SAPIENZA
UNIVERSITÀ DI ROMA

Control Architectures and Algorithms Design for the Aggregation of Flexible Loads for Network Services Provisioning

Faculty of Information Engineering, Informatics, and Statistics (I3S)
Department of Computer, Control, and Management Engineering Antonio Ruberti (DIAG)
Doctor of Philosophy in Automatica, Bioengineering and Operations Research, XXXIV Cycle

Roberto Germanà
Student ID 1527615

Supervisor
Prof. Francesco Delli Priscoli

A.A. 2021-2022

Acknowledgments

(intentionally left blank for the review process)

Abstract

The Electricity Energy scenario is currently subject to a radical transformation associated with the growth of both Distributed Energy Resources (DER) and Electromobility. This evolution is being investigated by the research community, the electric companies and European entities as a means to add flexibility to the electrical grid. This is done in an effort to increase the hosting capacity of DERs, with particular regard to Renewable Energy Sources (RESs) and electromobility, and their participation in the electricity energy market and in the network service provisioning. The thesis discusses the integration of flexible loads in the European network energy service scenario providing an incremental analysis that starts from a proof of concept and arrives at the design of realistic-like control systems. After introducing the transformations that are characterizing the Energy Market and the network service provisioning, a separation of Global and Local Ancillary Services is given. Based on this separation, the sequence of several incremental works provides the design and implementation of an increasingly sophisticated control system for the implementation of network services through Plug-In Electric Vehicles (PEVs) and Energy Storage System (ESSs), with considerations and evaluations of the technological aspects that characterize the fields of interest. The results obtained for Local Ancillary Services are examined and then extended and adapted to the Global Ancillary Services scenario. The provided extensions modify the electricity energy system scenario. The thesis exploits this new condition for the design of novel Global Ancillary Services based on flexible loads. All the proposed works are accompanied by simulations and emulations integrated with real ICT infrastructures. Simulation results are presented and extensively discussed, to highlight the effectiveness and the gaps of the proposed solutions.

Sommario

Il sistema dell'energia elettrica europeo nelle ultime due decadi è stato ed è protagonista di una profonda trasformazione. La sempre più elevata presenza di Risorse Energetiche Distribuite (DERs) - sparse oramai ad ogni livello della rete elettrica - insieme alla repentina crescita e diffusione dell'elettromobilità richiedono una revisione che arriva fino alle fondamenta del sistema elettrico. La profonda trasformazione del sistema elettrico ha riscosso l'interesse dalla comunità della ricerca scientifica, dalle compagnie elettriche e dagli enti europei. L'inclusione di carichi flessibili, distribuiti, e associati a Fonti di Energia Rinnovabile (FERs) tra gli attori partecipanti alla fruizione dei servizi ancillari come mezzo per aggiungere flessibilità alla rete elettrica, instaura nuove opportunità e sfide scientifiche, di mercato e di gestione del sistema a livello europeo. La tesi discute quindi l'integrazione dei carichi flessibili nella partecipazione dei servizi energetici di rete. La tesi fornisce un'analisi incrementale che, partendo da esempi applicativi arriva alla progettazione di sistemi di controllo realistici. Nella prima parte della tesi vengono introdotte e caratterizzate le trasnformazioni associate al sistema elettrico ed al mercato dell'energia elettrica, rimarcando la separazione tra Servizi Ancillari Globali e Locali. Sulla base di questa separazione, la tesi propone una sequenza di studi e lavori incrementali che hanno lo scopo di fornire gli strumenti, le considerazioni e le valutazioni necessarie per la progettazione e l'implementazione di un sistema di controllo sempre più sofisticato in grado di fornire servizi di rete tramite l'utilizzo di carichi flessibili, quali Veicoli Elettrici (PEVs) e Sistemi di Accumulo dell'Energia (ESSs). Nella prima parte della sezione 3 della tesi l'attenzione è focalizzata sui Servizi Ancillari Locali. Nella seconda parte della stessa sezione i risultati ottenuti a livello locale diventano oggetto di revisione ed estensione al fine di adattare l'impianto, costruito al livello di Servizi Locali, a scenari associati a Servizi Ancillari Globali. Tutti i lavori proposti sono accompagnati da simulazioni ed emulazioni integrate con infrastrutture ICT reali. I risultati delle simulazioni sono presentati e ampiamente discussi, per evidenziare l'efficacia delle soluzioni proposte ed aspetti che danno spunto per possibili sviluppi futuri.

Contents

List of Figures

Acronyms

ACER Agency for the Cooperation of Energy Regulators.

ADMM Alternating Direction Method of Multipliers.

aFRR Frequency Restoration Reserves with Automatic activation.

ARERA Autorità di Regolazione per Energia Reti e Ambiente.

BDE Dispatching Order.

BMS Battery Managment System.

BRP Balance Responsible Party.

BSP Balance Service Provider.

CPO Charging Point Operator.

CPS Cyber Physical System.

CQLF common quadratic Lyapunov function.

CS Charging Station.

CSP Control Service Provider.

DER Distributed Energy Resource.

D-LAA Dynamic Load Altering Attack.

DSM Demand Side Management.

DSO Distribution System Operator.

EC European Commission.

EMS Energy Managment System.

ESS Energy Storage System.

EV Electric Vehicle.

EVSE Electric Vehicle Supply Equipment.

IADS anomaly detection system.

ICT Information and Communication Technologies.

MEC Multi-access Edge Computing.

MGP Day-Ahead Market.

MI Intra-Day Market.

mMTC massive Machine Type Communications.

MPC Model Predictive Control.

MPE Spot Electricity Market.

MPEG Daily Products Market.

MSD Ancillary Services Market.

MTE Forward Electricity Market.

PEV Plug-In Electric Vehicle.

PMP Pontryagin minimum principle.

POC Point of Connection.

PV Photovoltaic.

RES Renewable Energy Source.

RMCU Remote Monitoring Control Unit.

RTT Round Trip Time.

RTU Remote Terminal Unit.

SCADA Supervisory Control and Data Acquisition.

S-LAA Static Load Altering Attack.

SOC State of Charge.

TSO Transmission System Operator.

URLLC Ultra Reliable Low Latency Communications.

UVA Enabled Virtual Unit.

UVAC Enabled Virtual Consumption Unit.

UVAM Mixed Enabled Virtual Unit.

UVAP Enabled Virtual Production Unit.

V2G Vehicle to Grid.

VPN Virtual Private Network.

VPP Virtual Power Plant.

Chapter 1

Introduction

Contents

This manuscript represents a *story* of the activity I have been carrying out during the last three years within' my PhD which has been developed in joint with the activities conducted in the *Network Control Laboratory*, *Dipartimento di Ingegneria Informatica e Automatica* (DIAG) at *Università degli Studi di Roma La Sapienza*. The arguments developed during the PhD were partially supported by the H2020 project 5G-SOLUTIONS (Grant agreement ID: 856691) and SAPIENZA - ATENEO 2017 "PROMETEO - Protezione di reti elettriche di potenza da attacchi ciber-fisici mediante strategie di controllo" (project, no. RM11715C7EFAF857)

During the PhD, I mainly focused my interest on the evolution of the energy market, in this perspective my research activities have been dedicated to the analysis of it with the aim of identify the opportunity and the issues concerning the metamorphosis of the *Electricity System*. In doing so, I have faced problems related to the inclusion of new actors in the Ancillary Service scenario and consequently in the definition of control algorithms for the integration of them in the Ancillary Services Market (MSD).

In this context, this manuscript focuses on the toward identification, develop and study of solutions, in terms of control algorithms and architectures, for enabling the participation of Vehicle Charging Areas and Energy Storage Systems (ESSs) in the Dispatching Services. In this sense, several case studies are provided -also considering commercial standard requirements- showing how the proposed control algorithms enable the participation of non-programmable sources in the Dispatching Services.

1.1 Motivation

The Electricity Energy Market and consequently the Disptatching Activity are rapidly developing due to the massive rise of Renewable Energy Sources (RESs), that have the peculiarity of being non-programmable, jointly with the growth and expansion of Distributed Energy Resources (DERs) and the progressive reduction of

programmable generation energy sources that historically guaranteed the equilibrium between electricity generation and demand. The power equilibrium is a key point for the efficient and secure operation of the network. The transition of the electricity energy scenario is in line with the European Objective to cut greenhouse gas emissions by at least 55% by 2030. The plan of Europe -becoming climate neutral by 2050- makes more urgent the update and innovation of Dispatching Services in terms of service provisioning, opening the participation to all the available convenient resources, and remuneration [4]. With the entry into force of the Third Energy Package in 2011, and in particular with the implementation of EC Regulation 714/2009 [5], the design of the wholesale electricity market of each Member State was subject to important processes of harmonization of the rules led by the European Commission and Agency for the Cooperation of Energy Regulators (ACER). The evolution of the Electricity Energy Market beside the requisites coming from the changes at the level of energy production, is got ahead with the intention of create a market structure that admit the coupling between the wholesale energy markets of the EU members, further harmonizing and sharing the Ancillary Services [6]. In the spirit of this evolution, it becomes necessary to review the definition of Ancillary Services provisioning and the strategy to provide and remunerate them. In the process of redefinition it is important to remove the barriers that currently exclude the participation of RESs, ESSs, DERs and Flexible Loads and then guarantee technological neutrality. To do that, several actions on the definition of the participation and responsibility of the participants to the electric system are making, sponsoring the aggregation and the use of the RESs, ESSs, DERs and Flexible Loads. These innovations bring the energy scenario a to re-evaluation of the Distribution System Operators (DSOs) in a context in which the impact of DER and Flexible Loads is not more negligible, with the consequent necessity of creating a new approach to manage the distribution branches.

1.2 Objective, Contribution and Structure of the Thesis

The objective of the thesis is to provide a comprehensive analysis of the electricity market evolution. The work aims are: highlighting the new potentialities, transforming them into operational scenarios, deriving the associated control problems, designing the control and providing critical analysis on results and implementation feasibility.

The structure of the thesis and the contribution of each part are described below: Chapter 2 provides an introduction on the Italian Electricity Energy Markets, taken as a reference for the developed scenarios, the market structure and the purpose of each market stage. The Italian market is then focused on the European Energy Market Structure and the Italians and Europeans directives are explained and contextualized in relation to the transformation of Electricity Energy Actors and Ancillary Services paradigm. Chapter 2 provides the knowledge base for the understanding of the next sections.

Chapter 3, the core chapter of the thesis, illustrates how the market evolution could be exploited to open the MSD to the flexible loads, in particular ESSs and PEVs. The chapter is divided into two sections.

Section 3.1 is dedicated to the Local Ancillary Service Provisioning, i.e. at the distribution node level. The discussion starts from the control of a single charging area for peak shaving and RESs integration goals and ends with the design, simulations and realistic tests of a distributed smart charging system, integrated with 5G network, able to carry out Demand Side Management (DSM) services, in compliance with international charging standards and ICT capabilities.

In Section 3.2 the results obtained at node level are examined and are used as the baseline for the designing of Global Ancillary Service. The section starts from the extension of the Demand Side Management (DSM) services provisioning, at a transmission-level node, investigate the utilization of PEVs for the power network frequency control, and ends with a control system able to robust stabilize a transmission network under attacks.

The designed services are contextualized in the European and Italian regulations scenario and linked with the current state of the art, both from literature, then industrial pilot projects points of view.

Chapter 3 contributes to the improvements of the conscious about the potentialities, benefits, limitations and current barriers that characterize the UVAMs control, providing control algorithms and architectures compliant with the industrial and technological requirements and constraints.

Finally, in Chapter 4 the conclusions of the work are drawn.

1.3 Contributing Publications and Project Documentations

Prior to this thesis, part of the contents presented in Chapter 3 was disseminated through the following publications:

- R. Germanà, A. Giuseppi and A. Di Giorgio, "Ensuring the Stability of Power Systems Against Dynamic Load Altering Attacks: A Robust Control Scheme Using Energy Storage Systems," 2020 European Control Conference (ECC), 2020, pp. 1330-1335, doi: 10.23919/ECC51009.2020.9143620.

- A. D. Giorgio, A. Giuseppi, R. Germanà and F. Liberati, "Decentralised Model Predictive Control of Electric Vehicles Charging," 2019 IEEE International Conference on Systems, Man and Cybernetics (SMC), 2019, pp. 3216-3222, doi: 10.1109/SMC.2019.8914040.

- F. Liberati, R. Germanà, E. De Santis and A. Di Giorgio, "Optimal Control of an Energy Storage System and Plug-in Electric Vehicles Fast Charging in a Grid-connected Service Area," 2021 29th Mediterranean Conference on Control and Automation (MED), 2021, pp. 202-207, doi: 10.1109/MED51440.2021.9480262.

- R. Germanà, F. Liberati and A. Di Giorgio, "Decentralized Model Predictive Control of Plug-in Electric Vehicles Charging based on the Alternating Direction Method of Multipliers," 2020 28th Mediterranean Conference on Control and Automation (MED), 2020, pp. 739-745, doi: 10.1109/MED48518.2020.9183137.

- Roberto Germanà, Emanuele De Santis, Francesco Liberati, Alessandro Di Giorgio "On the Participation of Charging Point Operators to the Frequency Regulation Service using Plug-in Electric Vehicles and 5G Communications", 21ST International Conference on Environment and Electrical Engineering (EEEIC2021), 7-10 Sept 2021, Bari, Italy

Part of the contents presented in Chapter 3 was result of the activities carried out in H2020 project 5G-SOLUTIONS (Grant agreement ID: 856691) and SAPIENZA - ATENEO 2017 "PROMETEO - Protezione di reti elettriche di potenza da attacchi ciber-fisici mediante strategie di controllo" (project, no. RM11715C7EFAF857).

Currently, the publication of the results of the PhD work is fully ongoing, with some papers under review and further ones about to be submitted.

Specifically, the results illustrated in section 3.2.2 is submitted to a control journal and 3.2.3 is about of submission.

Chapter 2

The Transformation of the Energy Market

Contents

2.1 The Energy Market Evolution

The Italian Electricity Energy Market was born in the 1999 from the Legislative Decree 79/99, which transposed the European Directive on the internal market in electricity (96/92/EC) [7] into the national legislation.

In line with the international experiences, the market has to meet specific requirements:

- promoting competition in electricity generation, sale and purchase, under criteria of neutrality, transparency and objectivity, through the creation of a marketplace;
- ensuring the economic management of an adequate availability of ancillary services.

In this sense, the Italian Market was conceived to ensure the the availability of the energy, in relation to the physical limits of the electricity system.

The Italian market (but in general all the electricity markets) was designed, making use of different market stages, to gradually meet, in relation to the approach of the time in which the estimated electric power must be effectively produced and absorbed, the demand and network requirements. Following this concept, the Electricity Energy Market in Italy is articulated in two different markets:

- Forward Electricity Market (MTE) : sellers and buyers can exchange large stocks of energy with a multi-year time horizon, thus safeguarding themselves from fluctuations in energy prices;

- Spot Electricity Market (MPE) : is designed to counteract to the power consumption and generation estimation errors which can be affected by weather variables, events, etc...

The MPE in turn is subdivided in different stages:

- Day-Ahead Market (MGP)
- Intra-Day Market (MI)
- Daily Products Market (MPEG)
- Ancillary Services Market (MSD)

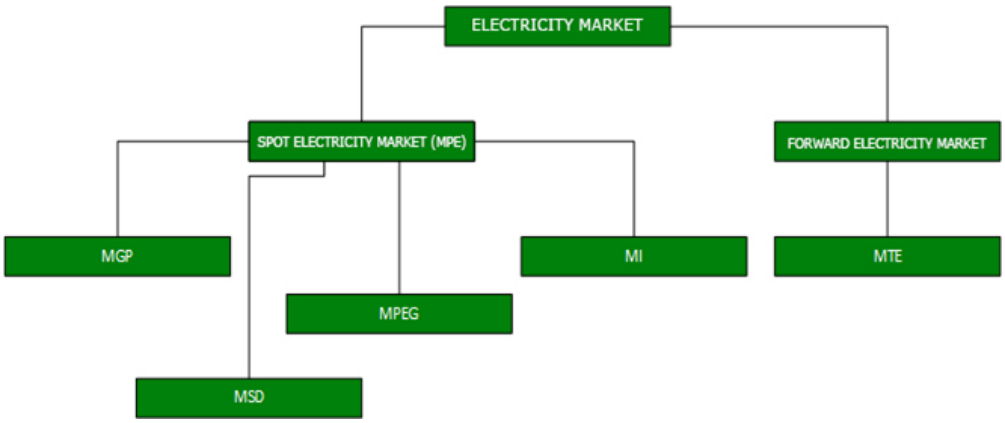

Figure 2.1: Articulation of the Italian energy market [1]

MGP and MI work on a time window horizons that varying from days to hours and are based on simplified versions of network model; the constraints are reduced to the power limits injection of the generation units and the withdraw of the participant of the market, to the representation of tie-line and congestion limits based on structural and/or recurrent events, neglecting the other network necessities as the reactive power requirement and consequently the voltage stability of the network.

The MGP, MI and MPEG are the venue for the trading of daily products with energy delivery obligation. The MSD is the stage of the market dedicated to the real time power balance in the network: the forecasting of power used in the MGP and MI doesn't fit exactly the real power consumption, the same consideration for the generation. This unbalance is intensified due to the RES penetration, with the uncertainties that characterize their power production, and due to the get crowed of electric energy based devices as air conditioning systems and Electric Vehicles (EVs). Unlike the MGP and MI, the MSD properly reflects the physical behaviour of the electric power system; the network is well represented right down to the nodal representation, as well the market offers are comprehensive of the real-time boundary conditions.

The presented structure of the Electricity Energy Market, in which MGP and MI provide initial dispatching of power in the system, based on the power injection and withdraw of the units tying tightly the physical and commercial nature of the market, limits the flexibility of part of the generation units that participated to the MGP and MI market phases. This condition not only reduce the flexibility, with the clear effects on the market but can bring the network's and units' to boundary operations conditions. The market process presented above limits the flexibility and the participation of actors in the MSD.

On 14 June 2019 the European Commission emanated the Directive 2019/994 of 5 June 2019 about the internal energy market regulations [8]. The directive introduced news related to the distribution grids, the portions of the network mainly impacted by the spread of ESSs and distributed RESs (take as example the solar panels located on the buildings). The directive has the aim of increases technological neutrality between the available energy sources with the final objective to reduce market distortions, widening the participation with a consequence of increase the competitiveness. The redefinition of the participants to the market, jointly with the promotion of the use of RESs, is combined with the rise of the DSOs as an active member in power management.

In this context, the 322/2019/R/EEL [9] identifies the main guidelines of intervention for the evolution of the dispatching service and for the coupling of the European markets. The key point is identified in the separation of the commercial actions and the schedule of the power units. The possibility of separate this two aspects allows to lose the restrictions imposed by the MGP and MI to the MSD; the rigidity of the scheduling defined during the MGP and MI denied the market participants to exploit information about the power generation and absorption forecasting in the near-real-time. The chance of declare the real-time scheduling of the units, without restrictions coming from the commercial positions, admits to increase the flexibility with benefits in terms of unbalance management. Moreover the separation between physical and commercial contexts admits the overcome of the sequentially of the market phases, enabling the necessary condition for the alignment with the European's markets. The MGP and MI, in this perspective, identify only the commercial participation decommissioned from the scheduling of the units that compose the commercial position. *The starting point of the MSD is not more exclusively defined by the previous markets' results.*

2.2 Ancillary services provisioning

The evolution of the Electricity Energy Market, with the separation of the commercial position and the physical intervention, as a matter of principle allows the participation of the RESs, or more in general, to non-programmable and distributed generation/load areas to the Ancillary Services. The opening up to these news participants, if from one side poses potential prospects in terms of energy efficiency, competitiveness and efficiency of the market, requires a non-trivial revision of the

Ancillary Services. Historically, the power equilibrium was entrusted by the programmable plants: the characteristic of guarantee power margins, the controllability of the plant and the high inertia characterizing these generation systems have ensured the functioning of the power network from the beginning. The RESs penetration, the spread of DERs, the increase of the power demand and its volatility, the evolution of the ESSs technology, with effects on the electromobility expansion, in conjunction with the progressive disappear of fossil-based generating systems made necessary the revision of the Ancillary Services, taking in to account these aspects as base for a long-term evaluation. The Ancillary Services provisioning has to be designed in order to include the RESs, ESSs, DERs and flexible loads (as example EVs), while always ensuring, eventually leveraging aggregation, all the needs for the safety and quality of the network operations. The revision includes the competence re-definition of two figures in the market scenario [9]:

- Balance Responsible Party (BRP): is the subject responsible of the *execution* of injection and withdraw programs of each units. In view the is also the responsible of the power unbalances and is the holder of the dispatching service contracts.
- Balancing Service Provider (BSP) is the subject responsible for the *ancillary service provision* results of obligation or MSD trading.

The innovation is in the separation of these two figures, indeed before the 300/2017/R/EEL [10] the two figures coincided. Summarizing, Balance Responsible Partys (BRPs) at the start of the MSD ex-ante [1] define the injection/withdraw schedules consistently with the physical limits of the units, Balance Service Providers (BSPs) offer the power capability for the MSD participation. The Transmission System Operator (TSO), in the Italy case *Terna* [11], based on the MSD ex-ante selects the BSPs' offers. The selection of the BSPs' services ironclad the scheduling making the BRPs responsible for the unbalances. In order to guarantee compliance with the principle of technology neutrality, the BSP can participate to the market by the aggregation of different units, the kind of units that compose the aggregated energy source defines different classes of virtual units called Enabled Virtual Units (UVAs) [10]:

- Enabled Virtual Consumption Unit (UVAC) - characterized by only consumption units;
- Enabled Virtual Production Unit (UVAP) - characterized by (non-relevant) production units [1] and ESSs;
- Mixed Enabled Virtual Unit (UVAM) - characterized by (non-relevant) production units including ESSs and vehicles charging areas that provide service to the network (i.e. Vehicle to Grid (V2G)). The UVAM definition is extended to other configurations untreated in this thesis, for details the reader may refer to [9].

[1] with a maximal nominal power of at least 5 MW

This thesis puts the attention on the UVAPs and UVAMs. The UVAM participation to the Ancillary Services is triggered by dispatching orders, defined *w.r.t.* a *baseline* defined by the BSP. The supply of the service by the UVAs can leverage the real-time conditions of the units that compose the aggregation. The separation between BRP and BSP allows a clever managing of the units that in aggregated form have to provide the services, the BSP can modify the contribution of the units without restrictions dictated by the single unit commercial position. However, whatever is the strategy used to define the intervention of the units the service has to be guaranteed.

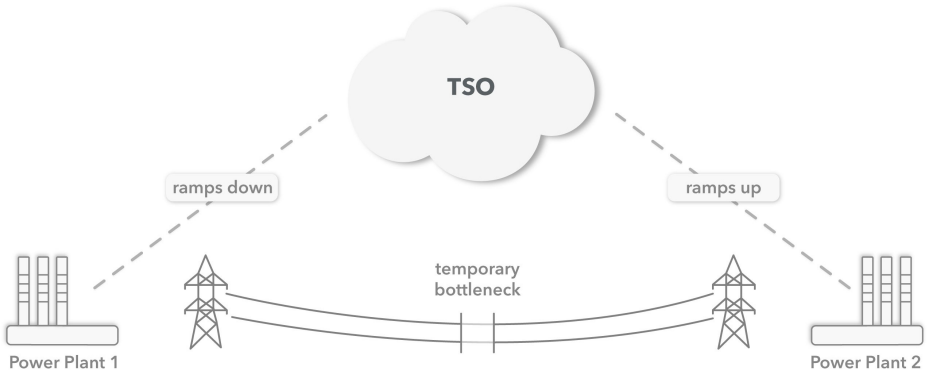

Figure 2.2: Graphical example of dispatching order. Credits [2]

2.3 The new role of Distribution System Operator

Traditionally the aggregation of loads concerning the distribution branch is consider a passive load, the power flow could be consider unidirectional and predicable. With the expansion of DERs, EVs and litte-size ESSs the view is changed: the presence of active components in the distribution network deeply modified the behaviour of the network making necessary a revision -together with the ancillary service redefinition- of the role of the Distribution System Operator (DSO).

The Ancillary Services, that we recall are the set of services needed to ensure the security of the electrical system, can be divided in two groups:

- global ancillary services: designed to ensure the security at the level of the electrical transmission system;
- local ancillary services: designed to ensure the security of the distribution grid.

The new role of the DSO is defined with respect to this separation:

- the DSO assumes the role of *neutral facilitator* for the supply - to the TSO- of the global ancillary services offered by BSPs. The DSOs have to be informed

about the MSD results of the units' production and consumption included in the UVAs. DSOs have to provide full cooperation to the TSO, and if necessary indicate ex-ante limitations to the movement of certain production and/or consumption units connected to their networks.

- the DSO assumes the role of buyer of local ancillary services to control the under responsibility distribution network. The DSO is responsible for the purchase of the services necessary for the efficient, reliable and safe operation of the distribution system.

The DSO can benefit from this new role: the possibility of provides Ancillary Services with the aggregation of DERs, ESSs and EVs charging areas contained in the distribution network can be used to ensure the efficiency of the distribution portion and at the same time opens to the participation, as BSP in the MSD.

Chapter 3

Control Systems for Integrating PEVs and ESSs into Ancillary Services Provisioning

Contents

In In this section case studies characterized by technological problems related to the different contributions that the flexible loads can provide in the management of electricity networks are presented.

The works are presented following an incremental discussion, showing the step-up improvements that characterized the research carried during the PhD.

The case studies are built in an incremental way, the section start with a proof of concept on the contribution of flexible load to the power flow control, on this proof of concept the discussion is augmented and specialized to specific services and integration aspect.

The main concept at the basis of the following works is based on the idea of exploit the presence of loads capable to store energy. The ability of storing energy introduces a degree of freedom that could be used to introduce elasticity in power injections and withdraws, creating a collaboration between loads in the same load area and/or between different load areas.

The works presented below gradually examine practical aspects related to the use of ESSs technologies in the real application. In this section are provided discussions in control architectures, computation and market participation perspectives. To evaluate the real possibilities and limitation coming from the on-field application, also the technological standards are taken into account,

The works presented in this thesis exploit the presence of ESSs, but it is important to clarify that this thesis has not the aim of entering in the detail the technology used to implement the ESSs. The reader may find an overview on the energy storage types, applications and recent developments related also to Electric Vehicles (EVs) in [12].

3.1 Local Ancillary Services

3.1.1 Optimal Control of a Grid-connected Service Area equipped with Energy Storage

As a result of the increasing charging rate implemented by car manufacturers in the new generation of plug-in electric vehicles (PEVs), charging point operators are continuously adjusting the charging infrastructure accordingly. In order to maximize the charging operator's return of investment and minimize the impact on the electricity grid, a key aspect is finding technical solutions which allow to downsize the nominal power flow at the point of connection between the charging station/charging area and the electricity grid, as the operating expenses are significantly affected by this parameter. In this regard, this study discusses the optimal control of an energy storage system (ESS) and PEVs fast charging for reducing the impact on the grid of the charging load in a charging area. A trade-off is achieved between the objectives of keeping limited the charging power withdrawal from the grid and the one of keeping limited the fluctuation of the state of charge of the ESS around a given reference, while keeping the charging power near to the nominal one. A deterministic solution, under the realistic assumption that the charging operator knows a piece-wise constant estimate of the aggregated charging power demand over the control period is presented. Numeric simulations are provided to validate the proposed approach.

3.1.1.1 Introduction

Among the main barriers to the large scale adoption of electromobility, the time needed for charging represents a key aspect for many drivers planning to buy a new vehicle without having the availability of a private parking for slow charging during the night or a Charging Station (CS) available at the workplace [13][14]. This is the reason why car manufacturers and charging infrastructure operators are working in the direction of technically enabling diversified charging services, and offering increasing level of charging power [15][16]. In the context of an electricity system subject to unbundling, a charging infrastructure operator may be a different player than the distribution system operator, so that the connection of its CSs to the grid

is subject to installation and operational costs which depend on the nominal power flow at the Point of Connection (POC). Consequently, finding technical solutions which allow to downsize the power flow at the POC is a key aspect to maximize the charging operator's return of investment (and indirectly minimize the impact on the electricity grid).

This works deals with the problem of controlling a grid-connected microgrid equipped with a set of CSs providing the fast charging service to PEVs, an electric ESS and potentially a source of power generation. We call such microgrid a "service area". The service area concept is relevant both for fast charging in urban scenarios and for fast charging during long-range trips. Since, in a fast charging scenario, there is limited possibility to modulate the single PEV charging sessions (as the priority is to serve customers as close as possible to the maximum power and in the minimum possible time), in this work an additional degree of freedom providing introduced by a ESS is taken into account, the additional flexibility is used to control the aggregated service area power exchange with the grid. More specifically, the control objectives for this work are:

1. To keep as low and smooth as possible the power flow at the point of connection of the service area with the grid. This lowers the operation cost of the service area, which is nowadays one of the main barriers for the deployment of the service area concept (the higher the power flow is, the higher the grid connection fees that the service area operator pays);

2. To keep the evolution of the State of Charge (SOC) of the ESS as close as possible to a desired reference value (usually, 50% of charge), to make sure the ESS has always a reserve of energy to charge or discharge; indeed, there is limited flexibility in the control actions if the ESS is operated close to the 0 or 100% SOC levels;

3. To keep the aggregated PEVs charging power in the service area as close as possible to a reference power curve, typically representing the nominal power, so as to minimize the PEVs dwelling time at the CS.

The above mentioned requirements work in opposition each other, giving raise to the need of formalizing an optimal control problem. Optimal control has been successfully applied in many applications dealing with resource management problems, see, e.g., [17], [18]. Control problems related to PEVs and microgrids equipped with several forms of controllable loads, storage devices and local generation are the subject of a wide literature. The contributions mainly differ for the application requirements, the control methodology and specific mathematical issues arising when modeling the control problem. Among the application scenario, [19] studied the problem of minimizing the voltage deviation in the microgrid in presence of distributed generation units, while [20] tackles the problem of reconfigurable microgrids to enhance security and reduce operation costs. Moreover, [21] faced the problem of energy management of smart homes in a microgrid environment. Several control methodologies, such as Model Predictive Control (MPC) [22][23], sliding mode

control [24], machine learning [25] have been investigated in several application contexts. Also the calculus of variations and the Pontryagin minimum principle (PMP) have found numerous applications in energy management, especially in the optimal control of hybrid vehicles (see, e.g., [26], [27], [28]) and microgrids (see, e.g., [29], [30]). One of the main obstacles in the adoption of these techniques in such problems is that it is not always possible to derive a causal or a closed loop solution. To address this, in literature some simplifications on the calculation of the costate from the necessary optimality conditions are discussed. In [26], the authors show that for the given hybrid vehicle control problem, the costate of the system can be assumed constant, simplifying the derivation of the optimal solution. In [28], in the context of the energy management of a plug-in hybrid electric bus, the authors combine PMP and MPC. In [29], a similar approach is used to optimize the energy flows in a microgrid hosting ESSs and renewables, with the objective of minimizing the ESS control effort and the deviation of the SOC from a reference value; also in [29], the costate is constant. However in many applications it is not possible to assume a constant costate.

The distinctive features of this work are as follows. First, we consider a deterministic formulation of the service area fast charging optimal control problem, which assumes the knowledge of the charging power demand in the service area over the control window. In this regard, charging infrastructure operators offering a booking service for charging are typically able to build a prediction of the near future value of the charging demand, which takes the form of a piece-wise constant signal and here represents a time-varying reference to be tracked by the actual aggregated charging power. Though quite realistic, the limitations resulting from this assumption are discussed in view of a future stochastic formulation of the proposed optimal control problem. Second, we model the above mentioned power tracking requirement through a cost term whose weight is dependent on the power demand, in order to mitigate the difference in the tracking performances resulting from different level of congestion (i.e. power demand) in the service area. Such a modeling choice gives raise to a two-point boundary value problem referred to a non-stationary dynamic system, for which an iterative procedure is proposed with the aim of explicitly calculating the initial costate. Third, we design an optimal control for a system subject to an exogeneous non-controllable signal - the short term prediction of locally generated power - which we assume to be known to the controller. Finally, to the best of the authors' knowledge, this work presents one of the first applications of the theory of calculus of variation to the problem of ESS and PEVs charging control in a smart charging area subject to the above mentioned requirements.

The reminder of this section is organized as follows. Section 3.1.1.2 presents the reference service area architecture and the proposed optimal control problem. Section 3.1.1.2 discusses the calculation of the optimal control. Section 3.1.1.3 presents and discusses simulations in a simplified but still realistic charging scenario. Section 3.1.1.4 concludes the work and discusses future directions of the work.

3.1.1.2 Problem formalization

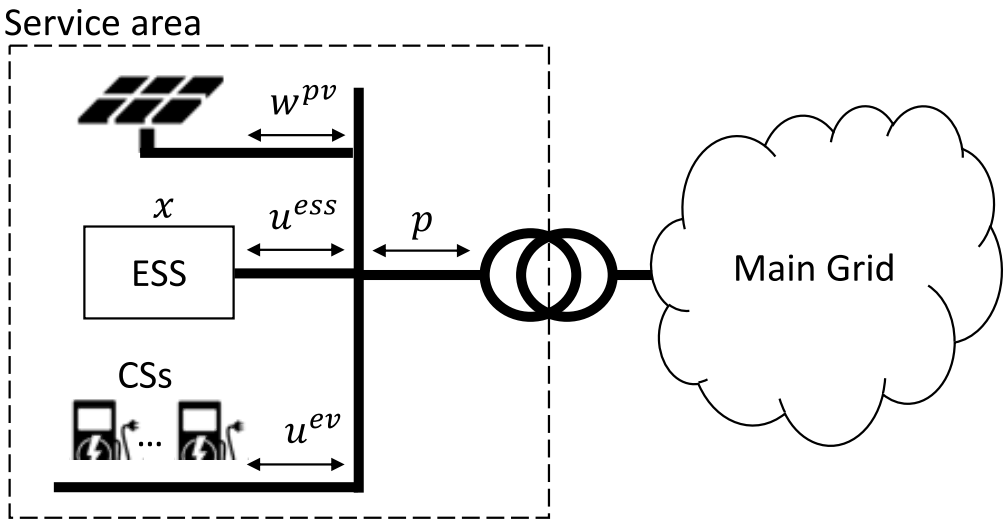

Figure 3.1: Reference service area architecture.

The reference service area architecture considered in this work is presented in Fig. 3.1. In this setup, the ESS, the CSs and the power generation are both directly connected to the POC. Let $p(t)$ denote the power flowing at time t at the POC, $u^{ess}(t)$ the ESS charging/discharging power, $x(t)$ the deviation of the ESS SOC from a reference value (typically, half of the full charge), $u^{ev}(t)$ the actual cumulative power absorbed by the PEVs, $\hat{u}^{ev}(t)$ the nominal cumulative PEVs power demand, $w^{pv}(t)$ the power generation in the area. The ESS dynamics is modeled as $\dot{x}(t) = f(x(t), u^{ess}(t), t) = u^{ess}(t)$. The service area is subject to the balance equation $p(t) = u^{ess}(t) + u^{ev}(t) - w^{pv}(t)$. In order to keep simpler the analysis of the problem, the obvious box constraints on $p(t)$, $u^{ess}(t)$ and $x(t)$ are neglected. Several works in literature (see e.g., [31], [32]) show how they can be handled, by including additional auxiliary state variables and accordingly expanding the Hamiltonian of the system.

Based on the control objectives introduced in Section I, the following optimal control problem is defined.

Problem 3.1. *(Service area fast charging optimal control problem). Given an initial and a final time of problem definition (respectively, t_i and t_f), given $\{\hat{u}^{ev}(t), t \in [t_i, t_f]\}$ and $\{w^{pv}(t), t \in [t_i, t_f]\}$ find*

$$\min_u \left\{ J(u) = S(x(t_f)) + \int_{t_i}^{t_f} L\big(x(t), u^{ess}(t), t\big) dt \right\}, \tag{3.1}$$

with

$$S(x(t_f)) = \frac{1}{2} s x(t_f)^2 \tag{3.2}$$

$$\begin{aligned} L\big(x(t), u^{ess}(t), t\big) = \frac{1}{2} \big[& q x(t)^2 + r p(t)^2 + \\ & + c(\hat{u}^{ev}(t)) \big(u^{ev}(t) - \hat{u}^{ev}(t)\big)^2 \big] \end{aligned} \tag{3.3}$$

subject to

$$x(t_i) = x_i, \tag{3.4}$$

$$\dot{x}(t) = u^{ess}(t), \quad \forall t \in [t_i, t_f], \tag{3.5}$$

$$p(t) = u^{ess}(t) + u^{ev}(t) - w^{pv}(t), \quad \forall t \in [t_i, t_f], \tag{3.6}$$

with $s, q, r > 0$. The weight $c(\hat{u}^{ev}(t))$ depends on the charging power currently requested. The idea is that it should be very high (ideally infinite) when the requested charging power is low (since there is not difficulty in this case to serve immediately the charging requests, at the requested power level), while it should progressively decrease as the requested charging power approaches the nominal maximum power available at the charging area (which denotes a state of congestion). In the following, for brevity, we write $c(t)$ in place of $c(\hat{u}^{ev}(t))$.

The optimal control Problem 1 can be solved via standard techniques from calculus of variations. The Hamiltonian of the system is

$$\begin{aligned}
\mathcal{H} &:= L\big(x(t), u^{ess}(t), t\big) + \lambda(t) f\big(x(t), u^{ess}(t), t\big) = \\
&= \frac{1}{2} q x(t)^2 + \frac{1}{2} r u^{ess}(t)^2 + \frac{1}{2} r u^{ev}(t)^2 + \frac{1}{2} r w^{pv}(t)^2 + \\
&+ r u^{ess}(t) u^{ev}(t) - r u^{ess}(t) w^{pv}(t) - r u^{ev}(t) w^{pv}(t) + \\
&+ \frac{1}{2} c(t) u^{ev}(t)^2 + \frac{1}{2} c(t) \hat{u}^{ev}(t)^2 - c(t) u^{ev}(t) \hat{u}^{ev}(t) + \\
&+ \lambda(t) u^{ess}(t)
\end{aligned} \tag{3.7}$$

Problem 1 is convex, and the resulting sufficient optimality conditions are

$$\dot{\lambda}(t) = -\frac{\partial \mathcal{H}}{\partial x(t)} = -q x(t), \tag{3.8}$$

$$\begin{aligned}
\frac{\partial \mathcal{H}}{\partial u^{ess}(t)} = 0 &\longrightarrow r u^{ess}(t) + r u^{ev}(t) - r w^{pv}(t) + \lambda(t) = 0 \\
&\longrightarrow u^{ess}(t) = -\frac{1}{r} \lambda(t) - u^{ev}(t) + w^{pv}(t),
\end{aligned} \tag{3.9}$$

$$\begin{aligned}
\frac{\partial \mathcal{H}}{\partial u^{ev}(t)} = 0 &\longrightarrow r u^{ev}(t) + r u^{ess}(t) - r w^{pv}(t) + \\
&+ c(t) u^{ev}(t) - c(t) \hat{u}^{ev}(t) = 0 \\
&\longrightarrow u^{ev}(t) = \frac{1}{c(t)} \lambda(t) + \hat{u}^{ev}(t),
\end{aligned} \tag{3.10}$$

$$\lambda(t_f) = \frac{\partial S}{\partial x(t_f)} = s x(t_f). \tag{3.11}$$

where the last step in (3.10) is achieved by noticing from (3.9) that $r u^{ess}(t) + r u^{ev}(t) - r w^{pv}(t) = -\lambda(t)$. Equation (3.8) is the costate equation, (3.9) and (3.10) the equations of the control, and (3.11) the transversality condition.

By plugging (3.10) into (3.9), we rewrite (3.9) as:

$$u^{ess}(t) = -\frac{1}{r'(t)}\lambda(t) - \hat{u}^{ev}(t) + w^{pv}(t), \tag{3.12}$$

where

$$r'(t) := \left(\frac{1}{r} + \frac{1}{c(t)}\right)^{-1} \tag{3.13}$$

After plugging (3.9) into the state dynamics, the state and the costate dynamics define the following two-point boundary value problem

$$\begin{bmatrix}\dot{x}(t)\\ \dot{\lambda}(t)\end{bmatrix} = \underbrace{\begin{bmatrix}0 & -\frac{1}{r'(t)}\\ -q & 0\end{bmatrix}}_{:=A(t)}\begin{bmatrix}x(t)\\ \lambda(t)\end{bmatrix} + \underbrace{\begin{bmatrix}-1\\ 0\end{bmatrix}}_{:=B} w(t) \tag{3.14}$$

with boundary conditions $x(t_i) = x_i$ and $\lambda(t_f) = sx(t_f)$, and where we have defined $w(t) := \hat{u}^{ev}(t) - w^{pv}(t)$.

Notice that (3.14) is a time varying system, because r' depends on $\hat{u}^{ev}(t)$. Its explicit solution can be however computed easily in the present case, by exploiting the fact that the reference $\hat{u}^{ev}(t)$ in practice is piece-wise constant.

First of all, partition $[t_i, t_f]$ into sub intervals over which the reference is constant, i.e., consider the time instants $t_i = t_1 < t_2 < ... < t_N = t_f$, with $N \geq 2$, such that, for any $n \in \{1, ..., N-1\}$, $\hat{u}^{ev}(t)$ is constant over the time interval $[t_n, t_{n+1})$.

Consider a time instant in the n-th time interval of the above-defined partition, i.e., $t \in [t_n, t_{n+1})$, with $n \in \{1, ..., N-1\}$. Then we have

$$\begin{bmatrix}x(t)\\ \lambda(t)\end{bmatrix} = e^{A_n(t-t_n)}\begin{bmatrix}x(t_n)\\ \lambda(t_n)\end{bmatrix} + \int_{t_n}^{t} e^{A_n(t-\tau)}Bw(\tau)d\tau, \tag{3.15}$$

where we write A_n to remind that it is the matrix A computed based on the value which the aggregate charging reference takes on the n-th interval (i.e., $\hat{u}^{ev}(t)$, $t \in [t_n, t_{n+1})$). In turn, $[x(t_n), \lambda(t_n)]^T$ can be computed based on the same formula, and starting from $[x(t_{n-1}), \lambda(t_{n-1})]^T$. The process can be iterated backward up to the initial state $[x(t_1), \lambda(t_1)]^T$. Based on this consideration, it is not too difficult to see that $[x(t_n), \lambda(t_n)]^T$, with $n \in \{2, ..., N\}$ (being $n = 1$ a trivial case), can be written as[1]

$$\begin{aligned}\begin{bmatrix}x(t_n)\\ \lambda(t_n)\end{bmatrix} = &\left(\prod_{k=1}^{n-1} e^{A_{n-k}\Delta t_{n-k}}\right)\begin{bmatrix}x(t_1)\\ \lambda(t_1)\end{bmatrix} + \\ &+ \sum_{h=1}^{n-1}\left[\prod_{j=1}^{n-1-h} e^{A_{n-j}\Delta t_{n-j}}\right] \\ &\left[\int_{t_h}^{t_{h+1}} e^{A_h(t_{h+1}-\tau)}Bw(\tau)d\tau\right],\end{aligned} \tag{3.16}$$

[1]Notice that, for $h = n-1$, the product $\prod_{j=1}^{n-1-h}$ in (3.16) becomes the empty product $\prod_{i=1}^{0}$, which is equal to one by convention.

where we have defined for simplicity $\Delta t_j := t_{j+1} - t_j$. Equation (3.16), substituted back into (3.15) provides the explicit solution for the optimal state and costate trajectories, as a function of $\lambda(t_1)$, which in turn is found by evaluating (3.16) for $t_n = t_f$ and substituting $x(t_f)$ and $\lambda(t_f)$ into the transversality condition (3.11), and finally solving for $\lambda(t_i)$. These calculations, though conceptually simple, are quite involved, and can be executed with a computer, through symbolic computation routines.

An alternative approach allowing to explicitly calculate the initial costate, which is a key information to determine the optimal control and trajectories of the system, is as follows. Consider the transition matrix characterizing the free evolution of system (3.14) in the generic time interval $[t_n, t_{n+1})$. After simple calculations, it takes the form

$$\begin{aligned} e^{A_n(t-t_n)} &:= \begin{bmatrix} \Phi_{n,11}(t-t_n) & \Phi_{n,12}(t-t_n) \\ \Phi_{n,21}(t-t_n) & \Phi_{n,22}(t-t_n) \end{bmatrix} = \\ &= \begin{bmatrix} \cosh\left(\sqrt{\frac{q}{r'_n}}(t-t_n)\right) & -\frac{1}{\sqrt{qr'_n}}\sinh\left(\sqrt{\frac{q}{r'_n}}(t-t_n)\right) \\ -\sqrt{qr'_n}\sinh\left(\sqrt{\frac{q}{r'_n}}(t-t_n)\right) & \cosh\left(\sqrt{\frac{q}{r'_n}}(t-t_n)\right) \end{bmatrix}. \end{aligned} \tag{3.17}$$

Evaluating (3.15) for $t = t_f = t_N$ and $t_n = t_{N-1}$, substituting $x(t_f)$ and $\lambda(t_f)$ into the transversality condition (3.11) and finally solving for $\lambda(t_{N-1})$ gives

$$\lambda(t_{N-1}) = s_{N-1}x(t_{N-1}) + \int_{t_{N-1}}^{t_N} H_{N-1}(t_N - \tau)w(\tau)d\tau, \tag{3.18}$$

where

$$\begin{aligned} s_{N-1} &= -\frac{\Phi_{N-1,21}(\Delta t_{N-1}) - s\Phi_{N-1,11}(\Delta t_{N-1})}{\Phi_{N-1,22}(\Delta t_{N-1}) - s\Phi_{N-1,12}(\Delta t_{N-1})} \\ H_{N-1}(t_N - \tau) &= \frac{\Phi_{N-1,21}(t_N - \tau) - s\Phi_{N-1,11}(t_N - \tau)}{\Phi_{N-1,22}(\Delta t_{N-1}) - s\Phi_{N-1,12}(\Delta t_{N-1})} \end{aligned} \tag{3.19}$$

Equations (3.18)(3.19) establish, with little abuse of nomenclature, a new "transversality" constraint linking λ and x at time t_{N-1}. In turn, $[x(t_{N-1}), \lambda(t_{N-1})]^T$ can be computed using (3.15) and starting from $[x(t_{N-2}), \lambda(t_{N-2})]^T$, which allows to establish a new constraint between λ and x at time t_{N-2}. Iterating the procedure backward up to the initial time t_1, the initial costate can be written as

$$\begin{aligned} &\lambda(t_i) = s_i x(t_i) + \\ &+ \sum_{k=1}^{N-1} \left[\prod_{j=1}^{N-1-k} d_j \right] \int_{t_{N-k}}^{t_{N+1-k}} H_{N-k}(t_{N+1-k} - \tau)w(\tau)d\tau, \end{aligned} \tag{3.20}$$

or equivalently, posing $h = N - k$, in the more compact form

$$\lambda(t_i) = s_1 x(t_i) + \sum_{h=1}^{N-1} \left[\prod_{j=1}^{h-1} d_j \right] \int_{t_h}^{t_{h+1}} H_h(t_{h+1} - \tau)w(\tau)d\tau, \tag{3.21}$$

in which

$$\begin{aligned} H_h(t_{h+1}-\tau) &= \frac{\Phi_{h,21}(t_{h+1}-\tau) - s_{h+1}\Phi_{h,11}(t_{h+1}-\tau)}{\Phi_{h,22}(\Delta t_h) - s_{h+1}\Phi_{h,12}(\Delta t_h)} \\ d_j &= \frac{1}{\Phi_{j,22}(\Delta t_j) - s_{j+1}\Phi_{j,12}(\Delta t_j)} \\ s_h &= -\frac{\Phi_{h,21}(\Delta t_h) - s_{h+1}\Phi_{h,11}(\Delta t_h)}{\Phi_{h,22}(\Delta t_h) - s_{h+1}\Phi_{h,12}(\Delta t_h)} \\ s_N &= s \quad h = 1, ..., N-1 \quad j = 1, ..., N-2. \end{aligned} \tag{3.22}$$

The above procedure completely determines the optimal solution. In particular, the optimal state and costate trajectories are determined by (3.15) (as said, after embedding (3.16) and the initial costate (3.21)); the optimal control of charging power w^{ev} is found from (3.10); the optimal ESS control from (3.9); and the optimal trajectory of the power at the point of connection with the grid from (3.6).

3.1.1.3 Numerical Simulations

Simulations were performed in Matlab 2018b and span 12 hours of operation of the service area. We empirically selected $q = 1$, $r = 2$ and $s = 10$, resulting in good performance of the control system. The weight $c(\hat{u}^{ev}(t))$ of the charging power error term in (3.3) was selected as in Fig. 3.2. It remains close to the maximum value for low charging power demands, then it drops to a minimum value as the charging demand approaches the maximum allowed in the service area (a congested state of the service area, in which curtailment of the power delivered to the charging stations is admissible).

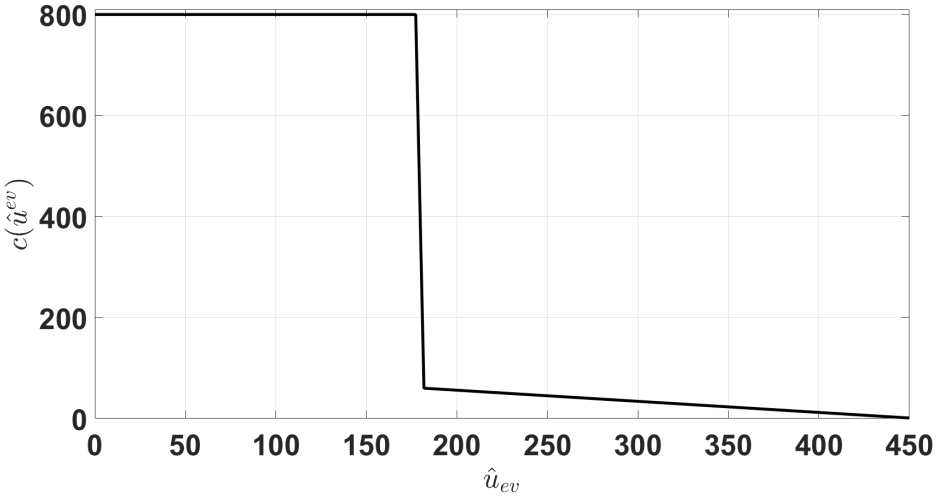

Figure 3.2: Shape of weight $c(\hat{u}^{ev}(t))$ used in the simulations.

The simulation was performed considering fast-charging at a maximum supply rate of $50kW$. Problem 1 and the associated optimal control handle the presence of

renewable generation in the service area. In this simulation we consider the presence of Photovoltaic (PV) power production at the service area; the forecasted PV power output is here assumed to have the form reported in Fig. 3.3, which is representative of an almost clear sky day, with two small perturbations approximately around 10:00 and 14:00.

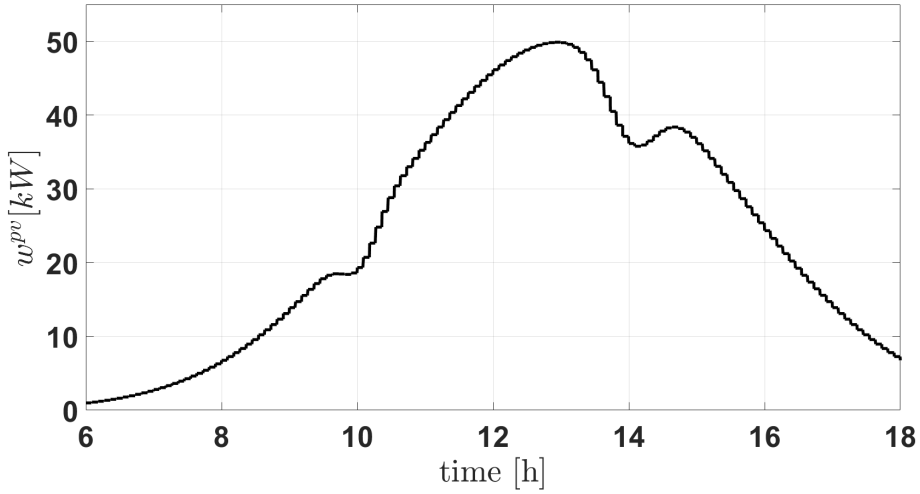

Figure 3.3: PV forecast profile.

Figure 3.4 displays the charging reference considered in the simulation (dashed line), and the resulting aggregated controlled charging curve u^{ev} (solid line). The charging reference reflects a test scenario, with different peaks of charging requests during the day. This simulation is aimed to study the behaviour of the system under high and low load conditions (the proposed control system naturally also works in conditions with no/reduced renewable energy, a scenario not discussed in this work; in that case, the charging energy will be provided only by the ESS and the POC). The reference is tracked with high fidelity when there are only 3 charging sessions active (see Fig. 3.4). As the number of simultaneous charging sessions increases, the tracking requirement is progressively relaxed, accordingly to the weight $c(\hat{u}^{ev}(t))$, allowing for an incremental mismatch between the reference charging profile and the controlled one. The zoom in Figure 3.4 highlights this behavior.

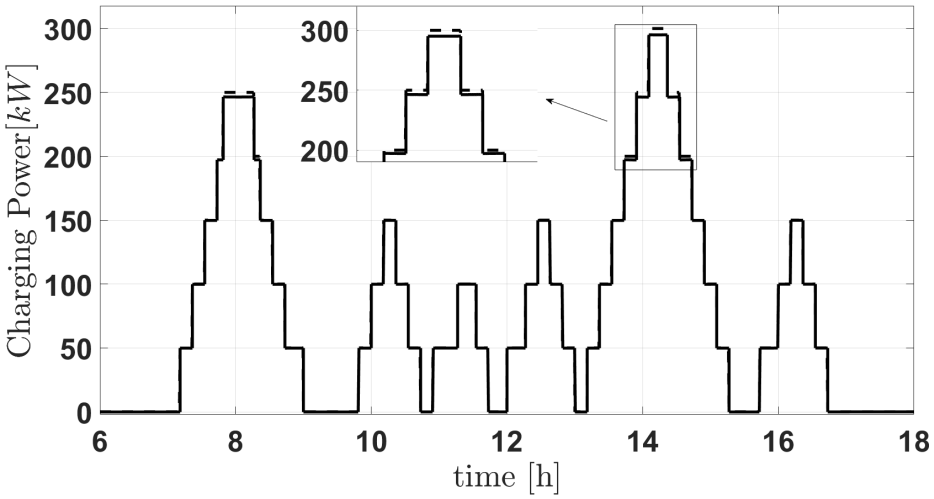

Figure 3.4: u^{ev} (continuous line), $\hat{u}^{ev}$ (dashed line)

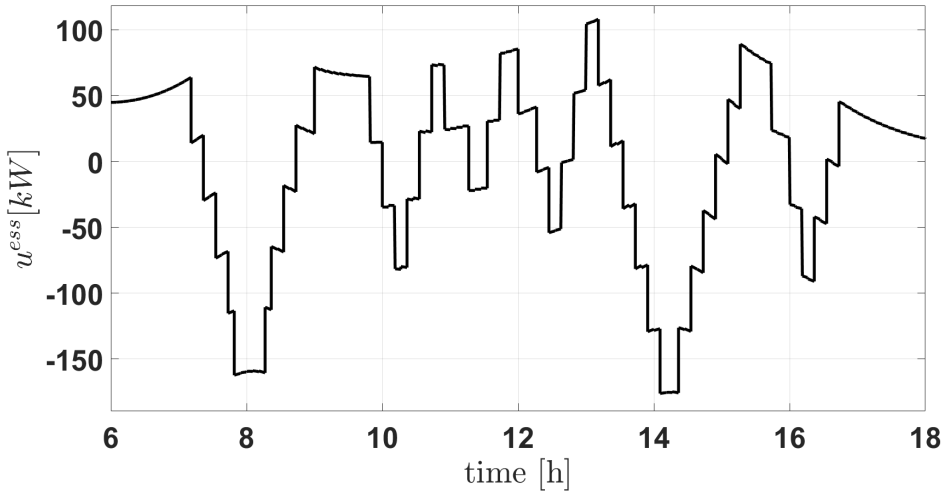

Figure 3.5: ESS charging/discharging power.

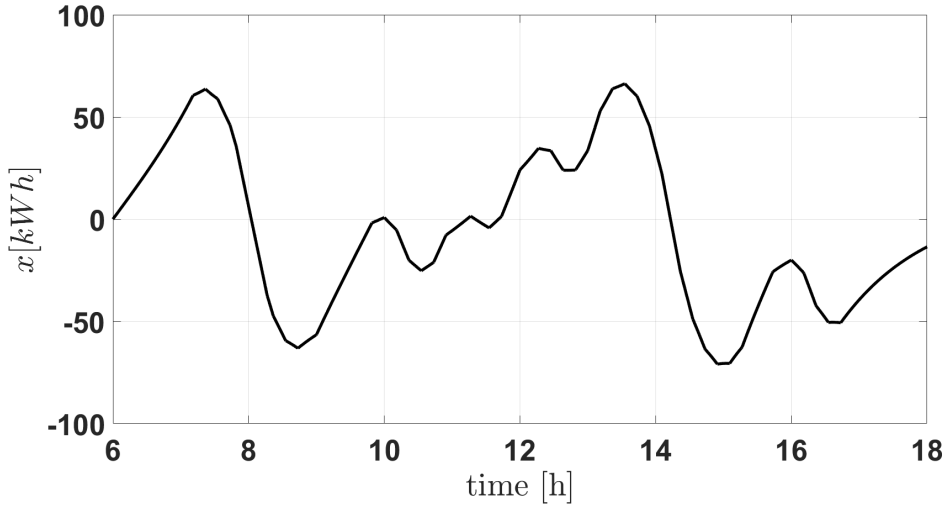

Figure 3.6: ESS SOC.

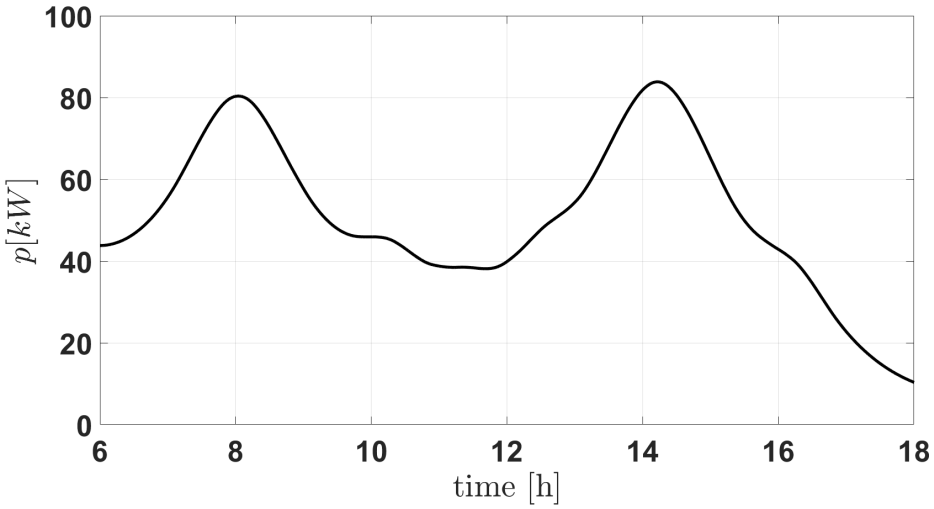

Figure 3.7: Power flow at the connection with the grid.

Figures 3.5 and 3.6 report the ESS charging/discharging power and the ESS SOC evolution, respectively. The piece-wise nature of the charging sessions reference signal is reflected on the power contribution of the storage. The ESS SOC evolution well reflects the strategy adopted by the storage, to smooth the power flow at the POC. The ESS recharges in advance, in prevision of the large peaks of demand, and later discharges to contribute during the peaks-periods, thus reducing the overall SOC error. Between the two charging peaks, the ESS recharges and balances the charging requests, thus smoothing their effect on the POC. Figure 3.7 reports the power flow at the point of connection with the grid. The resultant power flow is

smooth, in line with the desired requirement. The charging peaks in particular are significantly reduced, thus contributing to keeping low the power flow at the POC, as desired.

The results presented above show the effectiveness of the proposed control under the assumptions reported in Section I, in particular on the knowledge of the charging demand in the service area. Though quite realistic in a scenario where the charging point operator offers the charging service through a booking system, some practical remarks and limitations have to be considered. For example, from Figures 3.4 and 3.5 it can be seen that the ESS power profile has fast changes at the times in which a charging session starts or stops; as a consequence, in order to avoid undesired perturbations of the power flow at the POC, it is fundamental in practice to start and stop the delivery of charging power at the scheduled times, instead of synchronizing it with the actual times of connection and disconnection of the PEV at the CS. Further, the performances of the proposed control are clearly affected by PEVs connecting at the CSs after the time indicated in the booking system, as well as by drivers booking the charging service when the control window is already active. In order to properly take into account these limitations, and more in general to solve the same control problem in a more general scenario, where PEVs connect to the CSs without booking the service, it appears natural to formalize the same control problem under milder assumptions on the charging demand. In this regard, this work can be considered instrumental to the formalization of a future stochastic version of the proposed optimal control problem, in which the knowledge of the power demand is replaced by that of parameters characterizing the corresponding stochastic process (e.g. expected value, variance, etc). Also, re-optimization and the adoption of a receding horizon approach can be considered, in order to take into account the progressive update of the information available to the controller (not only the forecast of the charging demand, but also of the renewable power output, to which similar considerations apply). Finally the simulation results previously presented may be used as a benchmark for the evaluation of the performances achieved by the controller under the mentioned milder assumptions.

3.1.1.4 Concluding remarks

This work has presented an optimal control strategy for controlling the recharging of plug-in electric vehicles (PEVs) in a service area equipped with an energy storage system (ESS). The objective is to control the ESS and the PEV recharging process in order to serve the PEV users as fast as possible, while flattening the power profile at the point of connection with the grid (which results in lower operation costs of the charging area).

Future works will focus on the detailed modelling of the charging demand as a stochastic process, and consequently on the extension of the problem to stochastic optimal control [33], also considering a probabilistic formulation of constraints. Another line of research will address the inclusion into the problem of all the applicable constraints (on ESS charging power, POC, ESS SOC, etc.), as well as of the

PEVs' charging dynamics, for better capturing the recharging process. Also, re-optimization schemes to address uncertainties in the start and the duration of the PEV charging sessions will be analysed. Finally, in future works, an assessment of the economical benefits arising from the flattening of the power profile at the POC will be carried out.

3.1.2 Distributed MPC of Electric Vehicles Charging Service Area

Based on the results of the previous work, in which where showed how the presence of ESS in a smart charging load area combined with an optimal control algorithm able to control the charging and discharging set points of the elements in the smart-grid let a flatten power profile at the point of connection with the grid, this section presents a decentralised control strategy for the management of simultaneous charging sessions of electric vehicles.

The previous work does not take into account the PEVs' charging aspects, as the SOC of the vehicle and the power limits associated to the POC.

In this section, the proposed approach is based on the model predictive control methodology and the Lagrangian decomposition of constrained optimization problem which is solved at each sampling time. This strategy allows the computation of the charging profiles in a decentralised way, with limited information exchange between the electric vehicles.

The simulation results show the potential of the proposed approach in relation to the problem of shaving the aggregated power withdrawal from the electricity distribution grid, while still satisfying drivers' preferences for charging.

3.1.2.1 Introduction

In recent years the electric mobility has grown in popularity, pushed by the need to overcome the problems of pollution, depletion of natural oil and fossil fuel reserves, and rising petrol costs. The automotive industry is also motivated to adopt cleaner and more sustainable technologies by the governmental regulations and international agreements (see e.g. [34][35]). As largely recognized, massive PEV charging represents a concern for the operation of electricity distribution grids, but also an opportunity, due to the possibility of exploiting the flexibility offered by the vehicles during charging.

Over the last decade, this remark has motivated the investigation of several methodologies for the control of the PEV charging process according to a *pletora* of grid and drivers' requirements. Among the criteria used for classifying the control approaches, the centralized/decentralized nature of the control plays an important role, since it reflects two different visions of the new electromobility paradigm.

On the one hand the electric companies, as responsible for the secure operation of the electric network or interested players in the electricity markets, are interested in managing the charging processes in a centralized way; on the other car manufacturers are also interested in using the PEVs as a mean for enabling new business models and avoiding to share proprietary information related to the PEVs charger with other market players, which brings to the idea of a decentralized control.

Both these two classes of control have been proposed in the relevant literature for different purposes. Centralized control strategies have been developed for minimizing the peak load and avoiding distribution network issues [36, 37], reducing the power losses [38], avoiding network congestion and lower CO2 emissions [39],

minimizing the total cost of energy for users [40], maximizing aggregator profits and guarantee voltage regulation [41], tracking of target load curves [42][43], deliver balancing [44][45] and frequency regulation services [46]. Several studies also explore the possibility of utilising the PEV batteries as a distributed Energy Storage Systems [47] to offer additional seriveces to the grid, as service restoration [48] and resiliency improvements [49]. Similarly, decentralized control strategies have been proposed for avoiding overloads [50] [51], minimizing the total cost of energy for users and reducing power losses [52], maximizing aggregated profits [53][54], frequency regulation and integration of renewable energy sources [55], for reference power tracking [56], etc. An in-depth analysis of the many pursued objectives and proposed algorithms can be found for example in the comprehensive reviews [57] and [58].

This work targets a reference scenario consisting of a load area, namely a node of the distribution grid, equipped with a set of Charging Station for the delivery of charging services and proposes a decentralised control strategy aimed at maximizing the margin between the utility deriving to the drivers from the delivery of the charging service, and the cost for the operator deriving from the aggregated charging power withdrawal.

The proposed control is based on a MPC framework, which embeds a constrained optimization problem, taking into account both grid and drivers' requirements, which can be decomposed through Lagrangian relaxation. Several centralised control solutions based on MPC can be found for similar case studies in the literature [59, 60, 42], while in this work the computation of the charging load curves is performed by agents working at the level of each single PEV. Furthermore, the information exchanged with grid players is restricted to the computed load curve and energy price feedback from the market, elaborated according to the charging infrastructure congestion. Comparable scenarios have also been addressed by decentralised solutions, as in [61], in which a Mixed-integer optimisation formulation is utilised to model the optimization problem in which the various users trade their energy flexibility, in [62], where an aggregator agent dynamically modifies the energy pricing signal to steer a set of PEVs behaviour, and in [63] where a game-theoretic strategy is employed. In the envisaged scenario, the main innovation of this work are:

- The predictive and dynamic nature of the charging session scheduling, as the MPC scheme allows to attain optimal performances over its prediction window and, thanks to its receding horizon paradigm, it allows the system to easily respond to new charging requests.
- The focus on decentralisation, as the amount of information exchanged between the agents is limited thanks to the Lagrangian Dual Decomposition approach.
- The focus on the trade-off between economic performances and user satisfaction, captured by the utility and cost functions considered for the optimisation.

The remainder of the section is organized as follows. Section 3.1.2.2 recalls the fundamental concept of the MPC methodology and describes at high level how it is applied in this work. Section 3.1.2.3 presents the formalization of the open loop optimal control problem at the basis of the MPC scheme. Section 3.1.2.5 describes the decentralized solving procedure of the problem. Section 3.1.2.6 presents and discusses the simulation results and, finally, section 3.1.2.7 reports the conclusions and directions for future works.

3.1.2.2 Control methodology

The proposed controller is designed based on the discrete-time MPC methodology [64]. Discrete-time MPC is an optimization-based technique in which, at the generic discrete time t, the plant control signals are computed by solving a constrained optimization problem, usually referred to as open loop control problem, defined in a time window N steps in the future (i.e. $[t, t+N-1]$); the first sample of the computed control signals is applied to the plant (the remaining sequence is discarded) and then the process is reiterated at time $t+1$. The generic optimization problem at time t is built based on the feedback of the state plant at t, so that the closed loop properties of MPC arise from the combination of state feedback and continuous reoptimization.

MPC is one of the advanced control techniques most used in the industrial control practice, mainly because of its native ability and easiness in managing multi-variable constrained control. Also, great design flexibility is offered by the possibility of selecting and tuning the objective function and the constraints to be included in the optimization problem.

In standard MPC, the objective function terms are selected with the aim of stabilizing the plant state around a desired reference state, while minimizing the control effort. A distinctive aspect of the MPC here proposed is that the objective is designed to optimize the user satisfaction and the economical operation of the system.

In this work the control signals computed by the controller at each time t are the charging power of the PEVs; though the power flowing at the point of connection is a problem variable, in principle it does not represent a control variable, since it results from the PEVs controls in the load area. The feedback signals retrieved at each t for computing such an optimal control are the current State of Charge (SOC) of the PEVs in the network.

Further key input to the MPC controller at t are the boundary conditions and preferences characterizing the requests for the charging service, more specifically

- the arrival time at the charging station
- the initial SOC
- the departure time

- the desired state of charge

also the PEVs and the point of connection of the load area with the grid are characterized by their own technical and economic data.

Despite the potential large amount of critical data being part of the open loop optimal control problem, a distinctive aspect of this work is the one of being solved in a decentralised way; the information exchanged by the PEVs and the operator is restricted to power and energy price, while technical and economic information related to the equipment are not shared, then preserving user privacy and sensitive car manufacturers' data.

3.1.2.3 Control problem formalization

This section presents the open loop optimal control problem at the basis of the proposed MPC scheme. In what follows t will denote the current time, $T_t = \{t, t+1, \cdots, t+N-1\}$ the set of discrete time instants within the control window starting from t, τ the generic time instant within the set. The set R_t is introduced to denote the PEVs connected to a charging station at t and consequently being part of the control problem.

Agents behavioural models The behaviour of the agents being part of the control problem is modeled taking advantage of the concept of utility and cost functions usually applied in the context of microeconomics and resource management in telecommunication networks [65, 66].

Each PEV $r \in R_t$ is modeled by a utility function $U_r(p_r(\tau/t))$ which represents the level of satisfaction for the withdrawal of the charging power $p_r(\tau/t)$ at time $\tau \in T_t$, The utility function is requested to satisfy three properties: (i) it has to be continuous, (ii) monotonically increasing and (iii) strictly concave. From the modeling perspective, these requirements reflect the fact that the level of satisfaction of each driver grows up continuously with the level of charging power and is subject to saturation; from the theoretical point of view, this natural choice brings to the definition of a convex optimization problem. In particular, the utility function of the r-th PEV is here chosen as

$$U(p_r(\tau/t)) = w_r log(1 + p_r(\tau/t)) \quad \forall \tau \in T_t \tag{3.23}$$

where w_r is a weight introduced to differentiate the behaviour of the drivers.

The system operator is modeled in relation to the effect that multiple charging sessions have in terms of aggregated power withdrawal at the point of connection between the load area and the distribution grid. A cost function $C(P(\tau/t))$ is then introduced, where $P(\tau/t)$ is the power flowing at the point of connection at time $\tau \in T_t$. This cost function is requested to meet the following requirements: (i) it has to be continuous, (ii) monotonically increasing and (iii) strictly convex; as before, these are natural requirements, introduced to penalize the peaks of power

withdrawal from the grid. Specifically, the cost function is here chosen as

$$\begin{aligned} C(P(\tau/t)) = \alpha(P(\tau/t))^2 + \\ + \delta(P(\tau/t) - P(\tau - 1/t))^2 \quad \forall \tau \in T_t \end{aligned} \tag{3.24}$$

where α and δ are proper weights. The first term represents a penalty for excessive power withdrawal from the grid, while the second one is a ramping rate term aimed at avoiding fast variation of the power at the point of connection.

The utility and cost functions model counteracting requirements from different players. On the one hand, the drivers are interested in disposing of the highest possible level of charging power, on the other hand, the owner of the infrastructure is interested in minimizing the deriving operational cost. Then a trading mechanism is needed for establishing a proper trade-off allowing to meet driver needs for charging while guaranteeing acceptable operating conditions for the electrical infrastructure.

3.1.2.4 The open loop optimal control problem

In order to establish the required trade-off, the *social welfare*, defined as the difference between the total utility and cost in the area, is evaluated over all the control horizon, and the optimization criterion is consequently formalized as

$$\max_{\substack{p_r(\tau/t), P(\tau/t) \\ \forall \tau \in T_t}} \sum_{\tau \in T_t} \left\{ \sum_{r \in R_t} U_r(p_r(\tau/t)) - C(P(\tau/t)) \right\} \tag{3.25}$$

The optimal control sequences p_r^* and P^* are subject to three classes of constraints, taking into account the overall power balance, technical limitations and preferences at the level of the single PEVs and limitations of load area equipment. As far as it concerns the overall behaviour of the agent at load area level, the power balance has to be guaranteed at each $\tau \in T_t$, which is modeled as

$$\sum_{r \in R_t} p_r(\tau/t) = P(\tau/t) \ , \forall \tau \in T_t \tag{3.26}$$

At PEV level the feasibility of the charging session has to be guaranteed both in terms of allowed power withdrawal and driver preferences satisfaction.

$$p_r^{min} < p_r(\tau/t) < p_r^{max} \ , \forall r \in R_t \ , \forall \tau \in T_t \tag{3.27}$$

The driver preferences for charging are taken into account as follows. Let $e_r(\tau/t) = x_r(\tau/t) - x_r^{des}$ denote the deviation of the state of charge $x_r(\tau/t)$ of PEV $r \in R_t$ at time $\tau \in T_t$ from the desired state of charge x_r^{des}; this error signal is subject to the dynamics

$$\begin{aligned} &e_r(\tau + 1/t) = e_r(\tau/t) - (1 - \xi_r)\Delta t \, p_r(\tau/t), \forall \tau \in T_t, \forall r \in R_t \\ &e_r(t/t) = e(t), \forall r \in R_t \end{aligned} \tag{3.28}$$

where Δt denotes the sampling time, ξ_r the conversion losses coefficient and $e_r(t) = x_r(t) - x_r^{des}$ the actual error at current time t, evaluated using the feedback signal $x_r(t)$ and the desired state of charge x_r^{des}. The latter, which is in principle different from the maximum capacity of the battery x_r^{max}, has to be guaranteed at the departure time t_r^{dep} chosen by the driver, so that

$$e_r(t_r^{dep}/t) = 0 \ , \forall r \in R_t \tag{3.29}$$

As expressed in (3.26), the aggregated charging power is provided by the distribution grid at the point of connection (typically through a dedicated medium voltage to low voltage substation); due to the limited power rating of the transformers the power P is bounded as follows:

$$P^{min} \leq P(\tau/t) \leq P^{max} \ , \forall \tau \in T_t \tag{3.30}$$

In the light of the above, the open loop optimal control to be solved at each iteration of the MPC scheme can be stated as follows.
Open loop PEVs charging control problem. For a given load area characterized by operational cost (3.24), hosting a set R_t of charging PEVs having utility (3.23) and preferences (x^{des}, t^{dep}), solve (3.25), subject to the dynamics (3.28), control constraints (3.26), (3.27), (3.30) and state constraints (3.29).

Remark 1 In order for the optimisation problem to be feasible, it is required that all session requests have to be checked for consistency in terms of their departure time and desired state of charge, in such a way that they are compatible with the maximum PEV charging power. Furthermore, the aggregated charging session shall not require, over their time windows, more energy than the maximum output of the load area.

3.1.2.5 Decentralized solving procedure

The problem previously formalized is solved in a decentralised way taking advantage of the Lagrangian theory (in particular the duality theory [67]) and the specific form of the target function and constraints. For convenience of notation, as customary in the MPC literature, a vector is introduced to denote in a compact form each variable which is defined over the whole control horizon; in particular $\boldsymbol{p_r}(t) = \text{col}(p_r(t/t), p_r(t+1/t), \ldots, p_r(t+N-1/t))$ and $\boldsymbol{P}(t) = \text{col}(P(t/t), P(t+1/t), \ldots, P(t+N-1/t))$ will denote the r-th PEV and the load area power over the period respectively.

The Lagrangian function is introduced by combining the target function (3.25) and the power balance constraint (3.26) - the only one explicitly matching PEVs

and load area variables - as

$$\begin{aligned} L(\boldsymbol{p_r}(t),&\boldsymbol{P}(t),\boldsymbol{\lambda}(t)) = \\ &= \sum_{\tau\in T_t}\left\{\sum_{r\in R_t} U_r(p_r(\tau/t)) - C(P(\tau/t))\right\} + \\ &- \sum_{\tau\in T_t}\lambda(\tau/t)\left\{\sum_{r\in R_t} p_r(\tau/t) - P(\tau/t)\right\} \end{aligned} \tag{3.31}$$

where $\boldsymbol{\lambda}(t) = \mathrm{col}(\lambda(t/t), \lambda(t+1/t), \ldots, \lambda(t+N-1/t))$ is the vector of Lagrangian multipliers; as it will be clarified in the following, the multipliers represent an indicator of the energy price in the load area.

The dual problem is defined as

$$\min_{\boldsymbol{\lambda}(t)>0} D(\boldsymbol{\lambda}(t)) \tag{3.32}$$

where

$$D(\boldsymbol{\lambda}) = \max_{\boldsymbol{p_r}(t),\boldsymbol{P}(t)} L(\boldsymbol{p_r}(t),\boldsymbol{P}(t),\boldsymbol{\lambda}(t)), \tag{3.33}$$

subject to constraints (3.27) - (3.30).

The Lagrangian function can be decomposed as

$$L(\boldsymbol{p_r}(t),\boldsymbol{P}(t),\boldsymbol{\lambda}(t)) = \sum_{r\in R_t} f(\boldsymbol{p_r}(t),\boldsymbol{\lambda}(t)) + g(\boldsymbol{P}(t),\boldsymbol{\lambda}(t)) \tag{3.34}$$

where

$$f(\boldsymbol{p_r}(t),\boldsymbol{\lambda}(t)) = \sum_{\tau\in T_t}\{U_r(p_r(\tau/t)) - \lambda(\tau/t)p_r(\tau/t)\} \tag{3.35}$$

and

$$g(\boldsymbol{P}(t),\boldsymbol{\lambda}(t)) = \sum_{\tau\in T_t}\{\lambda(\tau/t)P(\tau/t) - C(P(\tau/t))\} \tag{3.36}$$

Taking advantage of this property the dual problem can be decomposed in subproblems, logically related to different agents, and solved iteratively. The generic *k-th* iteration of the procedure is as follows.

In the first step each PEV and the operator compute the respective optimal power, for a given value of multipliers $\boldsymbol{\lambda}_k(t)$. Each PEV solves the subproblem

$$\max_{\boldsymbol{p_r}(t)} f(\boldsymbol{p_r}(t),\boldsymbol{\lambda}_k(t)) \tag{3.37}$$

subject to constraints (3.27) - (3.29). This means finding, for a given $\boldsymbol{\lambda}_k(t)$, the optimal charging power $\boldsymbol{p_r}_k(t)$ over the time which maximizes the margin among utility and cost, while respecting technical constraints and charging preferences. Notice that, due to the assumption made on the utility function (3.23), the PEV subproblem is a convex optimization problem.

Similarly the operator solves the subproblem

$$\max_{\boldsymbol{P}(t)} g(\boldsymbol{P}(t), \boldsymbol{\lambda}_k(t)) \tag{3.38}$$

subject to constraint (3.30). Again, this means finding, for a given $\boldsymbol{\lambda}_k(t)$, the optimal power curve $\boldsymbol{P}_k(t)$ at the interface with the distribution grid which maximizes the margin among the benefit and cost, while keeping feasible operation of operator's equipment. As before, due to the properties of the utility function (3.24), the operator subproblem is convex.

In the second step of the procedure, once the powers $\boldsymbol{p_r}_k(t)$ and $\boldsymbol{P}_k(t)$ are known, the Lagrangian multipliers are updated following the anti-gradient of $D(\boldsymbol{\lambda})$. The updating rule is then

$$\boldsymbol{\lambda}_{k+1}(t) = \max(\boldsymbol{\lambda}_k(t) - \gamma \boldsymbol{\nabla D}_k, \boldsymbol{0}) \tag{3.39}$$

where

$$\boldsymbol{\nabla D} = \boldsymbol{P}_k(t) - \sum_{r \in R_t} \boldsymbol{p_r}_k(t) \tag{3.40}$$

and the step γ is chosen according to the Armijo's rule. Notice that $\boldsymbol{\lambda}_k(t)$ evolves according to the imbalance between the aggregated charging load and the power supply in the load area; specifically the values of the Lagrangian multipliers increase as the demand outbalance the supply and vice-versa, so that the multipliers can be interpreted as an indicator of the energy price in the load area.
The two-steps procedure is repeated using $\boldsymbol{\lambda}_{k+1}(t)$, until a k^* exists for which the exit condition

$$\|\boldsymbol{\nabla D}_{k^*}\| < \epsilon \tag{3.41}$$

is satisfied, for an arbitrary small positive real number ϵ. If (3.41) holds, the balance (3.26) between demand and supply is reached in practice, and the optimal solution of the dual problem is achieved. The point

$$(\boldsymbol{p_r}^*(t), \boldsymbol{P}^*(t), \boldsymbol{\lambda}^*(t)) = (\boldsymbol{p_r}_{k^*}(t), \boldsymbol{P^l}_{k^*}(t), \boldsymbol{P^s}_{k^*}(t), \boldsymbol{\lambda}_{k^*}(t))$$

represents the optimal control and price sequences over the control horizon, according to the boundary conditions characterizing the load area at current time t; consequently $(p_r(t), P(t), \boldsymbol{\lambda}(t)) = (p_r^*(t/t), P^*(t/t)), \boldsymbol{\lambda}^*(t/t))$ is the control and the price actually applied to the plant at current time t.

3.1.2.6 Simulation Results and Discussion

The proposed control algorithm has been validated at simulation level in order to provide a preliminary proof of concept. The simulation framework has been built in Matlab, leveraging Matlab built-in solver for the solution of agents' optimization problems; the simulation parameters are specified in Table 3.1, while the simulation scenarios are reported in Table 3.2 and 3.3. For simplicity, the desired final SOC has

been set to 90% for all the charging sessions, due to the fact that this value represents the bound beyond which the validity of model (3.28) becomes questionable.

Table 3.1: Simulation Parameters

Parameter	Value
Δt	$5min$
N	36
α, δ	0.5, 0.1
ϵ	0.1
$U(p)$	$\omega log(1+p)$
ω	15
ξ	0.05
p^{max}, p^{min}	$22kW, 0kW$
x^{max}	$24kWh$
P^{max}, P^{min}	$200kW, 0kW$

Table 3.2: Sim. I - Charging sessions

PEV ID	Start time	End Time	Initial SOC [%]
1	00:00	04:00	12.5
2	00:00	05:00	25
3	00:00	03:30	29
4	03:00	07:00	21

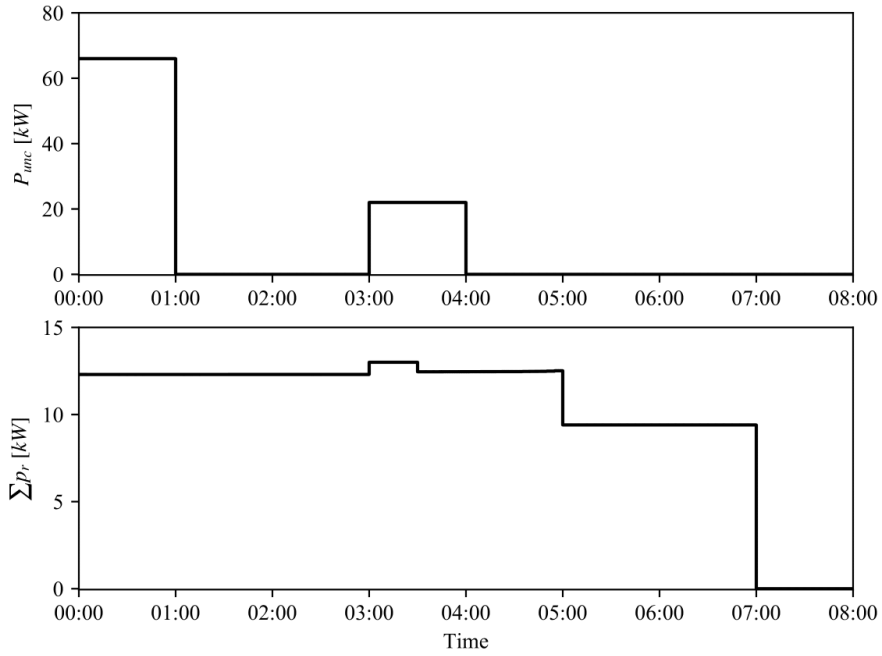

Figure 3.8: Sim. I - Aggregated charging power in the (a) uncontrolled and (b) controlled case.

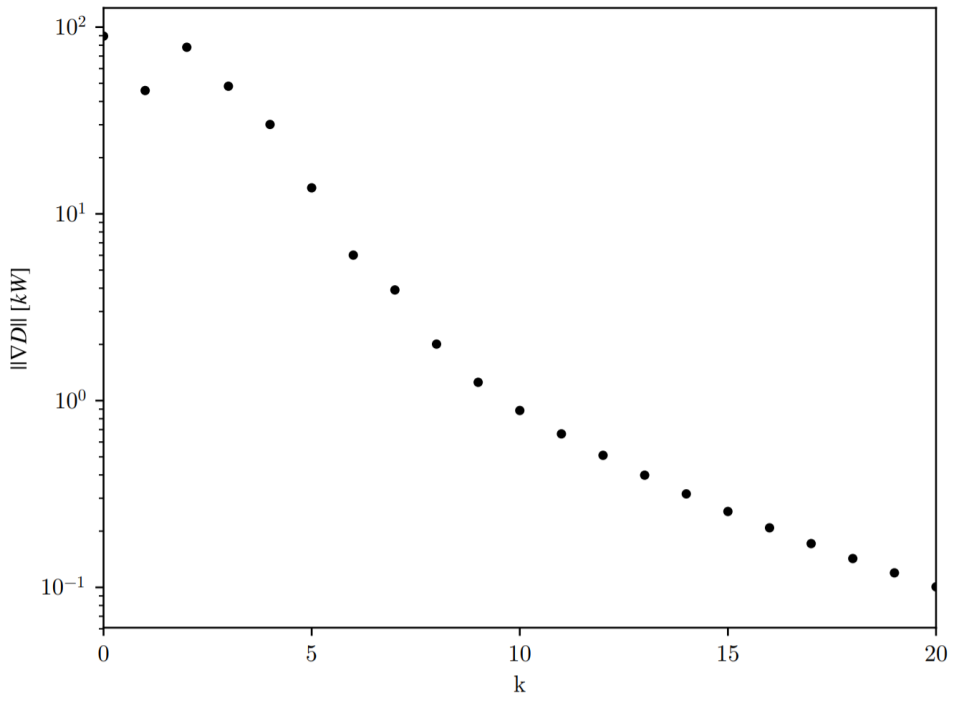

Figure 3.9: Sim. I - Evolution of $||\nabla D||$ for the optimization performed at 2:55.

The first simulation is intended to show how the algorithm works in a simplified scenario where it is straightforward to check for its effectiveness. Fig. 3.8 shows the aggregated charging power in the (a) uncontrolled case, in which the charging service is provided at rated power starting at the time of arrival, and in the (b) controlled one. It is immediate to see how the control distributes the charging power over the time in order to smooth the aggregated power profile. As far as concerns the decentralised optimization occurring at each iteration of the MPC scheme, Fig. 3.9 reports an example of the evolution of $||\nabla D||$ over the proposed decentralised optimization procedure: it is seen that $||\nabla D||$ has a fairly regular behaviour, and the convergence is achieved after 20 iterations of the procedure.

Table 3.3: Simulation 2 - Charging sessions

PEV ID	Start time	End Time	Initial SOC [%]
1	00:15	05:15	10
2	00:30	04:30	10
3	00:45	05:00	16
4	01:00	02:15	10
5	01:30	06:00	62
6	02:00	07:00	41
7	02:45	06:45	16
8	03:00	08:00	10
9	03:00	05:00	16
10	03:15	04:45	10
11	04:00	09:00	16
12	05:45	10:45	13
13	06:00	11:00	13
14	07:00	10:30	13
15	07:00	11:00	13
16	07:00	11:30	16
17	08:30	11:00	16
18	08:45	11:45	16
19	09:00	11:45	16
20	09:30	11:45	16

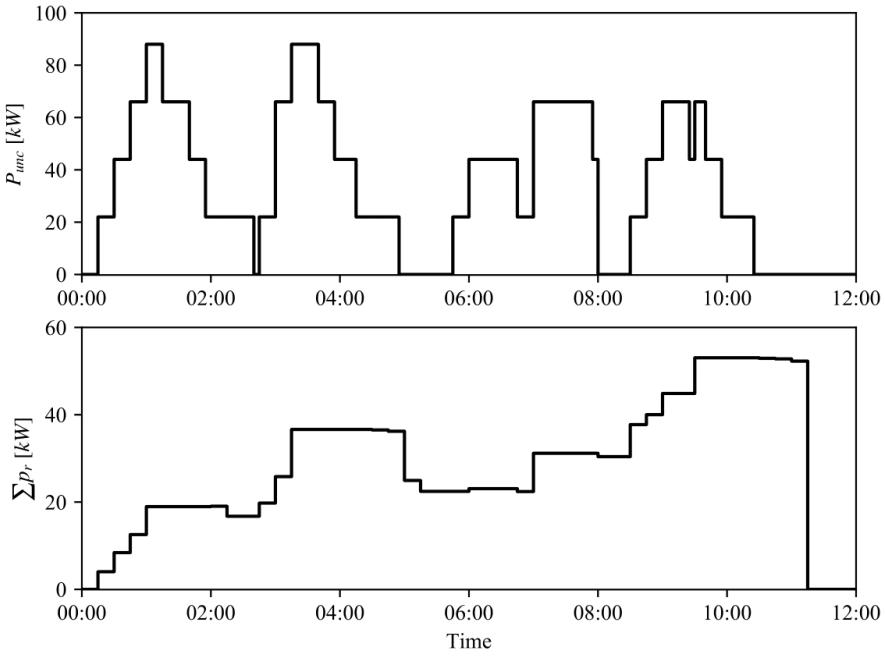

Figure 3.10: Sim. II - Aggregated charging power in the (a) uncontrolled and (b) controlled case.

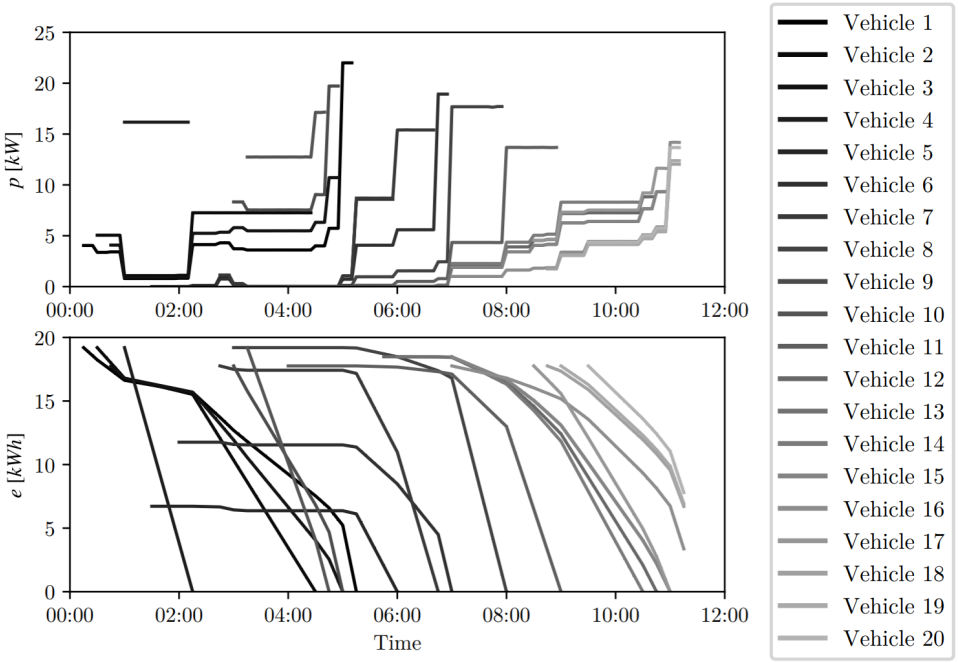

Figure 3.11: Sim. II - Evolution of (a) power and (b) SOC for each charging session.

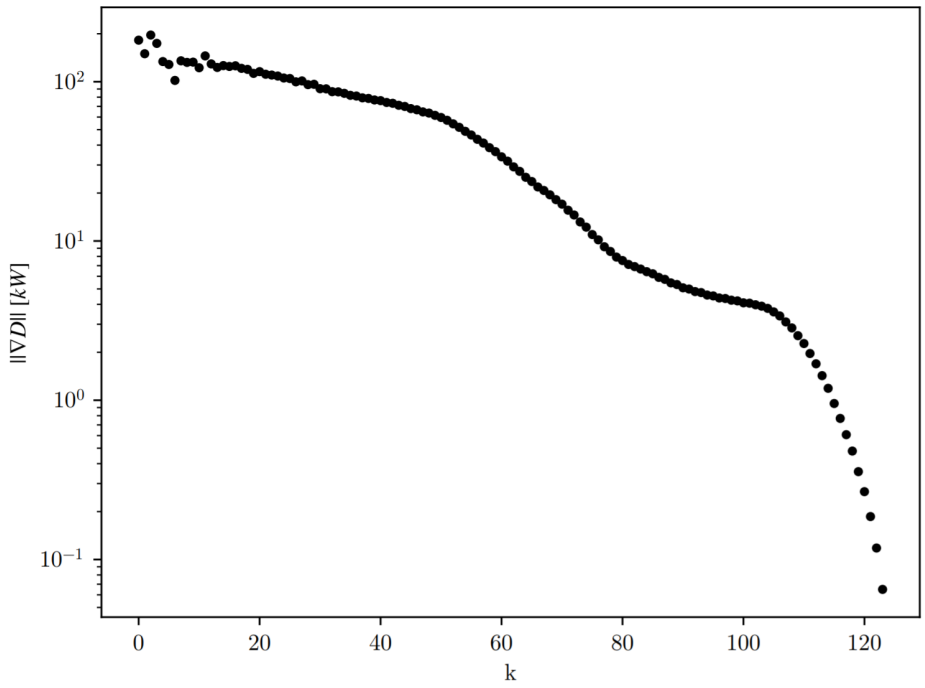

Figure 3.12: Sim. II - Evolution of $||\nabla D||$ for the optimization performed at 3:45.

Simulation II is characterized by a more complex and realistic scenario, in which the proposed control better show its potential. In absence of control, the charging requests produce a highly variable aggregated charging power characterized by peaks reaching approximately 90 kW (Fig. 3.10); the proposed control allows to significantly mitigate the variability of the aggregated power withdrawal while allowing to steer the SOC errors of all the charging sessions to zero (Fig. 3.11). Finally Fig. 3.12 reports the evolution of $||\nabla D||$ for the optimization procedure occurring at 3:45, a congested time in which 9 PEVs charge simultaneously. The convergence is achieved in approximately 120 iterations; though this value may appear quite high for an implementation of the method in a real system, it is important to remark that it is affected by the choice of ϵ and the sampling time; moreover, due to the low complexity of the optimization problem solved by each agent (with solving times in the range of a second or less), it can be concluded that the proposed method is compatible with a real time application characterized by the proposed sampling time.

3.1.2.7 Concluding remarks

In this work a real time decentralised control strategy for electric vehicles charging has been presented. The decentralised control mechanism is based on model predictive control methodology and Lagrangian decomposition of the optimization problem at its basis. The simulation results show the potential of the proposed approach, which can be implemented in practice in scenarios where the sampling time of the control action is in the typical range of power systems metering and scheduling applications. Possible directions for this work consider the integration of energy storage systems in the decentralised framework, the improvement of convergence performance and its theoretical validation.

3.1.3 Distributed MPC of Electric Vehicles Charging Service Area with Demand Side Management

The work presented in 3.1.2 is affected by different problems. First, from charging performance point of view the PEV's utility function does not well describe the desired preferences of the driver.

If the driver comes back before the defined time, the utility function (3.23) is not able to drive the SOC to a satisfactory value in function to the charging time, behaviour expected from the driver. Figure 3.11 shows that the vehicles are mainly charged during the last period of the charging sessions. This behaviour is also related to the formulation of the cost function associated to the power withdrawal from the grid.

The cost function (3.24) penalizes any power consumption, the first term of (3.24) can be seen as a cost on the tracking error on the 0 reference power. This formulations drive the system to utilize the minimum amount of power flattening the profile, but forcing on the long term a general reduction of the single charging sessions, slowing the charging.

The choice of the utility and cost functions are related to the decentralize solving procedure adopted in the previous work: to guarantee the convergence the functions that model the *social welfare* have to be: (i) continuous, (ii) monotonically increasing and (iii) strictly concave/convex.

Also, the decentralize solving procedure based on the duality concepts of Lagrangian theory [67] is sensitive to the parameter identification of the Armijo's rule, that in some case can deteriorate the convergence performances.

This work tries to overcome the above mentioned limitations. In this work, a reformulation of the open loop optimal control problem at the basis of MPC is provided. The optimization problem is modeled as a consensus with regularization optimization problem and solved by means of the decentralized Alternating Direction Method of Multipliers (ADMM). Simulations performed on a realistic test case show the potential of the proposed control approach and allow to provide a preliminary evaluation of the compatibility between the required computational effort and the application in real-time charging system.

Nomenclature

Table 3.4: Nomenclature

Symbols	Meaning
t	Current time
t_r^{dep}	Departure time of vehicle $r \in R_t$
T_t	Set of time instants in the control window
R_t	Set of charging PEVs at time t
p	PEV charging power
SOC	PEV state of charge
SOC^{ref}	Desired PEV state of charge
e	PEV state of charge error
ξ	PEV conversion losses
P	Scheduled aggregated charging power
P^{ref}	Reference aggregated charging power
E	Aggregated charging power tracking error
D	PEV cost function
C	Load area cost function
Δt	Sampling time
r, τ	Generic elements of sets R_t, T_t (subscript)
ρ	augmented lagrangian parameter
ϵ	ADMM tolerance

3.1.3.1 Introduction

Following the achievements of the 2020 climate and energy framework [68], the European Commission has established new challenging targets for 2030, with the objective of gradually decarbonizing the energy sector by moving away from fossil fuels [69]. In this context a key role is going to be played by plug-in electric vehicles (PEVs), provided that the aggregated power needed for charging is controlled to match power generation from renewables and keep feasible operation of electricity distribution grids [70, 71]. The problem of PEV charging control has been intensively investigated during the last decade: beyond the satisfaction of driver preferences for charging, typical requirements taken into account at network level involve voltage regulation [72, 73, 74], active power regulation [75, 76], minimization of power losses [77, 78], overload avoidance [79, 80, 81], balancing among charging power and local generation [82, 83, 84], etc. Several methodologies have been applied such as several forms of optimization [85, 86], learning techniques [87], model predictive control (MPC) [88, 89, 23, 37], etc.; among them MPC has been successfully field tested in the context of some EU research projects [90] and has been applied in pioneer production environments [91]. However the need of solving in real time the MPC inherent optimization problem raises concerns, especially when increasing the number and duration of simultaneous charging sessions. Though complexity can be partially

broken by clustering charging PEVs according to the electricity grid topology [44] and substations power rating, promising results are expected to come from the machinery of well established decentralized optimization techniques [92], using which a set of less challenging problems are solved in parallel and driven iteratively towards the optimal solution of the original centralized problem.

In this work an original application of the alternating direction method of multipliers (ADMM) to the problem of decentralized PEVs charging control, in presence of requirements concerning the regulation of the aggregated PEVs charging power and the respect of drivers' privacy [93] and charging preferences is proposed; the optimization problem is modelled at the basis of the MPC framework as a consensus with regularization optimization problem and the advantages of Alternating Direction Method of Multipliers (ADMM) are exploit in order to achieve an effective real time decentralized control implementable in practice in realistic charging scenarios. The proposed formulation reconsiders the control objectives characterizing the successfully field tested centralized formulation presented in [42] and [94], also taking into account some decentralized optimization concepts characterizing the preliminary work [95].

This work raises in the context of the EU research project 5G Solutions [96], which aims to show the effectiveness of the 5G communication technology in use cases defined over several application fields: in the context of smart grids, its low latency and high reliability are key features expected to allow real time decentralized PEVs charging control techniques characterized by a potentially large number of communications among the optimization agents.

The remainder of the work is organized as follows. Section 3.1.3.2 outlines the charging scenario and the control objectives. Section 3.1.3.3 presents the problem formulation. Section 3.1.3.4 at first recalls the main concepts and results at the basis of ADMM and consensus with regularization optimization problem, and then shows how the proposed formulation can be put in this latter form. Section 3.1.3.5 is dedicated to the presentation of simulations and the discussion of the related results. In section 3.1.3.6 the concluding remarks are drawn together with the expected future developments.

3.1.3.2 Scenario and Control Objectives

The reference scenario considers a load area, namely a node of the electricity distribution grid hosting a set of charging stations available for the provisioning of the charging service; all the charging stations share the same point of connection to the grid (typically a MV/LV substation). A reference charging power is assigned to the load area, representing a target load curve optimizing some operation criteria; this reference may be in principle time-dependent and subject to modifications over the time through short-term notification (Demand Side Management (DSM) signal). Each driver connecting his/her PEV to a charging station is expected to declare the initial and desired state of charge (SOC) and the time of departure from the charging station.

The control system is in charge of computing in real time the charging power setpoints that each PEV has to actuate during its charging session; in this work consider the following control objectives are considered:

1. *Power tracking.* The aggregated charging power in the load area has to track the time-dependent reference.

2. *Charging preferences.* Each PEV has to reach the desired SOC level no later than the departure time.

3. *Privacy.* The charging power setpoint has to be computed locally (i.e. at the level of each PEV) without sharing PEV parameters and driver's charging preferences with external agents.

For a detailed explanation of the reference scenario and related use cases the reader can refer to the previous work [42].

3.1.3.3 Control Problem Formalization

The proposed control is based on the well known MPC methodology [64]. At each sampling time a measure (or at least an estimation) of the SOC is taken from all connected PEVs; then, a proper open loop optimal control problem is solved, which provides an optimal control sequence over the control window for each PEV, whose the first sample is actually applied to the plant. The procedure is then repeated at the upcoming sampling time to realize a real time closed loop control framework.

In the following the open loop optimal control problem is defined at the basis of the MPC framework. In what follows t denotes the current time, $T_t = \{t, t+1, \ldots, t+H-1\}$ is the set of discrete time instants within the control window starting from t, τ the generic time instant within the set. The set R_t is introduced to denote the PEVs connected to the charging stations at t and consequently being part of the control problem.

The open loop optimal control problem is built taking into account the requirements reported in Section II, together with technical limitations and constraints related both to the PEVs and the load area. In order to model requirements 1 and 2 a target function of the following form is considered

$$J = \sum_{\tau \in T_t} \left[\sum_{r \in R_t} D_r(e_r(\tau/t)) + C(E(\tau/t)) \right] \tag{3.42}$$

in which D_r and C are proper functions accounting for performances at PEVs and load area levels respectively. As far as concerns each PEV, a function D_r is introduced to model the disutility resulting from the deviation of the current state of charge from the desired one. Defining the SOC error at τ as $e_r(\tau/t) = SOC_r(\tau/t) - SOC_r^{ref}$, the function D_r is taken as

$$D_r(e_r(\tau/t)) = \alpha_r e_r^2(\tau/t) \qquad \forall \tau \in T_t \tag{3.43}$$

where α_r represents a weight used to balance the charging preference requirements among different agents.

As far as concerns the load area, the function C is introduced to penalize the deviation of the aggregated charging power with respect to the reference power. Defining the tracking error at τ as $E(\tau/t) = P(\tau/t) - P^{ref}(\tau/t)$, the function C is taken as

$$C(E(\tau/t)) = \beta(\tau/t)E(\tau/t)^2 \qquad \forall \tau \in T_t \tag{3.44}$$

where $\beta(\tau/t)$ is a weight used to enforce the tracking at time instants near to the current time t. Combining the cost items (3.43) and (3.44) in the target function (3.42) and minimizing it introduces a trade-off between two competing requirements: the one of charging the PEVs as fast as possible and the one of smoothing the aggregated charging power so that it tracks a target curve which guarantees proper operation of the load area over the time. The connection among the above mentioned competing terms is given by the power balance in the load area and the SOC error dynamics. The former is expressed by the equality constraint

$$\sum_{r \in R_t} p_r(\tau/t) = P(\tau/t) \ , \forall \tau \in T_t \tag{3.45}$$

while the latter is modeled by the linear discrete time invariant system

$$\begin{aligned} &e_r(\tau+1/t) = e_r(\tau/t) - (1-\xi_r)\Delta t \, p_r(\tau/t), \forall \tau \in T_t, \forall r \in R_t \\ &e_r(t/t) = e_r(t), \forall r \in R_t \end{aligned} \tag{3.46}$$

where ξ_r is a parameter accounting for the conversion losses, Δt represents the sampling time and the intial SOC error $e_r(t)$ is the measure taken from the PEV at t. In order to enforce the satisfaction of charging preferences, the hard constraints

$$e_r(\tau/t) = 0 \ , \forall r \in R_t \ , \forall \tau \geq t_r^{dep} \tag{3.47}$$

is included in the problem formalization, where t_r^{dep} represents the departure time of the r-th vehicle.

Finally, other constraints come from the technical limitations on the PEV charging power and the aggregated charging power in the load area. The following box contraints are in this work considered

$$p_r^{min} \leq p_r(\tau/t) \leq p_r^{max} \ , \forall r \in R_t \ , \forall \tau \in T_t \tag{3.48}$$

$$P^{min} \leq P(\tau/t) \leq P^{max} \ , \forall \tau \in T_t. \tag{3.49}$$

In the light of the above, taking into account control objective 3 and introducing for notational convenience the vectors $p_r = \text{col}(p_r(\tau/t), p_r(\tau + 1/t), ..., p_r(\tau + H - 1/t))$, $P = \text{col}(P(\tau/t), P(\tau+1/t), ..., P(\tau+H-1/t))$, $P^{ref} = \text{col}(P^{ref}(\tau/t), P^{ref}(\tau+1/t), ..., P^{ref}(\tau + H - 1/t))$, the open loop optimal control problem at the basis of the MPC scheme can be stated as follow.

Problem 3.2. *For a given set R_t of PEVs, each one characterized by a pair of charging preferences (SOC^{ref}, t^{dep}), connected to a load area having an aggregated charging power reference P^{ref}, find a decentralized strategy allowing to compute the optimal values of the control sequences $p_r, \forall r \in R_t$, and P which minimize the target function (3.42), such that constraints (3.45), (3.46), (3.47), (3.48), (3.49) are satisfied.*

3.1.3.4 Decentralized solving procedure

In this section, theoretical background of ADMM are recalled and a discussion on how the open loop optimal control problem can be handled in order to solve it by means of a decentralized approach is provided.

Centralized ADMM The ADMM is an iterative algorithm which solves optimization problems blending the advantages coming from the decomposability of the dual ascent algorithm and the convergence properties of the method of multipliers [92]. Consider an optimization problem of the form

$$\begin{aligned} \min_{x,z} \quad & f(x) + g(z) \\ \text{s.t.} \quad & Ax + Bz = c \end{aligned} \tag{3.50}$$

where $x \in \mathbb{R}^n$, $z \in \mathbb{R}^m$, $f : \mathbb{R}^n \to \mathbb{R} \cup \{+\infty\}$, $g : \mathbb{R}^m \to \mathbb{R} \cup \{+\infty\}$, $A \in \mathbb{R}^{q \times n}$, $B \in \mathbb{R}^{q \times m}$ and $c \in \mathbb{R}^q$. Define the augmented Lagrangian as

$$L_\rho(x, z, \lambda) = L_0(x, z, \lambda) + (\rho/2)||Ax + Bz - c||_2^2 \tag{3.51}$$

where ρ is a positive tuning parameter and

$$L_0(x, z, \lambda) = f(x) + g(z) + \lambda^T(Ax + Bz - c) \tag{3.52}$$

is the unaugmented Lagrangian related to problem (3.50). Then consider the following assumptions.

Assumption 3.1. The functions $f : \mathbb{R}^n \to \mathbb{R} \cup \{+\infty\}$ and $g : \mathbb{R}^m \to \mathbb{R} \cup \{+\infty\}$ are closed, proper, and convex.

Assumption 3.2. The unaugmented Lagrangian L_0 has a saddle point.

Assuming assumptions 3.1 and 3.2 hold, the ADMM algorithm finds the optimal solution through the following iterations:

$$\begin{aligned} x^{k+1} &:= \arg\min_x \; L_\rho(x, \lambda^k, z^k) \\ z^{k+1} &:= \arg\min_z \; L_\rho(x^{k+1}, \lambda^k, z) \\ \lambda^{k+1} &:= \lambda^k + \; \rho(Ax^{k+1} + Bz^{k+1} - c). \end{aligned} \tag{3.53}$$

The procedure is iterated until when, for some k, the so called primal and dual residuals respectively satisfy the conditions

$$\begin{aligned} ||Ax^{k+1} + Bz^{k+1} - c||_2^2 < \epsilon \\ ||\rho A^T B(z^{k+1} - z^k)||_2^2 < \epsilon \end{aligned} \tag{3.54}$$

where the parameter ϵ is a proper tolerance value. Notice that both x-update and z-update tasks require the knowledge of x and z at previous or current iteration, so that this procedure can not be executed in parallel by independent agents.

Distributed ADMM In some cases the ADMM algorithm can be specialized to be executed in a decentralized way. Pose $x = \text{col}(x_1, x_2, ..., x_N)$, where the components $x_i \in \mathbb{R}^{n_i}$ take the name of local variables, and suppose that the function $f(x)$ can be expressed as a sum of N independent functions $f_i(x_i)$. Consider the problem

$$\begin{aligned} \min_{x,z,\widetilde{z}} \quad & \sum_{i}^{N} f_i(x_i) + g(z) \\ \text{s.t.} \quad & x_i - \widetilde{z}_i = 0, \quad i = 1 \dots N \end{aligned} \tag{3.55}$$

in which the auxiliary variables, components of $\widetilde{z} = \text{col}(\widetilde{z}_1, \widetilde{z}_2, ..., \widetilde{z}_N)$, are introduced to replace the local variables in the linear constraint linking x and z. This problem is known as consensus with regularization optimization problem. Considering the augmented Lagrangian of problem (3.55), the machinery of ADMM brings to the definition of the iteration scheme

$$\begin{aligned} x_i^{k+1} &:= \underset{x_i}{\arg\min} \;\; f_i(x_i) + \lambda_i^{kT} x_i + (\rho/2)||x_i - \widetilde{z}_i^k||_2^2 \\ (z^{k+1}, \widetilde{z}^{k+1}) &:= \underset{z,\widetilde{z}}{\arg\min} \;\; g(z) + \sum_{i=1}^{N}(-\lambda_i^{kT}\widetilde{z}_i + (\rho/2)||x_i^{k+1} - \widetilde{z}_i||_2^2) \\ \lambda_i^{k+1} &:= \lambda_i^k + \;\; \rho(x_i^{k+1} - \widetilde{z}_i^{k+1}) \end{aligned} \tag{3.56}$$

which converges to the optimal solution of (3.55) under the previously mentioned Assumptions 1 and 2.

Equations (3.56) define a decentralized ADMM algorithm able to be executed in parallel by N local agents each one optimizing a specific local objective $f_i(x_i)$, one global agent optimizing the regularization term $g(z)$, driven by the updates of the Lagrangian multipliers λ_i.

Open loop control problem decomposition It is straightforward to realize how the machinery of decentralized ADMM can be applied to the open loop optimal control problem defined in section III. Remembering the definition of tracking error and using equation (3.46), the target function (3.42) and the power balance constraint (3.45) can be rewritten in terms of the PEVs charging power and the aggregated charging power to define a problem of the form (3.50), in which

$x = p = \text{col}(p_1, p_2, ..., p_N)$, $N = |R_t|$ and $z = P$. Further the problem (3.50) is enriched with constraints (3.47), (3.48) and (3.49) affecting separately the behaviour of the PEVs and the load area. Additionally, considering that the target function is separable in the components p_r, by introducing the auxiliary variables $\widetilde{z}_i \in \mathbb{R}^{n_i}$, where $n_i = H$, the open loop optimal control problem takes the form (3.55), in which the global variable z is linked to the auxiliary variables through the power balance constraint $z = \sum_{i=1}^{N} \widetilde{z}_i$.

In the light of the above, the decentralized ADMM procedure (3.56) can be applied to the problem at study, provided that the x_i-update and the z-update are performed taking into account the respective additional constraints. Further, notice that the x_i-update is influenced by local parameters and the auxiliary variable $\widetilde{z}_i$, which embeds the behaviour of the other agents, without giving information about them.

3.1.3.5 Simulation Results

In order to validate the proposed problem formulation and solving procedure, two simulations have been performed. The control system has been set to work with a sampling time $\Delta t = 5$ minutes over a control window of 3 hours (36 sampling periods); the weight of the SOC error cost appearing in target function (3.42) has been set to $\alpha = 0.3$, while the weight of the tracking error cost has been chosen as the function $\beta(\tau/t) = 0.6/(\tau - t + 1)$. The augmented Lagrangian parameter and the tolerance of the ADMM algorithm have been set to $\rho = 1$ and $\epsilon = 0.001$. All the PEVs have a battery capacity $SOC^{max} = 24$ kWh, conversion losses parameter $\xi = 0.1$, minimum and maximum charging power $p^{min} = 0$ kW and $p^{max} = 22kW$. The minimum and maximum aggregated charging power in the load area are $P^{min} = 0$ kW and $P^{max} = 200kW$. The simulations have been performed using Julia 1.0.5 as simulation environment and Gurobi 8.1.1. as optimization solver, running on an Intel®Core™i7-8565U, 1.80 GHz processor. Though the proposed control is decentralized, the simulations are performed on the same processor, in order to assess the computational effort of the control in absence of communications latency among optimization agents.

Table 3.5: Charging sessions

PEV ID	Initial SOC [%]	Start Time	End Time
1	11.46%	00:30	03:10
2	22.92%	00:30	02:45
3	26.58%	00:30	02:50
4	19.25%	02:10	05:30
5	16.67%	02:10	04:40
6	19.25%	02:25	05:05
7	31.67%	02:55	05:35
8	8.75%	04:25	07:05
9	30.42%	04:50	08:10
10	19.25%	05:00	08:35
11	50,00%	06:25	08:50
12	35.83%	06:55	09:30
13	26.58%	07:05	10:40
14	0,00%	07:55	12:30
15	8.75%	08:50	11:20
16	19.25%	09:10	12:40
17	58.33%	09:35	13:45
18	8.33%	10:50	13:25
19	8.33%	11:40	15:25
20	11.46%	12:30	15:35

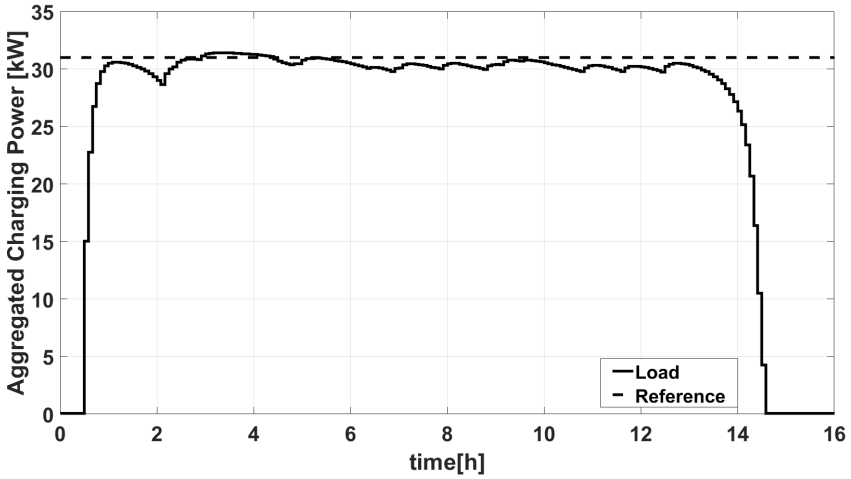

Figure 3.13: Sim. I - Aggregated load (continuous line), reference aggregated load (dashed line).

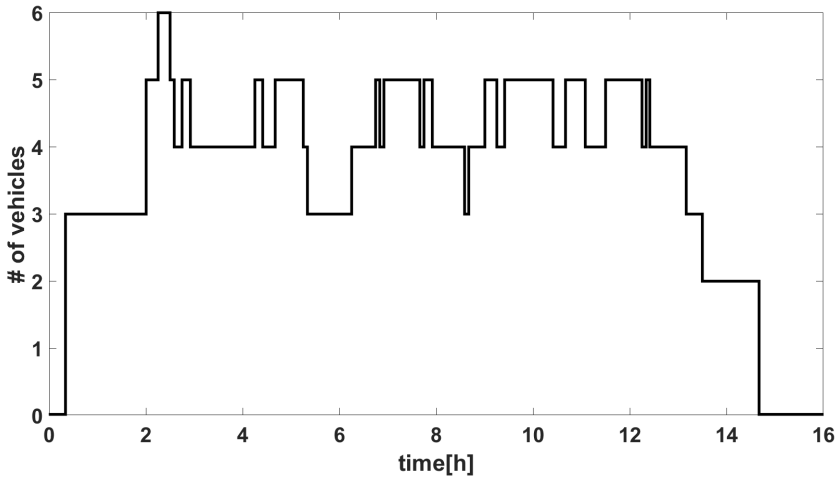

Figure 3.14: Sim. I - Number of connected PEVs over the time.

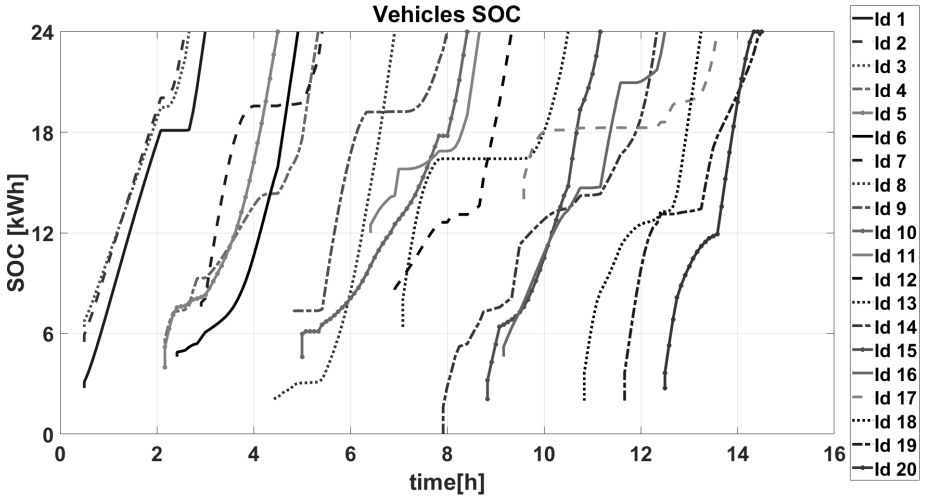

Figure 3.15: Sim. I - Evolution of the PEVs state of charge.

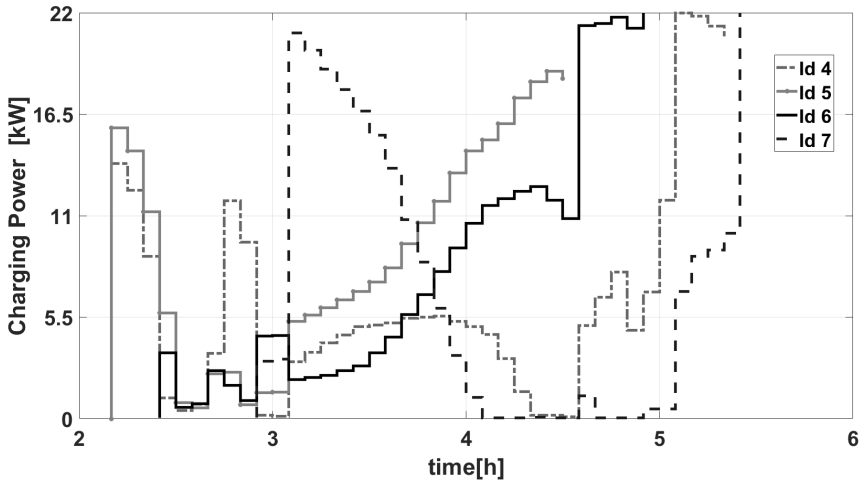

Figure 3.16: Sim. I - PEVs charging power, selection of 4 vehicles.

Simulation I The first simulation is based on the sequence of charging sessions reported in Table 3.5; all the session requests are characterized by a 100 % of desired SOC level. A flat reference power of 31.5 kW is assigned to the load area. As shown in Fig. 3.13 the proposed decentralized control allows to satisfy the tracking requirement pretty well; once reached the steady-state, the maximum tracking error is 7% of the reference power. The control properly manages the fluctuations in the number of connected PEVs (Fig. 3.14), smoothing the aggregated charging power. A careful comparison of Fig. 3.13 and 3.14 reveals that degradated tracking performances are expected at times when there is not sufficient request of power in the load area; consequently, the application in a real system requires to properly choose the power reference based on hystorical data, or to properly modify it over the time so that it can be actually tracked by the control system.

Fig. 3.15 shows the evolution of SOC over the time for all PEVs. All the charging preferences are satisfied in terms of desired SOC at the departure time. Fig. 3.16 reports the charging power schedules of 4 charging sessions taking place simultaneously. It is interesting to see that, though PEVs do not share information about preferences among them, they collaborate changing their own controls over the time so that the charging preferences of all PEVs in the cluster are met. See for example how PEV 7 changes its schedule at time 03:05 to let PEVs 5 and 6 complete the charging session before their departure time.

Looking at the ADMM performances, Fig. 3.17 reports the number of iterations needed to find the solution of the open loop optimal control problem at each sampling instant. It is worth noting that large peaks in the number of iterations arise at times when a new charging session becomes part of the optimization problem. Looking at the evolution of the primal and dual residual over the iterations, for the worst case occuring at 08:00 (Fig. 3.18), it can be noticed that relaxing the tolerance to 0.01 would imply the algorithm to converge approximately within 20 iterations.

Finally it is interesting to see how the chosen sampling time affects the convergence performances of the algorithm in terms of needed iterations and related computation time, neglecting the latency of communications among the optimization agents: Fig. 3.19, related to the first nontrivial optimization occurring at 00:30, provides a realistic indication about the minimum sampling time that can be used in a real time application of the proposed control scheme, and represents a benchmark for assessing the impact of communications latency on the control system performances.

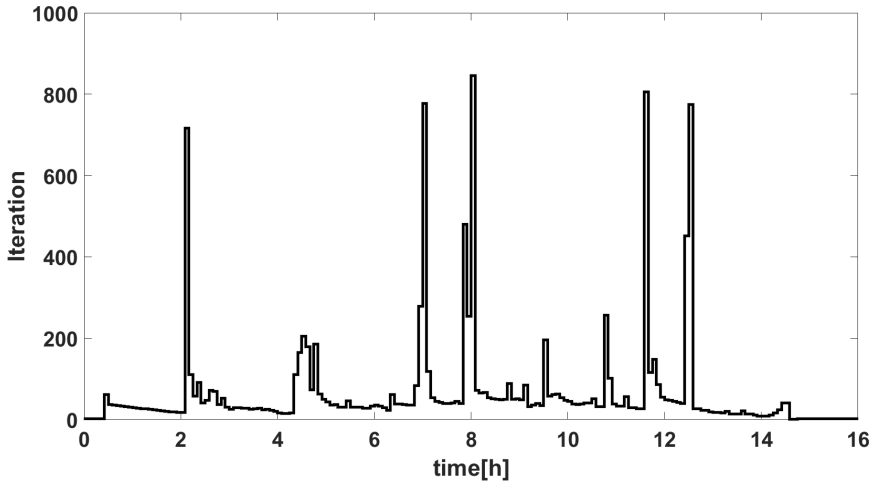

Figure 3.17: Sim. I - Number of iterations needed for convergence.

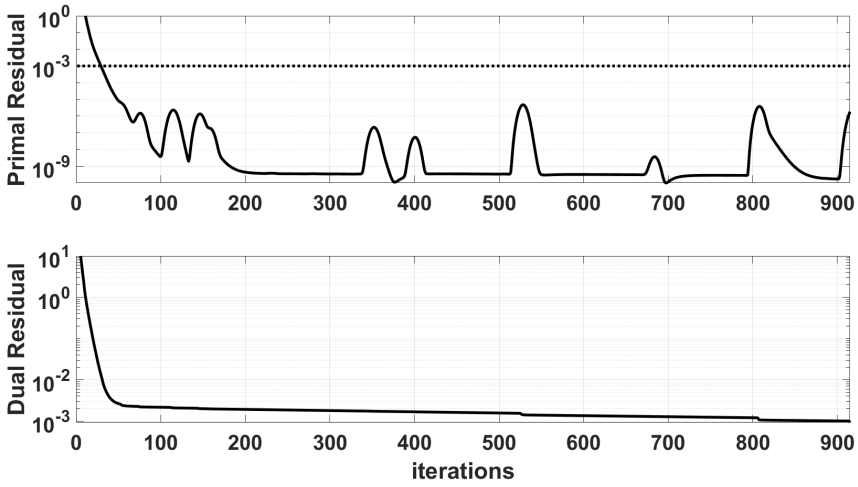

Figure 3.18: Sim. I - Evolution of primal and dual residuals for the optimization performed at 08:00.

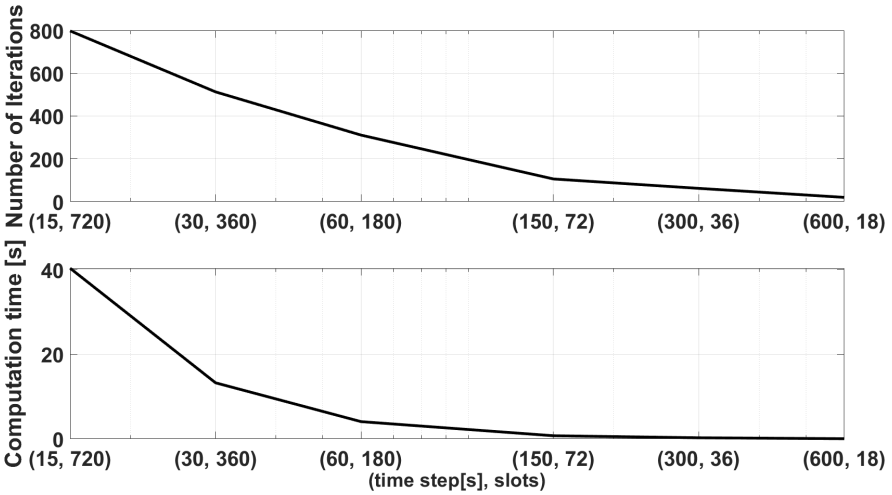

Figure 3.19: Sim. I - Number of iterations needed for convergence and computation time versus sampling time, for the optimization performed at 00:30.

Simulation II The second simulation is aimed at testing the ability of the control system to react to a short-term modification of the load area reference power (DSM signal); examples of application in a real scenario are the provisioning of a power balancing service to the network operator and the reaction to an update in the forecast of power generation from renewable energy sources. To this purpose the same test case characterizing simulation 1 is reconsidered and a DSM signal in sent to the controller notifyng that the reference power is modified starting from 04:00 to gradually relaxing the aggregated charging power to 22 kW over a 6 hours temporal window. Fig. 3.20 shows the aggregated schedule which is actually realized at the end of the simulation period: the control system continues to guarantee good tracking performances (9% of tracking error), while still guaranteeing proper evolution of PEVs' SOC towards the desired SOC.

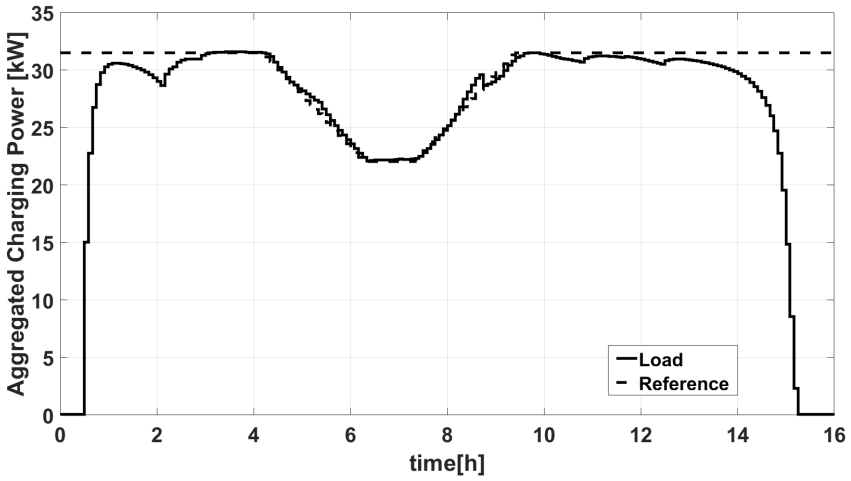

Figure 3.20: Sim. II - Aggregated load (continuous line), reference aggregated load (dashed line).

3.1.3.6 Concluding remarks

In this work a MPC based PEVs charging control scheme has been presented. The open loop optimal control problem at the basis of MPC has been modeled as a consesus with regularization optimization problem and solved by means of a decentralized ADMM algorithm. The proposed approach allows to jointly meet control requirements at load area level (reference charging power tracking) and at PEVs level (charging preferences and privacy). The computational effort related to the decentralized optimization algorithm has been preliminary assessed in terms of number of needed iterations to reach optimality and computation time, assuming zero communication latency among optimization agents. As a result, this study provides a proof of concept about the potential of the proposed control approach and a preliminary evaluation of the computational effort; future works will consider additional requirements (according to the IEC 61851 and ISO 15118 international standards) and the impact assessment of communications reliability and latency on the control system performances, as a result of the design and demonstration activities carried out in the context of the EU 5G Solutions research project.

3.1.4 Smart Charging System: architecture, integration with telecommunication system and compliance with industrial standards

The work presented in section 3.1.3 has provided a prof of concept on the use of PEVs for the network services provisioning. The work has highlighted two main aspects:

- the feasibility of considering a charging area as an aggregated load that is able to adapt the charging sessions in the function of network requirements, the base concept of the network services. The ability of adapting the aggregated power withdrawal enables actors like DSOs and Charging Point Operators (CPOs) to become buyers and sellers of services for the distribution network;
- the necessity, in case of distributed control computation strategy, of a fast and reliable communication.

Regarding the communication aspect, 5G infrastructure can be used for reliable real time scheduling of charging sessions: 5G capabilities, as the Ultra Reliable Low Latency Communications (URLLC) and massive Machine Type Communications (mMTC) are suitable for providing fast reschedule in case of network necessity, as an overload or contractual arrangements on the number of simultaneous charging sessions, or in case of electric power generated from renewable suddenly falls short of the predictions and so on.

Currently, charging platforms performing smart charging tasks leverage centralized computation schemes working at the level of charging infrastructure back-end. In this section, in relation to the work 3.1.3 a decentralized control scheme will be investigated and tested by using different communication technologies and a 5G like infrastructure. In this way, the computational effort will be distributed among session agents communicating with each other through 5G communications.

3.1.4.1 Introduction

Currently the charging stations used to charge plug-in electric vehicles are connected to the charging infrastructure operator back-end through mobile communications, mainly 3G technology. The reason for this technical choice mainly lies in the distributed nature of such an infrastructure. On the one hand, the access to the internet through whatever form of wired connection would imply dedicated civil works for installation of each charging station, resulting in additional costs and a slow growth of the charging infrastructure. Further, the idea of relaying on a subset of charging stations to establish a WiFi connection to the others is generally not effective for public large scale installations, due to the dispersed nature of the charging stations in the electricity distribution grid. Consequently, mobile communications are the most used solutions for the deployment of the charging infrastructure.

The computation of the smart charging setpoint is typically performed at the level of the back-end, based on proper discrete time centralized control and optim-

ization algorithms [42]. In this regard a fundamental role is played by the sampling time characterizing the measurement, computation and actuation chain. Indeed, the smaller the sampling time, the higher the granularity and consequently the effectiveness of the control, with positive consequences on the business opportunities.

The performances of the control chain are naturally affected by the sensors and actuators dynamics, but a really critical point is the computation of control. Computational complexity typically depends on a number of factors, including the sampling time, the number of controlled charging sessions and the vehicle's dwelling time. A fundamental requirement to achieve a real time control is to compute the charging power setpoints within the time interval established by the sampling time, so that it can be actuated at the beginning of the upcoming sampling period.

In order to improve the operation of the smart charging infrastructure, a promising solution may be the shift of the control strategy from a centralized approach to a decentralized one.

This is the reason why a high reliable and low latency communication technology is needed in order to quickly compute the charging setpoints (reducing the time wasted in the communication process needed at each iteration) and potentially let the whole decentralized control framework to work with smaller sampling times with respect to the centralized one. In summary, using 5G technology is expected to guarantee high reliability, very low communication latency and, consequently, enable a low sampling time control framework.

This section is devoted to analyze aspects related to the smart charging not covered by the previous works. The previous works were centered on algorithmic aspects, without spent particular attention on the other components that build the smart charging services, as the control architecture, the communications, the presence of limitation imposed by technical aspects and industrial standards.

3.1.4.2 Smart Charging Architecture

The fast-growing of electric vehicles market introduces new challenges in the management of energy sources to ensure at the same time charging performances, the profitability of the Charging Point Operator and security in terms of grid operations. The 5G technologies, in this scenario, can provide significant improvements of computational capabilities exploiting the property of Ultra Reliable Low Latency Communications (URLLC) that allows to demand and distribute computations of complex control algorithms to the devices that want to benefit of the smart charging service and at the same time allows to breakdown the management of the electrical vehicles overall infrastructure, increasing the competitiveness. In what follow a will be proposed a control architecture that exploits the presence of 5G technology communication and is adapt to the implementation of the distributed smart charging algorithm presented in 3.1.3. The architecture is composed of the following operational blocks and entities:

- The 5G block, that represents the 5G infrastructure;

- Transmission System Operator, that is an external part, has the capabilities to send dispatching orders that can modify the operativity conditions;
- The Charging Point Operator boots up the charging sessions and activates the sequence of actions needed to computing the charging schedules. The Charging Point Operator (CPO) Layer contains two main elements:
  - the E-Mobility back-end, that has a central role in the communication between the different layers. In this block there are the interfaces and communication protocols needed to the interaction between the TSO, Load Area and Control Service Provider (CSP). The E-mobility back-end is in charge of:
    * handle new charging session and notify them to the CSP;
    * collect measurements from the Load Area and forward them to the CSP for the computation of the charging schedulings;
    * accept and put into effect the charging session schedules coming from the CSP;
  - The Load Area hosts the controllable nodes such as Charging Station and Electric Vehicles. Charging Station is the CPO hardware capable of charging an Electric Vehicle according to IEC 61851 and ISO 15118 standards. The Load Area is in charge of:
    * get the charging schedules coming from the E-Mobility Platform;
    * actuate the charging schedules on the electric vehicles;
    * provide to the E-Mobility Platform the power measurements.
- The Control Service Provider offers the service of controlling the flexible loads in a distributed fashion. The CSP layer is composed by two different blocks, the CSP Back-End, that contains what in the architecture is called Master Control Agent and the distributed components, identified below by Local Control Agents.
  - Master Control Agent has many roles it is in charge of managing and coordinating Local Control Agents, it executes part of the schedulings computation (together with the Local Controllers), but it also works as interface with the CPO Layer in details:
    * the Master Control Agent communicates to the E-Mobility Platform in order to:
      · notify the starting of new Charging Sessions;
      · collect and manage the electrical measurements and operativity conditions;
      · send Schedulings for the Charging Stations;
    * the Master Control Agent interacts with the Local Control Agents in order to manage the distributed computational phase, in details:

  - notifies the charging request, so enables the Local Control Agents to take part to the computation;
  - sends the information needed for the computation, in this architecture identified by the arrow Measurements;
  - continuously interacts with them exchanging control signalling during the scheduling computation loop;
  - the Master Control Agent, as mentioned before, contributes also in the computation of the charging schedule;

- Local Control Agents are in charge of computing the Schedulings in a distributed way. A Local Control Agent communicates only with the Master Control Agent and it is designed to:
  - receive charging requests and measurements from the Master Control Agent;
  - have computational capability in order to compute the scheduling;
  - interact with the Master Control Agent through what in the architecture is called Control Signalling. This exchange of information is needed to the distributed computation of the Schedulings.

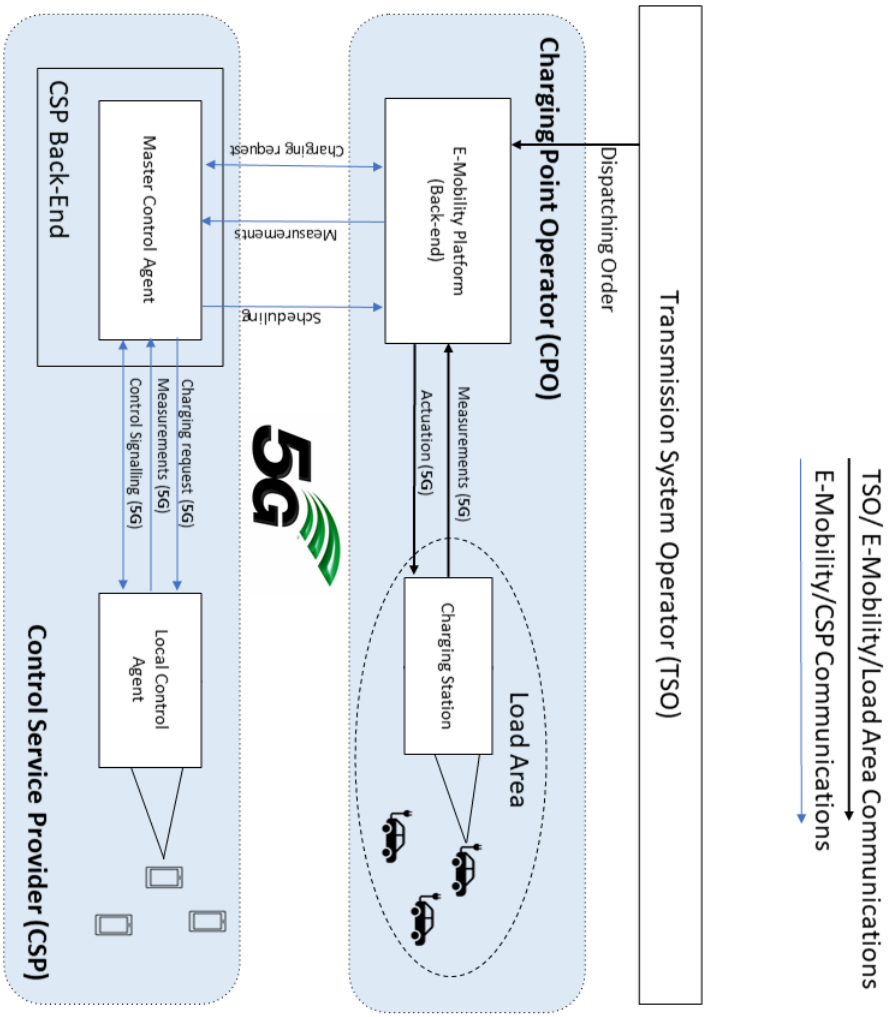

Figure 3.21: Control architecture for decentralized smart charging using 5G technology

When a user (identified by a the Local Control Agent hosted in the smartphone) asks for a new charging session, the request is sent to the Master Control Agent, which notifies the request to the E-Mobility Platform; this request triggers a set of communications between the Local Control Agents and the Master Control Agent for the acquisition of needed control information and for initialization of a set of computations. The computation phase requires a lot of fast and reliable communications between Master and Local agents; at the end of the computation the schedule is sent back to the E-Mobility Platform that will actuate the power setpoints. Similar actions are repeated iteratively during all the charging sessions to control and adjust the charging schedule to the eventually new boundary conditions given by the TSO or in general to compensate for the inevitable uncertainties in the system.

3.1.4.3 Integration with communication system

In this section, the smart charging algorithm presented in section 3.1.3 is studied considering the integration with the architecture presented in 3.1.4.2 and telecommunication system. In this section the focus is on the CSP layer. Master and Local Control Agents implement the iterative scheme (3.56) where local control problems are solved by Local Control Agents and the regularization problem is solved by the Master Control Agent. What will be shown in the next paragraphs provide an analysis on the importance of communication quality for the efficient computation of the charging set points. In section 3.1.3 were performed simulations emulating the distributed nature of the computation algorithm. This simulations are valid to test the main idea beneath it, but hide the important influence of telecommunication in the whole process. To understand the influence of the communication system, without the availability of 5G RAN, 5G technology was replaced with fiber technology. To understand the influence of the communication time, experiment were performed using a 4G commercial network.

The setup of the experiment considers two PCs, both connected to the same 4G smartphone (one through Wifi Hotspot and one through Tethering USB), that run 3 instances of the local control agent and 1 instance each of the local control agent proxy. The master control agent, instead, runs in the 5G Multi-access Edge Computing (MEC) server in Turin. The PCs that host the Local Control Agents are connected to the 5G MEC server through a Virtual Private Network (VPN).

In what follows, representative simulations will be shown to highlight the main results. Tests have been be performed considering a load area hosting 3 charging stations, the weight of the SOC error cost appearing in target function has been set to $\alpha = 0.3$, while the weight of the tracking error cost has been chosen as the function $\beta(\tau/t) = 0.6/(\tau - t + 1)$. The augmented Lagrangian parameter and the tolerance of the ADMM algorithm have been set to $\rho = 1$ and $\epsilon = 0.01$. All the PEVs have a battery capacity $SOC^{max} = 24kWh$, conversion losses parameter $\xi = 0.1$, minimum and maximum charging power $p^{min} = 0kW$ and $p^{max} = 22kW$. The minimum and maximum aggregated charging power in the load area are $P^{min} = 0kW$ and $P^{max} = 200kW$. The reference load area power is a flat signal of $28.5kW$. In

the following the schedule presented in Table 3.6 will be considered. The windows horizon is set as 3 hours. Tests with different sampling time will be performed and their effects will be evaluated.

Table 3.6: Charging sessions

PEV ID	Initial SOC [%]	Start Time	End Time
1	11.46%	00:30	03:10
2	22.92%	00:30	02:45
3	26.58%	00:30	02:50

Sampling Time The sampling time plays a fundamental role: from a vertical point of view, a lower sampling time allows more efficient management of the resources, on the other side, the use of a lower sampling time will increase the complexity of the optimization problem, that requires to solve more times more complex optimization problems. Figure 3.22 and Figure 3.23 show respectively the aggregated power on the load area (continuous line) and the aggregated charging reference (dashed-dot line) when the sampling time is 5 minutes and 1 minute. If the dwelling time and the charging preference are satisfied, in both cases (Figure 3.24 and Figure 3.25) the performances on the load area side degrade when the sampling time increases. This degradation is a clear consequence of the stiffness of the charging set points when the sampling time is high. Figure 3.26 and Figure 3.27 show the charging set points sent to the vehicles at each sampling time; as expected, both solutions share a common shape, but the flexibility provided by the lower sampling time allows to make small adjustments to the charging schedule, obtaining a smoother evolution and improved tracking performances. The weaknesses of the granular solution are the complexity and the number of problems that have to be solved; the simulations shown are characterized by approximately 2:40h of simulation time. The associated control problems change their dimensions according to the sampling time in the following way:

- in case of 5 minutes sampling time, the prediction and control horizons will have a dimension of 36 steps and, to reach the end of the charging sessions, 32 MPC instances need to be solved;
- in case of 1 minute sampling time, the prediction and control horizons will have a dimension of 180 steps and, to reach the end of the charging sessions, 160 MPC instances need to be solved.

So, reducing by an order N the sampling time the dimension associated to optimization problem of an MPC instance increases by a factor N, as the number of problems to be solved in the same simulation time. Moreover, note that to be consistent with the dynamic of the system, more complex problems have to be solved in less time.

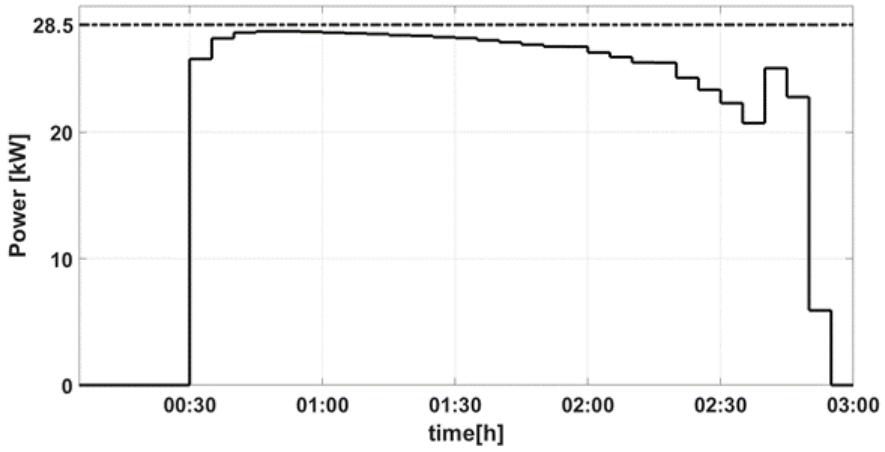

Figure 3.22: Integration with TLC system - aggregated charging load area power evolution with sampling time of 5 minutes

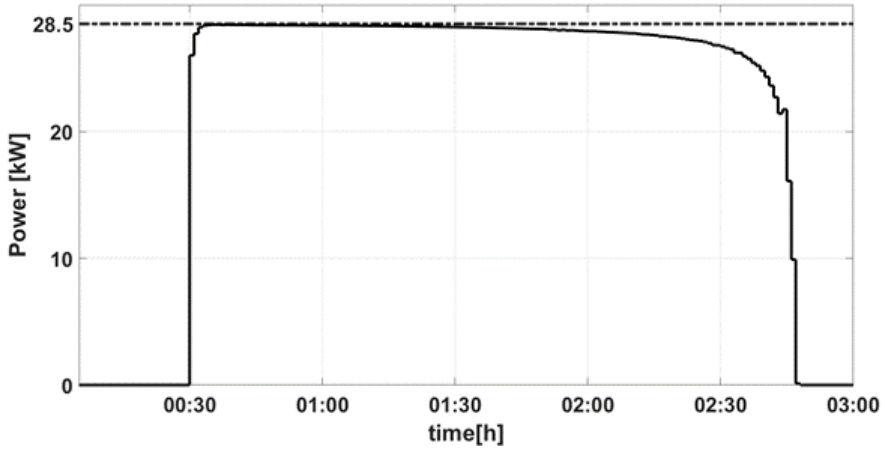

Figure 3.23: Integration with TLC system - aggregated charging load area power evolution with sampling time of 1 minute

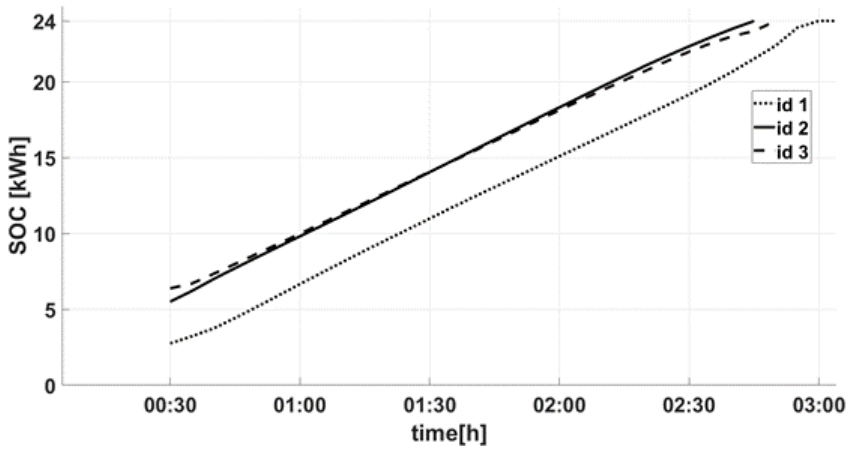

Figure 3.24: Integration with TLC system - state of charge evolution with sampling time of 5 minutes

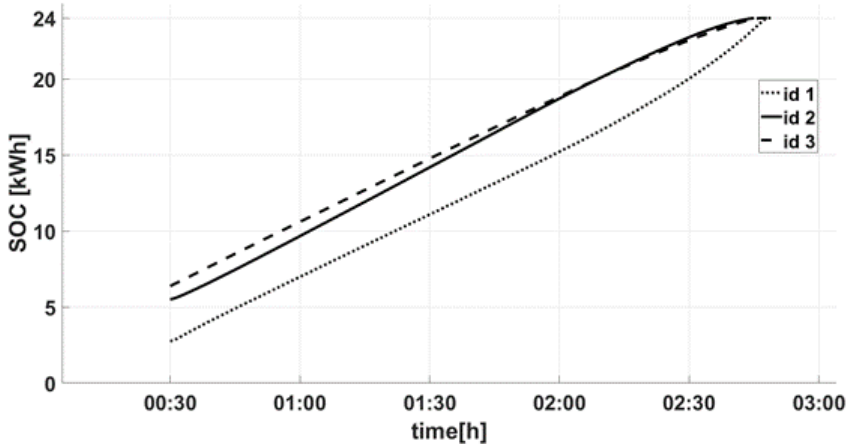

Figure 3.25: Integration with TLC system - state of charge evolution with sampling time of 1 minute

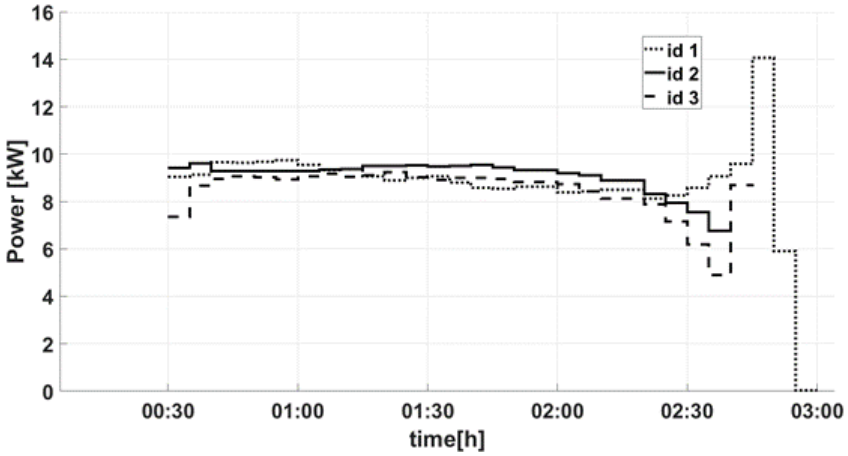

Figure 3.26: Integration with TLC system - charging power setpoints evolution with sampling time of 5 minutes

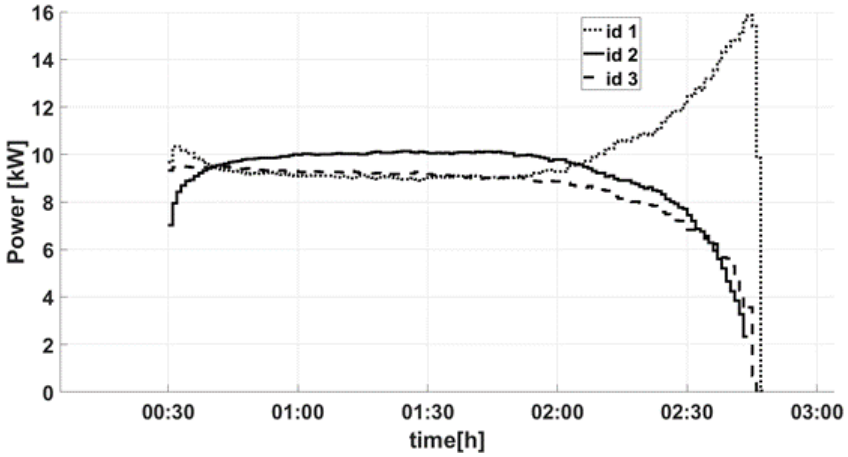

Figure 3.27: Integration with TLC system - charging power set point evolution with sampling time of 1 minute

In the simulations presented above some typical implementation details were not shown.

Typically, when a vehicle is plugged to the charging station the charging session starts with the maximum charging power; these power withdraw is maintained at least for one sampling time, that is the minimum time needed to schedule a power set point to the new vehicle. This operational sequence introduces spikes of power in the aggregated charging profile. The ability to reduce the sampling time not only improves the flexibility of the system, and consequently enhance the overall performance of the vertical during the smart charging session, but it is also useful during the preliminary stages of the charging session, when the charging power is

not yet controlled by the smart charging system.

Communication Latency As explained above, the sampling time affects considerably the performances of the overall system. The drawback of having a lower sampling time is directly correlated with the complexity of the problem that has to be solved, and consequently its required time. To this regard an additional test is designed also to evaluate the effects of the communication technologies on execution time. The main goal of this test case execution is to provide a comparison of the algorithm execution with respect to the communication technology employed. To provide this outcome without having the possibility to access the 5G RAN , the algorithm has been tested using Fiber communication technologies, between the Local Control Agents at and the Master Control Agent on 5G MEC server. The comparison has been made executing the tests also using commercial 4G communication technologies. The algorithm execution and performance depend on a multiplicity of aspects: the MPC algorithm is influenced by the weights assigned to the cost function, the convergence speed depends on the choice of tunable parameters and initial guess, the computational time depends on the machine performance, etc. For all the executions shown below these parameters are kept fixed to actually represent the contribution of communication time on the algorithm execution. The executions presented beneath refer to the configuration presented before with a sampling time of 1 minute. Figure 3.28 shows (in blue) the overall time spent to complete a single MPC step, i.e., to provide a new set of charging set points using 4G technology. The dashed line represents the theoretical time limit in which the solution of the optimization problem has to be computed (i.e., before the next MPC step starts). As it is possible to see from Figure 3.28, the MPC instances often require more time than the available one. On the same figure are represented (in orange) the estimation (made by measurements of the end-to-end Round Trip Time (RTT) of the communications between Master Control Agent and Local Control Agents) of the time spent in communication in each MPC instance: this execution clearly shows how the communication time contributes in the violation of the time constraints imposed by the sampling time. Nevertheless, the communication time is not the main bottleneck, the majority of the time is spent in the computational phase, but the communication time provides an important contribution to the total time. Reduce the communication time helps the overall system to match the time requirements. Figure 3.29 shows the same test execution, but performed using fiber technology. Two characteristics are evident: the number of times that the overall computation time is greater than the sampling time is remarkably reduced, and the impact of the communication time on the overall MPC instance time is significantly reduced.

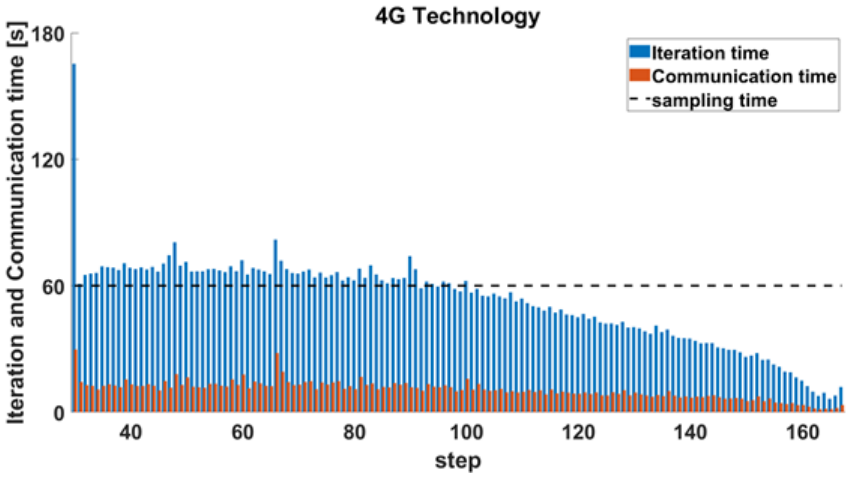

Figure 3.28: Integration with TLC system - iteration and communication time with a sampling time of 1 minute using 4G technology

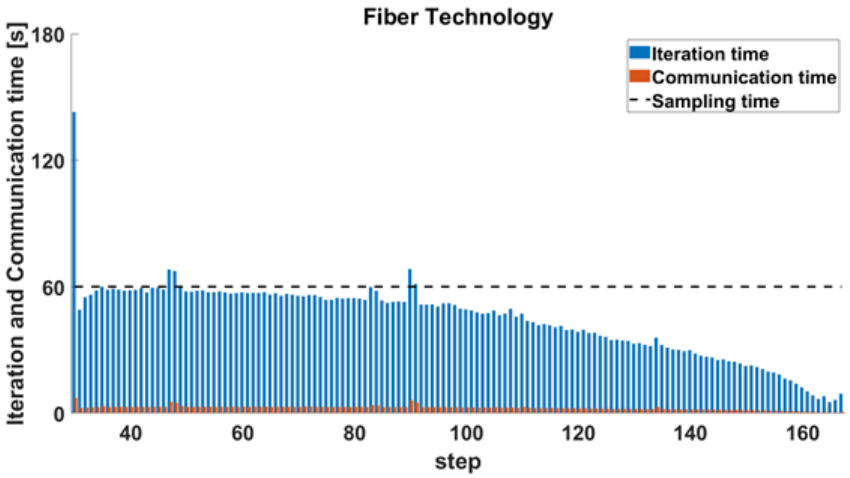

Figure 3.29: Integration with TLC system - iteration and communication time with a sampling time of 1 minute using fiber technology

3.1.4.4 Industrial Standards and operational conditions

In this section the attention will be focused on the impact of the standards and realistic operational conditions on the functioning of the smart charging system. In the works presented earlier were implicitly assumed the following assumptions:

1. the charging infrastructure is able to read the the SOC of the vehicle;
2. the power limits of the charging sessions correspond to the nominal power limits of the station/vehicle;
3. the charging dynamic model in the MPC fits the real one.

If the assumption 3 is not reasonable in practice, assumptions 1 and 2 can be managed exploiting the presence of the standard ISO 15118 [97].

IS0 15118 Assumptions 1 requires the communication between the vehicle, the charging station and the CPO's back-end, and assumption 2 respectively does not consider the limitation imposed by the charging station power electronics and the battery management system.

The communication system associated with assumption 1, could be used to overcome the limitations introduced by assumption 2. The availability of indication on the actual power limits associate with a specific charging session is beneficial for the optimization of energy resources management.

The share of information and the possibility of using them to command the vehicle in dependence to real-time conditions permit to figure out the implementation to the charging system shown in Figure 3.21 and the smart-charging algorithm presented in 3.1.3.

In terms of network services, the share of information between stations, vehicles and power infrastructure can endorse the development of local and global ancillary services. The presence of the ISO 15118 standard, that implements the required communication channel that validates assumption 1 and overcome assumption 2 spotlights the validity of the concepts at the basis of the thesis: *the improvement of the charging system, both with the expansion of the charging standards brings the charging system to an evolution that open to the participation of electric vehicles in the management of the electrical grid.*

The expected massive roll-out of PEVs, with the general idea to mix PEVs with other energy sources, encourages the studies on the constitution and control of UVAMs, both for local and global ancillary services provisioning.

The PEVs expansion has a huge impact at the DSO level, especially on the medium and low-voltage lines, where the UVAMs can be used to manage the distribution branches and nodes. The ISO 15118 standard considers the possibility for different actors to influence the energy transfer schedule (in line with the control architecture 3.21), maximum power profile and power limits. The presence of different actors able to modify the power limits as the Energy Managment System (EMS), Battery Managment System (BMS) and Electric Vehicle Supply Equipment (EVSE), influences the behaviour of the load area and charging sessions.

The communication channel introduced by ISO 15118 allows exchanging the real-time charging conditions. The sharing of information, as the SOC or additional constraints, augments the knowledge of the EMS that can take into account the new information to adapt the control actions to the new circumstances.

The charging sessions constraints can be expressed for example in terms of maximum power during a certain period of time, positive for charging or negative for discharging, also in financial or environmental terms.

The presence of more actors that can influence the boundary conditions of the charging sessions, but at the same time, the presence of interactions and commu-

nications between these agents influence the assumptions 1 and 2. The assumption 1 is valid, ISO 15118 considers the capability to read the SOC of the vehicle, but the assumption 2, is not valid. ISO 15118 considers also the capability to read these power limits in real-time, so in a real application, the box constraints (3.48) will become time-variant. Coherently with the MPC framework, the box constraints will be considered constant during the prediction and control horizon, but piece-wise constant w.r.t. the MPC instances. Formally, with the introduction of ISO 15118 the box constraints (3.48) can be modified as follow:

$$p_r^{min}(t) \leq p_r(\tau/t) \leq p_r^{max}(t) \ , \forall r \in R_t \ , \forall \tau \in T_t \tag{3.57}$$

The assumption 3, the perfect consistency between prediction and real model it is not applicable. Considering to the capability of ISO 15118, and assuming reasonable performance of the EVSE system, the model component mainly affected by uncertainties is the conversion losses coefficient ξ. The uncertainties on the conversion losses coefficient and the variability introduced by the non constant power limits have effects on the consistency and feasibility of Problem 3.2.

The uncertainties affect in an indirect way the dwelling time constraint (3.47): MPC considers the same box constraint for all the horizon, a condition that does not reflect the time-varying power constraints, threatening the feasibility of the optimization problem.

Suppose that the controller is solving a MPC iteration that contains the constraint (3.47), and it decides to split the charging rate in two different stages contained in the control horizon, in the first one the vehicle is charged with a low power rate, in the second stage, to recover the energy gap, the charging rate is increased. Suppose now that in proximity of the change of stage the EVSE is informed about a reduction of maximum power rate, that result lower than the scheduled charging power rate. In this case the unavailability of power can result in an unfeasible condition of constraint (3.47). Note that the charging sessions infeasibility are independently one from each other (the dependence arise only when the load area is undersized, formally when $P^{max} < \sum_r^{R^{max}} p_r^{max}$ where R^{max} represents the maximum number of contemporary charging sessions that could be present in the load area). The assumption of well-sized load area is reasonable, in general power system infrastructures are designed with large tolerances.

Working with the assumption of a well-sized load area, if the optimization problem associated with the local control agent results is unfeasible, the constraint (3.47) could be relaxed to avoid a dead-lock of the optimization algorithm. The MPC technique is adapt to face the effects of the relaxation: suppose that in a certain time step, the power limit associated to an agent make the associated optimization problem infeasible requiring the relaxation of constraint (3.47), only the fist step of the computed control horizon is actuated. In the next MPC the algorithm will recognize the adverse condition in which the agent is and try to feed it to recover the situation.

ISO 15118 - Integration In this paragraph the Problem 3.2 will be relaxed and a representative simulation aimed to discuss the effect of the introduction of ISO

15118 and related relaxation will be provided. The independence of the feasibility of each local optimization problem and the distributed optimization algorithm allow the relaxation of the dwelling time constraint, with effects on the formalization of the problem, maintaining the optimization algorithm unchanged. When the infeasibility is detected a new slack unbounded variable s_r is introduced in the optimization problem and (3.47) is modified as follows:

$$e_r(t_r^{dep}) = s_r \ , \forall r \in R_t \tag{3.58}$$

The slack variable s_r introduces tolerance on the final state of charge of the vehicle. The unbounded nature of the slack variables reflects the fact that the error is computed *w.r.t.* a state of charge reference SOC^{ref} that could be different (lower) that the battery capacity, so in case of necessity a vehicle can also overcharged (this case happens when the conversion loss coefficient is overestimated). The feasibility of the computed state of charge is still guaranteed by the SOC limit constraints.

To limit the side effects produced by the relaxation, the cost function associated to the local control agent is modified as follows:

$$D_r(e_r(\tau/t)) = \alpha_r e_r^2(\tau/t) + s_r \qquad \forall \tau \in T_t \tag{3.59}$$

Before start the algorithm (3.56) each local control agent evaluates the feasibility of the local optimization problem considering the formulation provided in section 3.1.3 and replacing the box constraints (3.48) with (3.57). If the problem results infeasible the local optimization problem is relaxed through the introduction of slack variable s_r, substituting the constraint (3.47) with (3.58) and the local cost function (3.43) with the relaxed version (3.59).

Figure 3.30 shows the simulation results based on the scenario of Sim. I presented in section 3.1.3.5. In addition to the original simulation scenario, the simulation treats the presence of signals from the vehicles that modify the power box constraints coherently with (3.57) and the conversion losses coefficient of each vehicle varies during the time in a range of 10%.

Comparing Figures 3.30 and 3.13 you can notice that the MPC control scheme is in general able to manage the uncertainties still obtaining good tracking performances. Differently from Figure 3.13, where the simulation was performed considering nominal conditions, in Figures 3.30 you can recognise two peaks of power (between 4:00 h and 6:00 h and between 8:00 h and 10:00 h). The presence of these peaks are related to the relaxation (3.58). The control system, especially when the problem associated with the PEV is feasible, tries to remove (or in case of infeasibility reduce) the error boosting the charging session, at the price to degrade tracking performances.

Figure 3.31 shows the final state of charge error reached by each vehicle. The maximum error is -1.25 kWh, that in percentage correspond to an absolute error of 5.20% that can be reduced with a different tuning of the MPC algorithm.

Convergence performance are not significantly affected by the introduced uncertainties (Fig. 3.32)

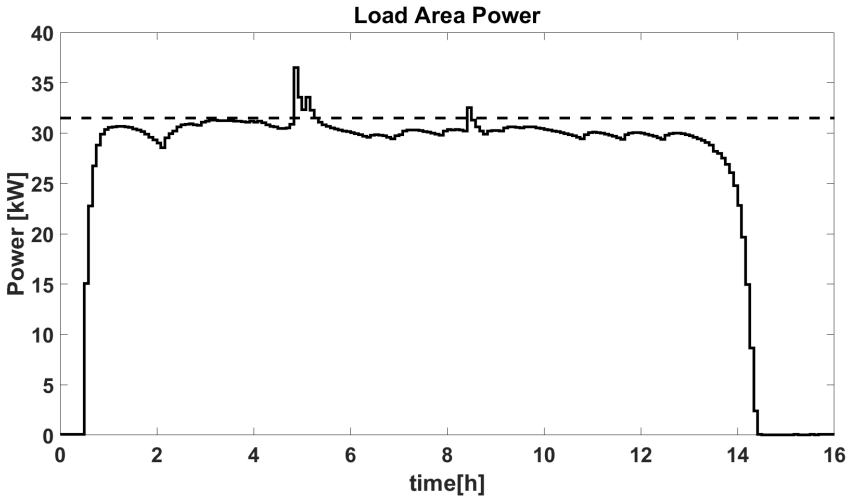

Figure 3.30: ISO 15118 - Aggregated load (continuous line), reference aggregated load (dashed line)

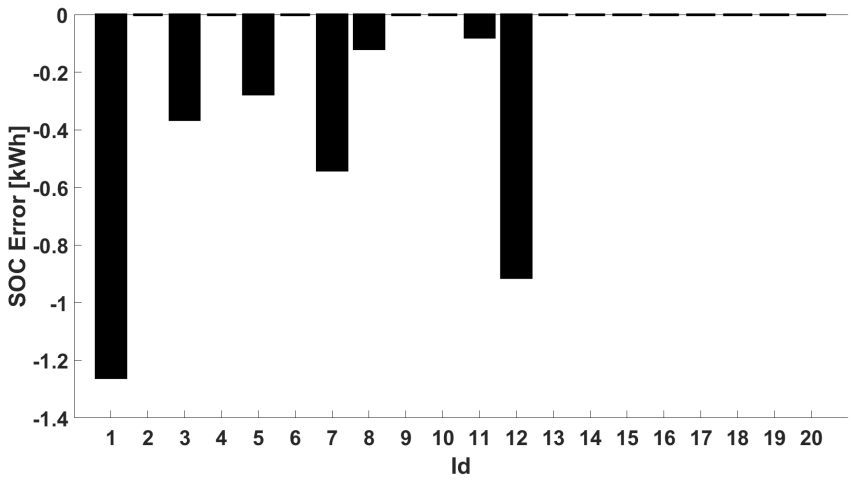

Figure 3.31: ISO 15118 - Error of the PEVs state of charge

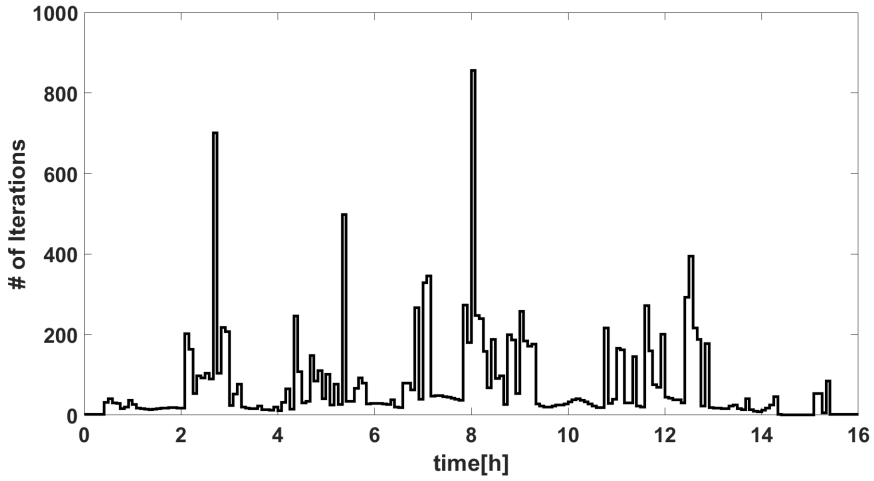

Figure 3.32: ISO 15118 - Number of iterations needed for convergence

3.2 Global Ancillary Services

In section 3.1 a deep discussion on how use the PEVs and ESSs to implement local Ancillary Services was provided. The discussion was performed in an incremental way: initially was shown how the presence of flexible loads allows to control the power at the POC, after that the discussion was driven in the direction of DSM service provisioning, identifying in the MPC solved by ADMM the right strategy for the satisfaction of control, computational, and privacy requirements. Finally the results and functionalities were analyzed and integrated through the design of control architecture scheme. The overall control system was contextualized, implemented and deployed in a realistic-like-scenario, considering Information and Communication Technologies (ICT) and charging standard requirements. The overall control system was evaluated with the support of standard-compliant experiments executed on real ICT infrastructure.

The results obtained in the previous sections can be partially extended and used to implement *Global Ancillary Services*.

In this section the smart charging paradigm will be used to implement Dispatching Service extending the logic of DSM. In this section will be also shown how the smart charging mass-deployment scenario introduce suitable condition for the participation of PEVs in the Frequency Regulation Services.

Finally, in relation to the Frequency Regulation Services, a different approach based on the use of ESSs for the robust stabilization of the transmission network under attack (that can be seen as a special case of frequency regulation service) is provided.

3.2.1 Dispatching Services Provisioning through PEVs and ESSs

Nomenclature

Table 3.7: Nomenclature

Symbols	Meaning
t	Current time
t_r^{dep}	Departure time of vehicle $r \in R_t^s$
T_t	Set of time instants in the control window
R_t^s	Set of charging EVs at time t under substation s
B^s	Set of ESSs under substation s
p	device power
SOC	state of charge
SOC^{ref}	Desired state of charge
e	state of charge error
ξ	conversion losses
P_p	Charging power at primary substation level
P_s	Charging power at secondary substation level
P_p^{ref}	Reference primary substations charging power
ΔP_s	Secondary substations charging power oscillations
E	Primary substations charging power tracking error
D	PEV cost function
W	Secondary substations cost function
C	Primary substations cost function
Δt	Sampling time
r, τ, b, s	Generic elements of sets R_t^s, T_t, B^s, S (subscript)
ρ	augmented lagrangian parameter
ϵ	ADMM tolerance
S	number of secondary substations

3.2.1.1 Introduction

The goal of this section is to show how the service provisioning strategy developed in Section 3.1, with appropriate extensions, enables the participation of flexible loads, in particular PEVs and ESSs, in the dispatching activities.

The extension of the DSM paradigm to medium/small production/load units, that aggregated form a Virtual Power Plant (VPP) with scalable capacities, facilitates the inclusion of new actors in the energy market, increasing competitiveness.

As a result of the high penetration of renewable sources and the decentralization of production sources, network managers of many countries are facing the problem of an increasing instability of their networks and the consequent disservices for users [98]. The key is to transform the presence of distributed generation as an advantage, i.e., create a VPP based on of several and different load and production

units geographically spreads and potentially in continuous evolution (e.g. in the PEVs case not only the power charging demand, but also the spacial distribution of flexible sources vary fluctuate during time).

The distributed approach is also related to the computational aspect, a central control strategy brings with itself computational problems; the huge number of aggregated loads needed to form a VPP would require important computation capability, with the associated time and cost requirements.

The work presented in section 3.1.3 is extended with the aim to consider the *Global Ancillary Services*.

The objective of this work is to design a system that is able to control the aggregate loads which constitute an UVAM, compliant with the requirements coming from 300/2017/R/EEL [10], and able to work in a centralized and decentralized way on the basis of need.

3.2.1.2 Italian Market and Regulation

The following work is referring to the control of a node of the transmission network, root of a distribution branch. The distribution system is composed by several secondary substations that could host charging stations, the charging stations that share the same point of connection are aggregated to a load area. According to the currently regulation, a day-ahead profile power consumption at transmission level is dispatched by the TSO and is considered as a reference for the aggregated overall distribution chain [2]. Differently from the Section 3.1.3 where the load areas work independently one to each other, the PEVs must collaborate and assist the distribution system in the fulfilment of TSO's dispatching orders, while support in the implementation of secure and efficient distribution network operation, breaking down the limits related to the load area affiliation.

The scenario presented above fits with the expectations of the Italian's and European's plans [9]. The participation in the dispatching service provision - for the sake of clarity is the set of services finalized to ensure the balancing between injection an withdraw of power- is reserved to systems that are able to guarantee margins of power modification in the order of MW in a specific range of time and fed/connected to specific source of power. The Autorità di Regolazione per Energia Reti e Ambiente (ARERA) in the may 2017 approved 300/2017/R/EEL [10] that *for the first time* opens the dispatching market to production units connected to renewable sources and storage systems. Starting from this first steps, the TSO has launched pilot projects in order to explore the possibility of introducing in the set of enabled systems new entities. In June 2018 the Italian TSO TERNA [11] opens the discussion for the inclusion of VPPs that include both consumption and generation units, also related to renewable sources. These activities bring to a new vision of the MSD, with the objectives to:

[2] for sake of simplicity, in this work only the charging power is considered. This assumption does not affect the validity of the work as the profile of the other loads can be considered as an offset

- Adapt the MSD to the new generation energy resources, maintaining the consistency with the principle of technological neutrality;
- Increase the amount of available sources to improve service performance and security;
- Sterilize possible distortions with respect to the energy, capacity and services markets.

To achieve these objectives, is necessary to update and refine the dialogue with respect to the new MSD participants [10]. The VPP of our interest, can be identified in the Italian regulation as UVAM. UVAM as the aggregation of consumption, production and storage units, so in general points connected to the grid at any voltage level [9].

It important to underline that the UVAM can be composed also by charging stations functional to "e-mobility" [10].

The participation to the UVAM in the MSD requires less restrictive conditions with respect to the policy before may 2017, but these less restrictive requirements bring limitations to the service that can be covered. To participate to the MSD the UVAM have to guarantee the following requirements:

- Maximum UVAM Control Power at least 1 MW;
- Ability to modulate the total energy withdrawn by the UVAM within 15 minutes of receiving the Dispatching Order (BDE);
- Ability to withstand the change in load for at least 2 consecutive hours.

When these requirements are satisfied, the UVAM can participate to the following MSD services:

- Congestion resolution;
- Tertiary Control;
- Balancing.

The BDE are computed with respect to a baseline (D-1), that represents the day ahead prediction of the aggregated UVAM power. This baseline have to be sent within a established deadline (in Italy by 5:00 p.m. of the day before) and has to have a granularity of 15 minutes, as the available reaction time of the UVAM. As definition, UVAM is an aggregation of load and generation units, potentially strew and far in space. The same point of aggregation can host a huge number of loads, conceptually different. The needed of manage this amount of loads introduces the necessity of define a scalable computation strategy, if possible distributed, that is able to provide control actions overstepping the problems related to a centralized computation strategy, in particular memory occupations and computational capacity. Distribution brings with itself the necessity to dealt with communications

issues, that sometimes could be prohibitive in terms of reliability and latency; the presence of new communication technologies (5G) can help in the overcome of these limitations. When it is not possible, the proposed algorithm should be able to reduce the contemporary memory occupations, allowing to switch from decentralize to centralize computation technology when necessary. The switch between the two computation strategies has to be supported also by an appropriate architecture.

3.2.1.3 Control Architecture

Figure 3.33 shows a control architecture that could be seen as an extension to different load areas of the 3.21.

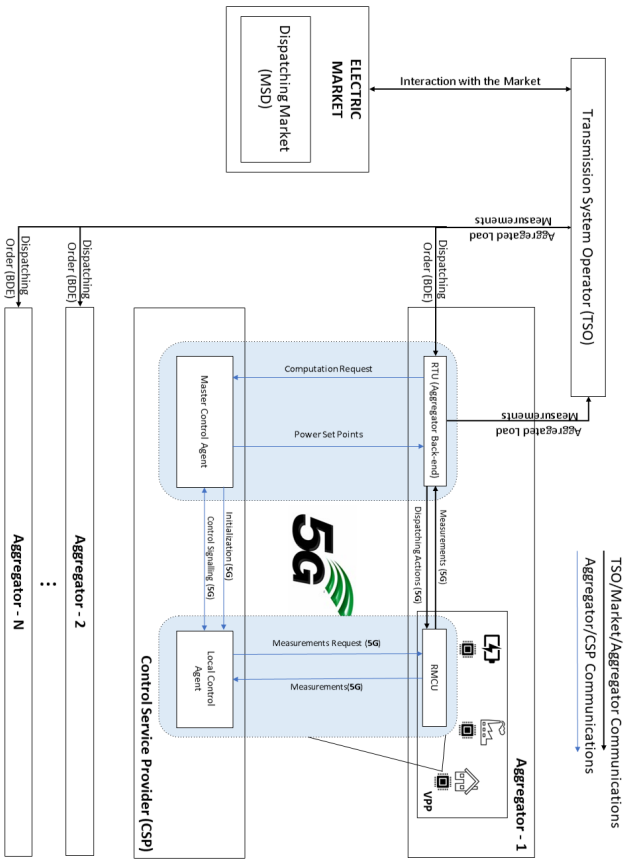

Figure 3.33: Control architecture for the UVAM using 5G technology

It is possible to identify 3 layers of competence:

- Transmission System Operator (TSO) Layer;
- Aggregator Layer;
- Control Service Provider (CSP) Layer;

The overall control architecture is supported by the presence of a 5G facility that allows using the 5G network for the communications. The architecture is composed of the following operational blocks and entities:

- The 5G block, that represents the 5G infrastructure;
- Transmission System Operator, that is an external part, has the capabilities to send dispatching orders that can modify the operativity conditions. These dispatching orders are sent to the Aggregator layer, in particular to the Remote Terminal Unit (RTU). The TSO, according to the deliberation receive periodically, the VPP aggregated load measurement.
- The Aggregator Layer collects two main entities:
  - The RTU, that encloses the Back-end of the operator. This block is design to cover a multiplicity of tasks, indeed is in charge of works as interface between all the layers, it is in charge of receive: dispatching orders, measurements from the field and the power setpoint that has to be actuated on the flexible loads, send charging requests to the Control Service Provider and the actuation signals to the field device;
  - The Virtual Power Plant VPP, is composed by the flexible load and Remote Monitoring Control Units (RMCUs). RMCUs are devoted to the communication with the RTU in order to send electrical measures and perform electrical actuation actions, they communicate also with the distributed part of the Control Service Provider, the Local Control Agents, to provide the measurement needed for the computation of optimal setpoints.
- Control Service Provider CSP Layer, it encloses the operational blocks that allow to provide the services needed to participate to the Dispatching Market, in this layer we can identify two operational blocks:
  - The Master Control Agent, is a central node of the distributed architecture of the CSP, it is in charge to communicate with the RTU to receive requests of the service and to communicate the optimal setpoints that should be actuated. It is connected as central node of a star topology with the Local Control Agents, the Master Control Agent initializes all the Local Control Agents to perform the computations and iteratively exchanges control signalling with them to reach the result of the control algorithm;

– The Local Control Agents are the distributed components of the CSP layer, their main role is in the computation of local optimization problems, their results will be used to compute the optimal power setpoints. They communicate with RMCUs to obtain the measurements needed for the computation and with the Master Control Agent (with what is called Control Signalling) to take part in the overall control algorithm.

The proposed architecture is structured in a way to exploit the above-mentioned control decentralization; as indicated in the figure, the TSO takes measurements of aggregated loads from the Aggregator participating to the MSD through the RTU. In case of network imbalance the Electric Market strives In order to find some parties that are able to re-balance the network. Once the Market finds the parties and the prices, then the TSO sends a Dispatching Order BDE to the Aggregators' RTUs (through IEC 60870-5-104 protocol [11]).

After receiving a Dispatching Order from the TSO through the Aggregator, the RTU (that represents the Aggregator back-end) calls proper services exposed by the Master Control Agent. These services orchestrate a series of communications among the Master Control Agent, the RTU and the Local Control Agents. The Master Control Agent gets the RMCU power measures from the RTU and activates each Local Control Agent present in the VPP in order to compute in a distributed way the optimal power target for each of the loads/generators present in the VPP. The computation of such optimal power targets is done through iterative algorithms, indeed the ADMM algorithm presented in section 3.1.3 will be reused to compute the optimal sequence of control actions. Coherently with what already discussed in section 3.1.4.2, the number of communications among the Agents can high, especially with a lot of loads/generators, so the communication delay can become an issue in guaranteeing that the new setpoints for loads and generators are computed and actuated within the time provided by the TSO.

In order to reduce as much as possible the communication delay (and so give more time for the actual computing and actuation of the new power setpoints) and to guarantee an high level of reliability, the proposed architecture envisages the use of 5G technologies for the communication among the Agents, leveraging on Ultra-Reliable Low-Latency Communication URLLC service of 5G communication. At the end of the computation phase, the Master Control Agent communicates to the RTU the Dispatching Actions, i.e. the new power targets for the loads and generators of the VPP, and the RTU sends these setpoints to the RMCUs, that are in charge of modulate the load/generator power according to the new setpoint.

3.2.1.4 Use Case Scenario

In this section, the network shown in Fig 3.34 will be used as a use case scenario to validate the application of the proposed control strategy. The Fig 3.34 although it is very simple, is able to represent the potential ability of the control strategy and its compliance with the 300/2017/R/EEL [10]. The scenario considers a distribution branch composed by three buses, at each bus corresponds a secondary

substation: looking at the commercial offers, distribution networks generally operate with secondary substations with nominal power of $630KVA$. Considering the minimum power requirement for the participation of the UVAM to the ancillary services ($1MW$), this simple network is, from minimum threshold power point of view, eligible. In this scenario, each secondary substation can host two type of loads, PEVs and ESSs. The main differences between these two type of loads are on the objectives that they perceive:

- PEV has to guarantee, in a certain range of time indicated by the user, the attainment of reference SOC;
- ESS has to compensate the lack (or conversely the exceed) of charging power demand w.r.t. the baseline and BDEs resulting on the primary substation at the root of the distribution network;
- ESS has to guarantee a suitable SOC in order to be able to properly react in case of necessity;
- both of them have to collaborate in order to follow the baseline and BDEs coming from the TSO.

It is important to note that the ESS lies on a node of the distribution network that does not contain any charging station, so the power contribution of the ESS has to be spread over the grid.

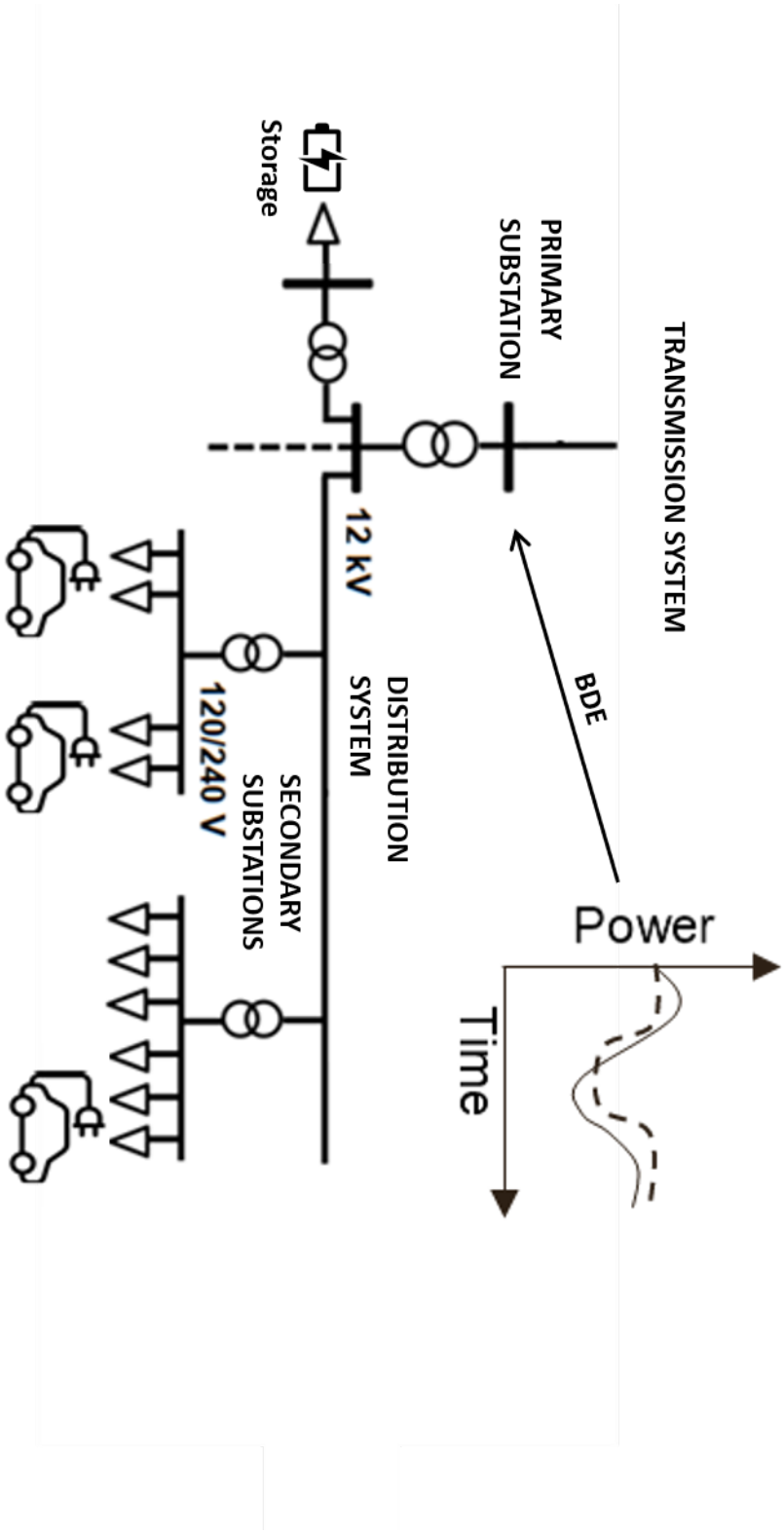

Figure 3.34: Reference scenario

3.2.1.5 Control Problem Formalization and solving procedures

As an extension of 3.1.3 the problem will be dealt with MPC strategy. The associated optimization problem has to be formulated in order to match the structure of (3.55). In this scenario more agents *w.r.t.* 3.1.3 can be recognized, indeed the entities involved in the process are:

- Primary Substation: the BDEs are defined at the transmission node level, the agent is in charge of guaranteeing the aggregated power tracking;
- Secondary Substations: the power flow at the distribution level has to be consistent with the power tracking requirements while safeguard the internal power flow. The agents work in the direction of tracking the aggregated power profile while flattening the internal power flow;
- PEVs: have to modify the charging schedules in order to satisfied the tracking and power profile requirements;
- ESS: is in charge of compensating the power gaps and surplus.

The general concept is to manage different energy sources, subject to different constraints (the dynamic of the sources, technical constraints...), different usages/objectives $f_i(x_i)$ (distortion w.r.t. reference power curve, state of charge deviation...) and correlations (an intuitive aspects could be the the power balance). The service provisioning is identified by the regularization function $g(x)$. The optimization problem (3.60) summarizes the overall concept.

$$\begin{aligned} \min_{x} \quad & \sum_{i}^{N} \overbrace{f_i(x_i)}^{\text{local target}} + \overbrace{g(x)}^{\text{service provisioning}} \\ \text{s.t.} \quad & \text{i-th local constraint}, \quad i = 1 \dots N \\ & \text{correlations between agents} \\ & x = \cup\, x_i \end{aligned} \tag{3.60}$$

In line with the 300/2017/R/EEL [10], the aggregated plant has to follow the D-1 baseline, and reacts to the baseline distortions commanded by the BDEs, this requirement is similar to the DSM service presented in 3.1.3 and could be treated in the same way:

$$\begin{aligned} \min_{p_r, p_b, P_s, P_p} J = \sum_{\tau \in T_t} \Bigg[\sum_{s \in S} \Bigg[W(\Delta P_s(\tau/t)) + \sum_{r \in R_t^s} D_r(e_r(\tau/t)) + \\ + \sum_{b \in B^s} D_b(e_b(\tau/t)) \Bigg] + C(E(\tau/t)) \Bigg] \end{aligned} \tag{3.61}$$

s.t.

$$D_r(e_r(\tau/t)) = \alpha_r(\tau/t)e_r^2(\tau/t) \qquad \forall\tau \in T_t,\ \forall r \in R_t^s,\ \forall s \in S \tag{3.62}$$

$$D_b(e_b(\tau/t)) = \alpha_b(\tau/t)e_b^2(\tau/t) \qquad \forall\tau \in T_t,\ \forall b \in B^s,\ \forall s \in S \tag{3.63}$$

$$W(\Delta P_s(\tau/t) = \beta^s(\tau/t)(P_s(\tau+1/t) - P_s(\tau+1/t))^2 \qquad \forall\tau \in T_t,\ \forall s \in S \tag{3.64}$$

$$C(E(\tau/t)) = \gamma(\tau/t)(P_p(\tau/t) - P_p^{ref})^2 \qquad \forall\tau \in T_t \tag{3.65}$$

$$\begin{aligned} &e_r(\tau+1/t) = e_r(\tau/t) - (1-\xi_r)\Delta t\, p_r(\tau/t), \forall\tau \in T_t, \forall r \in R_t^s, \forall s \in S \\ &e_r(t/t) = e_r(t), \forall r \in R_t^s, \forall s \in S \end{aligned} \tag{3.66}$$

$$e_r(t_r^{dep}) = 0\ ,\ \forall r \in R_t^s, \forall s \in S \tag{3.67}$$

$$\begin{aligned} &e_b(\tau+1/t) = e_b(\tau/t) - (1-\xi_b)\Delta t\, p_b(\tau/t), \forall\tau \in T_t, \forall b \in B^s \\ &e_b(t/t) = e_b(t), \forall b \in B^s \end{aligned} \tag{3.68}$$

$$\sum_{r \in R_t^s} p_r(\tau/t) + \sum_{b \in B^s} p_b(\tau/t) = P_s(\tau/t)\ ,\ \forall\tau \in T_t, \forall s \in S \tag{3.69}$$

$$\sum_{s \in S} P_s(\tau/t) = P_p(\tau/t),\ \forall\tau \in T_t \tag{3.70}$$

$$P_s(\tau/t) = L_s\theta_s(\tau/t) \forall\tau \in T_t,\ \forall s \in S \tag{3.71}$$

$$p_r^{min} \le p_r(\tau/t) \le p_r^{max},\ \forall r \in R_t^s,\ \forall\tau \in T_t,\ \forall s \in S \tag{3.72}$$

$$p_b^{min} \le p_b(\tau/t) \le p_b^{max}\ ,\ \forall b \in B^s\ ,\ \forall\tau \in T_t,\ \forall s \in S \tag{3.73}$$

$$P_s^{min} \le P_s(\tau/t) \le P_s^{max},\ \forall\tau \in T_t,\ \forall s \in S \tag{3.74}$$

$$P_p^{min} \le P_p(\tau/t) \le P_p^{max},\ \forall\tau \in T_t \tag{3.75}$$

$$\theta_s^{min} \le \theta_s(\tau/t) \le \theta_s^{max},\ \forall\tau \in T_t,\ \forall s \in S \tag{3.76}$$

Since this work is based on concepts already presented in Section 3.1.3, in what follows I highlight only the differences.

The cost function (3.61) of the associated optimization problem, is modified to consider the presence of several secondary substations (S), that can host a time varying set of charging PEVs (R_t^s) and a set of ESSs (B^s). The modification does not affect the cost function properties (quadratic and convex), so the assumptions

necessary for the ADMM convergence are still valid. Accordingly to the roles identified below, specific cost functions were defined, in details: (3.62) and (3.63) penalize the SOC error respectively for PEVs and ESSs, (3.64) penalizes the power oscillations at secondary substations level, (3.65) penalized the tracking error at primary substation level. The PEVs' and ESSs' dynamics are modelled as a simple integrator, (3.66) (3.68), but only PEVs are subject to dwelling time constraints (3.67). Correlations between agents are modelled through the power balances equations at secondary substations level (3.69), primary substation level (3.70) and with DC linearized power flow network equations (3.71) [99]. DC Power flow network equations will be discussed in detail in Section 3.2.3, so for the purpose of this discussion it is enough to know that DC Power flow network equations will be used to guarantee the feasibility of the power exchange across the network (3.76).

The optimization problem, with simple manipulations can be put in the (3.60) form. The optimization problem is solved by ADMM, a valid candidate for the computation of the optimal solution with respect to the mathematical properties of the optimization problem, and for the objectives illustrated in Section 3.2.1.1.

3.2.1.6 Simulation

The reference scenario of the following simulation is the same presented in figure 3.34. The control system has been set to work with a sampling time $\Delta t = 5$ minutes over a control window of 3 hours (36 sampling periods). All the PEVs have a battery capacity $SOC^{max} = 24kWh$, conversion losses parameter $\xi = 0.1$, minimum and maximum charging power $p_r^{min} = -22kW$ and $p_r^{max} = 22kW$, so differently from the previous simulations, in compliance with the ISO15118 standard discussed in Section 3.1.4, the V2G case is considered. The minimum and maximum power in the load areas that host PEVs are $P_s^{min} = 0$ kW and $P_s^{max} = 200kW$, while the load area that hosts the storage is limited by the storage power capacity, $p_b^{min} = -50kW$ and $p_b^{max} = 50kW$. The simulation is based on the sequence of charging sessions reported in Table 3.8; all the session requests are characterized by a 100 % of desired SOC level.

Table 3.8: Charging sessions

PEV ID	Substation	Initial SOC [%]	Start Time	End Time
1	1	11,46%	1:15	4:35
2	1	10,42%	1:15	4:15
3	1	9,83%	1:15	4:30
4	1	11,46%	1:15	4:15
5	1	22,92%	1:15	4:25
6	1	26,58%	1:15	4:55
7	1	19,25%	1:40	4:55
8	1	9,17%	2:10	6:10
9	1	11,92%	2:40	6:10
10	1	19,25%	3:10	6:20
11	1	11,46%	4:50	8:40
12	1	22,92%	5:25	9:50
13	1	11,46%	4:45	9:25
14	1	22,92%	6:25	9:30
15	1	26,58%	6:30	9:40
16	1	19,25%	5:45	9:30
17	1	9,88%	5:40	8:55
18	1	19,25%	7:00	9:00
19	1	21,33%	6:40	9:50
20	2	11,46%	1:15	4:50
21	2	22,92%	1:15	5:10
22	2	11,46%	1:15	4:55
23	2	22,92%	1:15	4:15
24	2	26,58%	1:50	5:00
25	2	19,25%	2:20	5:50
26	2	9,88%	2:55	6:05
27	2	19,25%	3:40	6:35
28	2	21,33%	3:40	5:45
29	2	11,46%	5:55	9:25
30	2	8,33%	4:40	8:00
31	2	11,46%	5:15	9:25
32	2	22,92%	4:55	7:35
33	2	26,58%	5:35	9:30
34	2	19,25%	4:40	7:50
35	2	9,88%	5:20	8:40
36	2	19,25%	4:40	8:45
37	2	21,33%	4:50	8:50

The simulation is aimed at testing the ability of the control system to react

to dispatching signals, so a short-term modification of the aggregated power at transmission level node. Figure 3.35 shows the D-1 baseline (dotted line). During the simulation, the D-1 baseline is modified by the dispatching signals, so during the run-time simulation the control system tracks the short-term reference load (Figure 3.35, dashed line). The immediate information that this figure provides is the ability of the system to track the short term reference signal.

Figure 3.36 shows the power profile at secondary substation level. The profiles are smooth. This is the result of the cooperation of the vehicles at load area level (Figure 3.37 and Figure 3.38) and the contribution of the ESS. Vehicles collaborate by each others, charging power is exchanged from and to the grid in order to satisfy the tracking requirement, at the level of load area charging power is internally exchanged to guarantee the satisfaction of charging requirements, while maintaining the aggregated power profile smooth. This mechanism is supported by the storage that absorbs and injects power in the network to relive the vehicles. The control system modulates the ESS' power setpoints in order to avoid big displacement between the SOC and the SOC reference value (Figure 3.39).

The trade-off between tracking error and ESS SOC displacement is evident in the final part of the simulation, between h 10 and h 12. The ESS has supported, with preventive charging and discharging actions the tracking requirement. In the last part of the simulation, several vehicles need to be charged, while the baseline associated with the charging power goes to zero. Storage preventive increases its state of charge and injects power in the network during the negative ramp. This procedure results in good tracking performance, while the ESS SOC is characterized by a displacement with respect to the desired value. In absence of other energy sources, the storage is forced to violate the power reference to recover its state of charge.

The distributed computational strategy well scales the optimization problem, Figure 3.40 shows how the number of needed iterations remains contained.

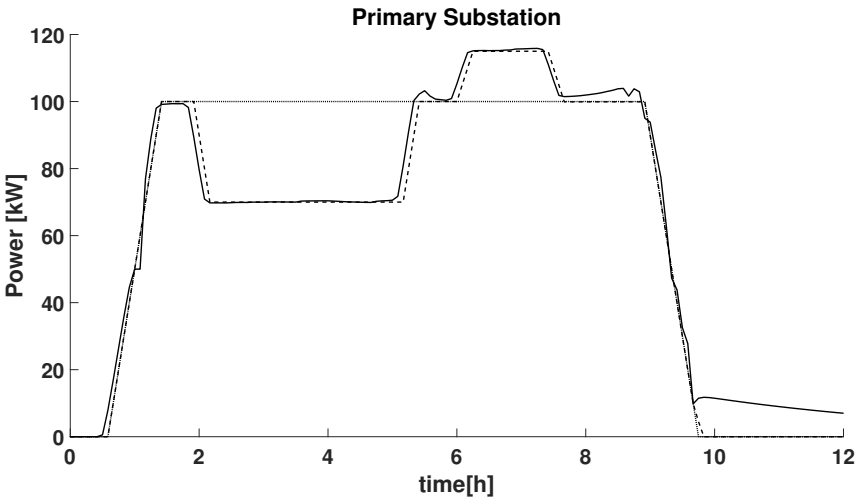

Figure 3.35: Aggregated load (continuous line), D-1 Baseline (dotted line), short-term reference aggregated load (dashed line)

Figure 3.36

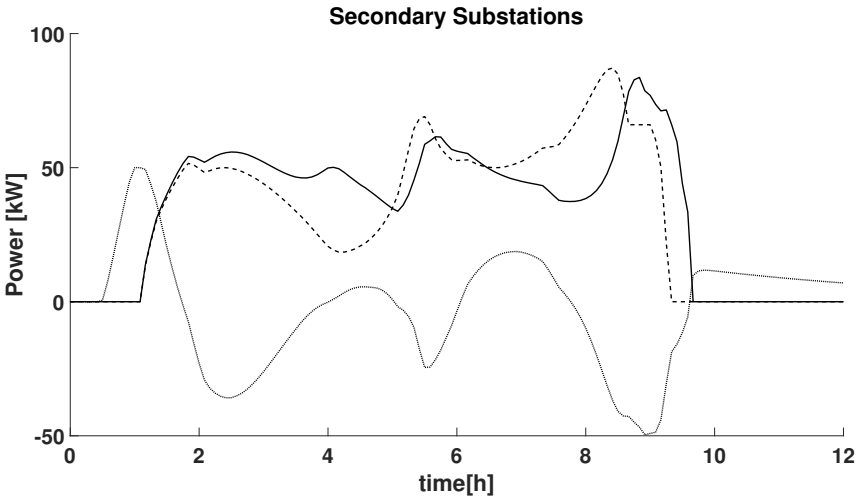

Figure 3.36: Secondary substations aggregated power profile of secondary substations that hos PEVs (continuous and dashed lines), and power profile of the secondary substation that hosts the ESS (dotted line)

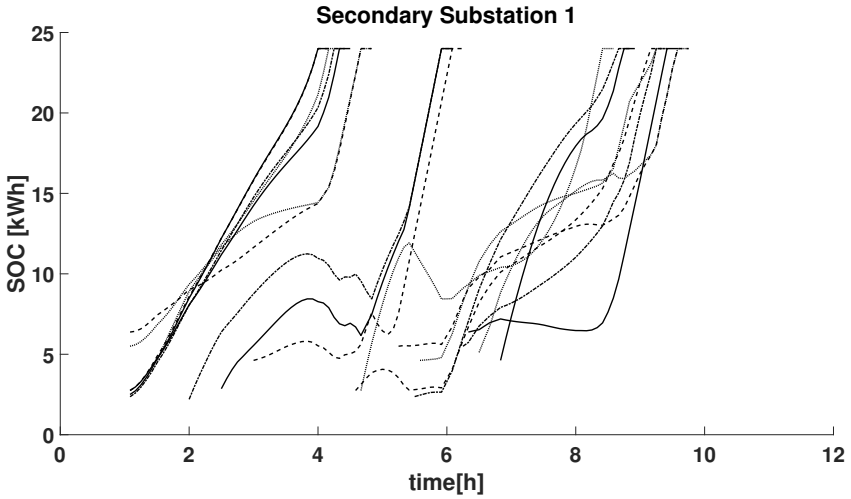

Figure 3.37: Evolution of the PEVs state of charge at substation 1

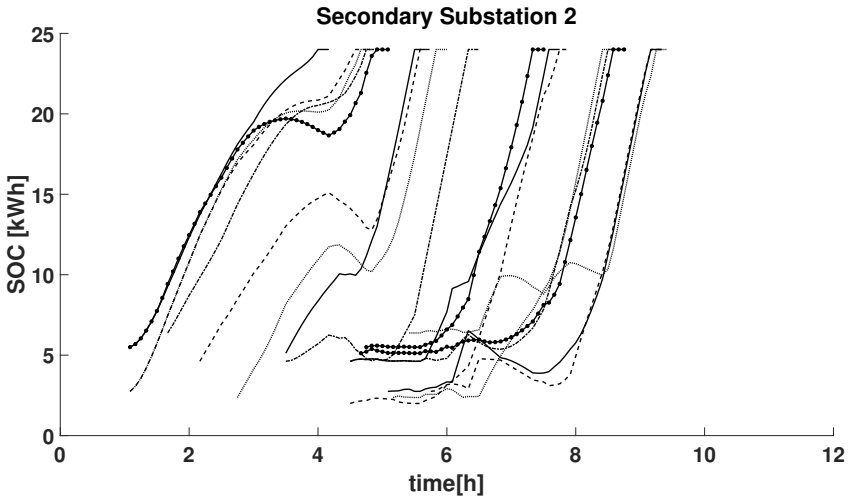

Figure 3.38: Evolution of the PEVs state of charge at substation 2

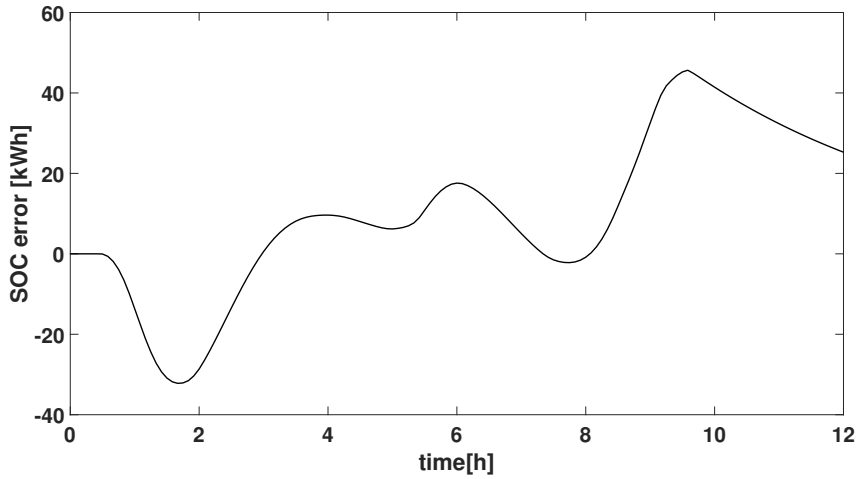

Figure 3.39: Evolution of the ESS state of charge

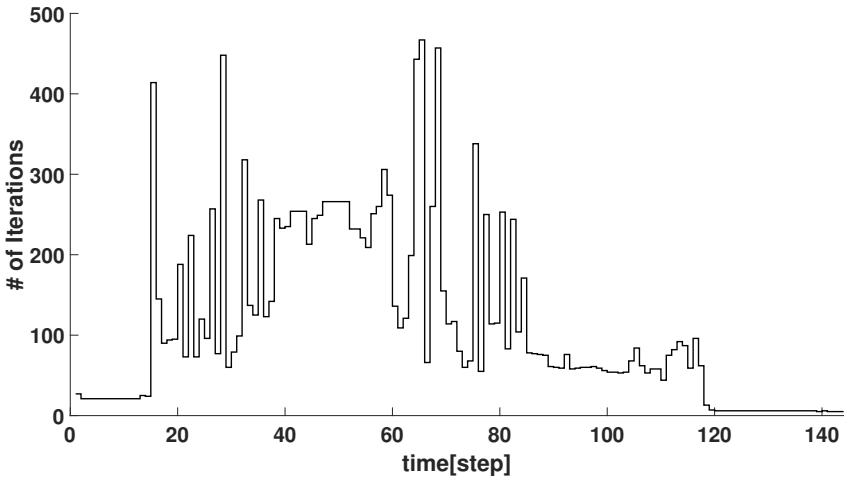

Figure 3.40: Number of iterations needed for convergence

3.2.1.7 Concluding remarks

This section presented how the results obtained at the distribution node level can be effectively extended to the transmission node level, the DSM service is augmented and transformed to dispatching service. Given the increase of the agents, the distributed structure of the optimization algorithm allows the management of simultaneous charging sessions, making effective the aggregation of small loads for the implementation of the UVAM.

3.2.2 Automatic Frequency Restoration Reserve using Plug-in Electric Vehicles and 5G Communications

In the previous section is illustrated how the results obtained at the local level can be applicable also in a mass-deployment condition, prerequisite for the implementation of Global Ancillary Services. In this section, the opportunity of large-scale aggregation will be used to enable the participation of PEVs in frequency control service provisioning.

3.2.2.1 Introduction

The safe and efficient operation of a power system strictly depends on two physical quantities: the frequency and the voltage level of the network [100]. The deviation of frequency and voltage from their nominal values are the effect of disequilibrium in terms of active and reactive power in the network. The so called ancillary services are then designed for the injection/withdraw of active and reactive power to balance the power mismatch. The evolution of the electricity network system and the spread of active components [101], make the involvement of new actors and technologies in the provisioning of ancillary services possible. The growth of electromobility in the last decade has pushed the scientific community and the power system stakeholders to develop new control strategies and concepts in order to improve and implement new paradigms to the ancillary services. The high penetration of RESs, with the associated transition of the power systems from synchronous-machine-based systems to inverter-dominated systems, pushed the development of the virtual inertia concept, in which also the inclusion of PEVs is expected to play an important role [102]. From this trend, several works that explore the potential and the issues of PEVs usage for the frequency regulation have been studied. In [103], a review of the strategies used to include the participation of electric vehicles in frequency regulation is provided; the review considers both technical and economic aspects, showing different points of view that have to be faced to move towards the development of ancillary services that include PEVs.

A recent paper in line with the activities of this work is [24], which proposes the use of PEVs for the provisioning of frequency regulation services. The work proposes some control strategies for the optimal control of PEVs' contributions, considering also the impact that such a service has on the battery degradation.

In this work, I elaborate on the design of a frequency regulation service based on the use of PEVs. The coexistence of the frequency regulation service with the smart charging one is tackled, and the advantages and challenges of the proposed scheme, considering also relevant ICT integration aspects, are analyzed. The section reports preliminary concepts and results established in the context of the European research project "5G Solutions" [96], where innovative use cases enabled by 5G communication technology in the field of smart energy grids are under design.

The remainder of the section is organized as follows. In section 3.2.2.2, the reference scenario is presented, contextualizing the problem and formalizing the ob-

jectives of the section. In section 3.2.2.3, the architecture designed to deal with the objectives is presented. Based on the proposed architecture, in section 3.2.2.4 the superposition of the smart charging service and the frequency regulation one is discussed. Finally, in section 3.2.2.6, the feasibility of the integration between the proposed architecture and the telecommunication systems, including 5G, is discussed.

3.2.2.2 System scenario and objectives

The scenario of this work considers the evolution of the European Energy Market and the related separation of the BRP and BSP roles [9]. The diffusion of distributed generation plants, favoured also by the European decarbonisation objectives [69], and the diffusion of small-sized storage systems, together with the spread of electric mobility, bring to the need of carrying out an important revision of the role played by distribution companies. As already mentioned in section 2 the DSOs are considering the possibility of assuming two additional roles compared to those that are traditionally under their responsibility: (i) the role of neutral facilitator for the provisioning of ancillary services made available by the BSP, that are needed for the safe operation of the overall system, and (ii) the role of purchaser of these services.

Moreover, this evolution changes the role of the CPO: the separation between BRP and BSP, that breaks up the physical positioning and market correlation of generation units and load plants. This separation allows the owner of energy sources to provide only ancillary services without having to care about balancing constraints. This results in the opportunity to participate to the Energy Market in an aggregated way. The separation of physical contribution and market position enables the aggregation of energy sources and, together with the possibility to sell services both at the level of distribution and transmission network, opens to the participation of new actors in the dispatching market, putting the CPO in an interesting market position.

In this context, the CPO can exploit the PEVs flexibility to create the necessary conditions for the participation in the dispatching market.

The potentiality of the use of the flexibility offered by PEVs was already discussed in the previous sections where the smart charging system empowers the load area with the capability of actuating DSM signals.

The presence of a smart charging system responsive to external signals introduces an additional factor in the context of smart charging in a load area: the possibility to have *power margins*; indeed, in section 3.1 it is shown how it is possible to drive the aggregated charging sessions power to track a target load curve; even in case of several charging sessions running at the same time, the smart charging system proposed is able to avoid the power saturation of the load area, while ensuring the drivers' requirements. The existence and the proper management of power margins are necessary for resource qualification to the provisioning of ancillary services. Ancillary services are historically entrusted to synchronous machines hosted by the generation units. The reasons why these services are provided by

the generators are multiple; focusing on the aspects of interest for this work, there are mainly two reasons: the capability of easily controlling the power generation, thus ensuring the presence of power margins, and the unidirectionality of the distribution network power flow. The change of paradigms presented above for DSOs and Energy Market also affects the way the distribution networks are modelled and, consequently, their role in the power system. Distribution networks become hosts of active loads, storage systems and generation units; the presence of them changes the distribution networks into a set of active nodes with bidirectional flow that can potentially supply ancillary services. The vision of disseminating the provisioning of ancillary service on different portions of the network is nowadays supported and enforced by official entities and stakeholders [104].

The work presented in this section focuses on the Frequency Restoration Reserves with Automatic activation (aFRR). aFRR is currently entrusted to generation plants relying on synchronous machines. The extension of the aFRR service to the participation of flexible loads is subject of studies and experimentation in Europe. For example, in the Pilot Project *Fast Reserve* [3] the inclusion of UVAM - that can be composed by PEVs [9] - in the aFRR service and their impact are investigated. This pilot project imposes specific performances to the units that are involved in the service provisioning like a specific degree of sensitivity to the frequency variations and precise reaction time requirements.

In the light of the considerations made above, the reference scenario is as follow: a smart charging load area is considered, the smart charging capabilities are used to introduce power margins at single charging session level and, consequently, in aggregated form at load area level. The presence of charging session margins is exploited by applying a real-time frequency based modification of the smart charging setpoints with the aim of providing the aFRR service. In this work, the Pilot Project *Fast Reserve* requirements are used to drive and validate the results.

In this context, 5G communication technologies, able to guarantee low end-to-end latency and high reliability compared to legacy technologies, together with modular virtualized network functions offered by the 5G Core Network architecture, represent enabling factors. These technologies are expected to allow the communication of frequency measurements to the charging stations within the strict time constraints imposed by the frequency regulation service, instead of relying on frequency meters installed in each unit of the UVAM. Considering the size, the number and the dispersed nature of the flexible loads needed in the aggregate, 5G technologies enable the UVAM to provide the frequency regulation service in a more cost-effective way.

The objectives of this work are: (i) to present an efficient control architecture that enables the exploitation of PEVs for the provisioning of aFRR, (ii) to provide the rationale for the integration between smart charging and the aFRR service provisioning and (iii) to discuss the impact of the telecommunication technologies on the service provisioning requirements and on the quality of the service.

3.2.2.3 System architecture

In order to match the objectives described before, a new system architecture has been designed. This system architecture represented in Fig. 3.41 shows the main components of the frequency regulation control system, together with their logical interfaces. The proposed system makes use of a single frequency meter for each Load Area (reducing a lot the cost for the deployment of such an architecture), that can be installed inside a single Charging Station or in its neighbourhood. Moreover, the proposed system exploits the novel 5G network architecture, where telco operators make some computing power very near to the Radio Access Network (RAN) available for their customers. These computing resources are named Multi-access Edge Computing (MEC) and enable very-low latency application to work efficiently, since the data packets can be processed (or pre-processed) in the neighbourhood of the customer requiring the service, with a substantial reduction of the end-to-end latency, that is reduced almost only to the radio access link latency (that is further reduced by 5G New-Radio standards, compared to the 4G LTE one).

The proposed architecture makes use of Local Control Agents, installed inside the Charging Stations, in order to compute the control signals in response to frequency disturbances. Each of these control signals can be superimposed over its corresponding slower smart charging scheduling signal computed by a separate system (see section 3.1), in order to enable the Load Area both to smart charging functionalities and to frequency regulation functionalities.

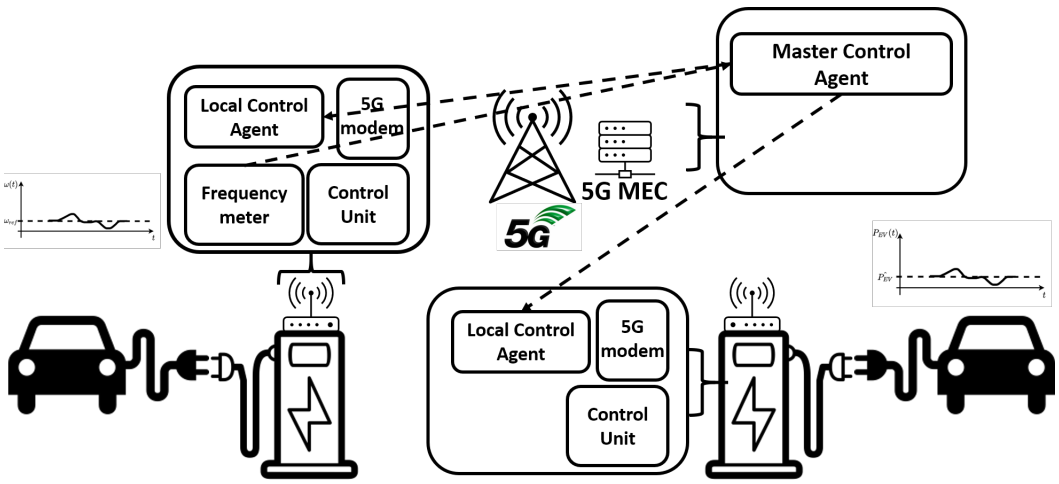

Figure 3.41: System Architecture

In the proposed architecture, the MEC hosts a Master Control Agent module that is in charge of spreading frequency measurements coming from the single frequency meter of the Load Area (that may be installed inside a Charging Station in order to make use of its 5G Modem) to all the Local Control Agents. The possibility to put the Master Control Agent inside the MEC enables a low-latency broadcast of the frequency measurements, avoiding to place a frequency meter inside each

Charging Station, while still having the measurements spread with an high reliability offered by 5G communication services and with a delay in line with the time requirements of the frequency regulation services, which will be better investigated in Section 3.2.2.6.

3.2.2.4 The smart charging problem and the power-frequency curve assignment

The integration between smart charging and aFRR service presented before must consider aspects related to the quality of the charging sessions, while have to guarantee the presence of power margins capable to realize a power-frequency curve that satisfies precise properties. The power-frequency curve properties can differ depending on the country. In this work, the Pilot Project Fast Reserve [3] directed by the Italian Transmission System Operator (TSO) *Terna* is considered as a reference for the forthcoming discussion. The requirements of the above pilot project are many, and the present work doesn't aim to address all of them. The attention is focused on the power-frequency curve shape and on the reaction time; in particular:

- the power-frequency curve has to be symmetric, continuous and the actuation has to be self regulating;
- the power-frequency curve has to consider the possibility to implement a dead band;
- the fast reserve unit has to react to the frequency variation in a time window less then 300 ms and it should reach the steady state in maximum 1 second.

Figure 3.42 shows an example of the expected response. In this work, the transient specifications, such as the overshoot and the steady-state error, which are strictly related to the power electronics components of the EVSE, are not considered.

The extension of smart charging with a frequency response base service is explained by the example shown in Fig. 3.43. The example of Fig. 3.43 considers a PEV subject to a V1G smart charging session. The figure is composed by two plots: the first one represents the network frequency, the dashed line represents the network frequency nominal value (in Europe $50Hz$) f_n, the continuous line represents the measured network frequency $f(t)$. In the example, the time trajectory of the frequency network is characterized by different distortions, with corresponding frequency deviation $|\Delta f| = |f(t) - f_n| \geq \overline{\Delta f}_{min}$ where $\overline{\Delta f}_{min}$ represents the frequency deviation threshold implemented by the dead-band. The second plot shows the superposition of the frequency response service on the smart charging session: the dashed line represents the nominal charging setpoint $\tilde{p}(t)$ assigned by the smart charging system at different time instants; the continuous line represents the actual setpoint commanded by the system. The charging session presented in the example well shows the concept behind the introduction of power margins: if the power setpoint for the charging session is between maximum and minimum charging power, the power gaps can be used to modify the charging power as a function of

frequency deviation. In the figure, the deviation is represented by Δp. The pair of the two plots explains the concept at the basis of the service integration. During nominal frequency operation, the EVSE follows the charging reference generated by the smart charging scheduler. In presence of a frequency deviation greater than the dead-band, the EVSE superimposes an additional contribution $\Delta p(\Delta f)$ to the smart charging setpoint, in order to participate to the actions aimed at steering the network frequency back to the reference value. A crucial point consists in the construction of the power-frequency (p-f) curve, that defines the variation of the charging power as a function of the frequency deviation. In this work, I aim at illustrating and discussing different possible strategies, highlighting the differences in terms of performance and compliance with the requirements discussed before.

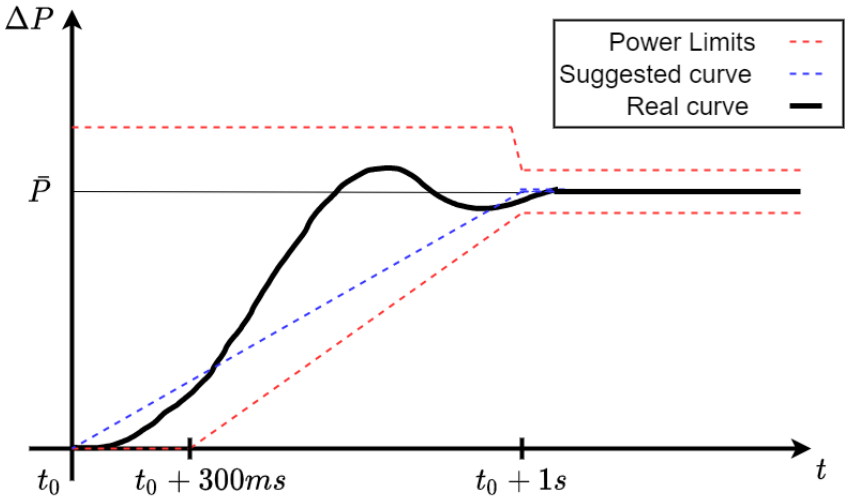

Figure 3.42: Expected response of a fast reserve unit [3]

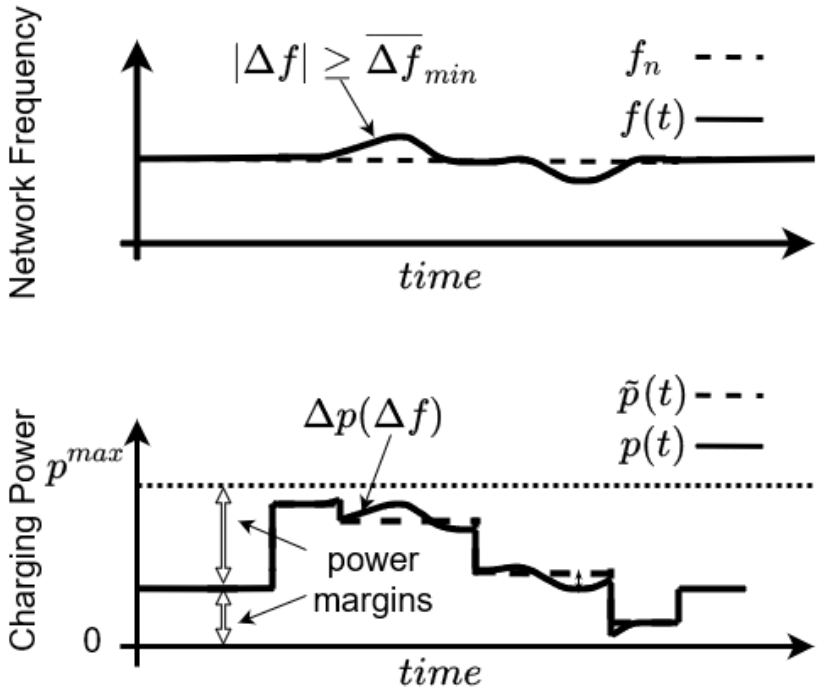

Figure 3.43: Example of the superposition of smart charging and frequency regulation services: top - network frequency time evolution, bottom - associated charging session

Case I - linear interpolation A first attempt for the p-f curve assignment is a strict separation between the smart charging service and the frequency regulation service. In this case, the smart charging system does not provide an active contribution for aFRR service, but it only introduces power margins (since typically the PEVs will not be recharged at maximum power, and thus some power margins will be available for the provisioning of aFRR services). Each EVSE equipped with a Local Control Agent, receiving the smart charging power setpoint $\tilde{p}$ and knowing the power limits of the whole charging system, linearly interpolates with two separated curves the points $(\overline{\Delta f}_{min}, \tilde{p})$, $(\overline{\Delta f}_{max}, p^{max})$ and $(-\overline{\Delta f}_{min}, \tilde{p})$, $(-\overline{\Delta f}_{max}, p^{min})$ where $\overline{\Delta f}_{max}$ characterizes the frequency deviation over which the EVSEs have to provide the full power margins. Figure 3.44 shows a representative example of this approach in a V2G scenario: the main advantages of this strategy are the decoupling between smart charging service and aFRR service, the possibility to compute the p-f curves at the level of EVSE and the exploitation of all the available margins at the level of EVSE. The drawback of this strategy is in the resulting shape of the load area curve (that is composed by the curves of each active session in the Load Area). Indeed, with this approach, the symmetry requirement for the aggregated power-frequency curve is in general not ensured (see Fig. 3.44b).

Case II - linear interpolation with load area control The presence of smart charging service is exploited not only to create margins at the level of the EVSE, but it can be also used to manage the power margins at the load area level. As in [42] [105] where an external signal is used to drive the aggregated load area power in order to satisfy a DSM service, the same methodology is used to impose a specific aggregated power withdrawal, i.e., half of the nominal power of the active charging sessions present in the load area at the given time. In this condition, by applying the linear interpolation strategy presented before, even if at the level of the single EVSE the curves are not symmetric, the aggregate p-f curve satisfies the symmetry requirement (Figure 3.45). Nonetheless, this strategy is characterized by different issues and limitations: first of all, the load area should be operated at half of the nominal power capacity. In addition, the symmetry is strictly related to the ability of the smart charging system to follow the load area power setpoint.

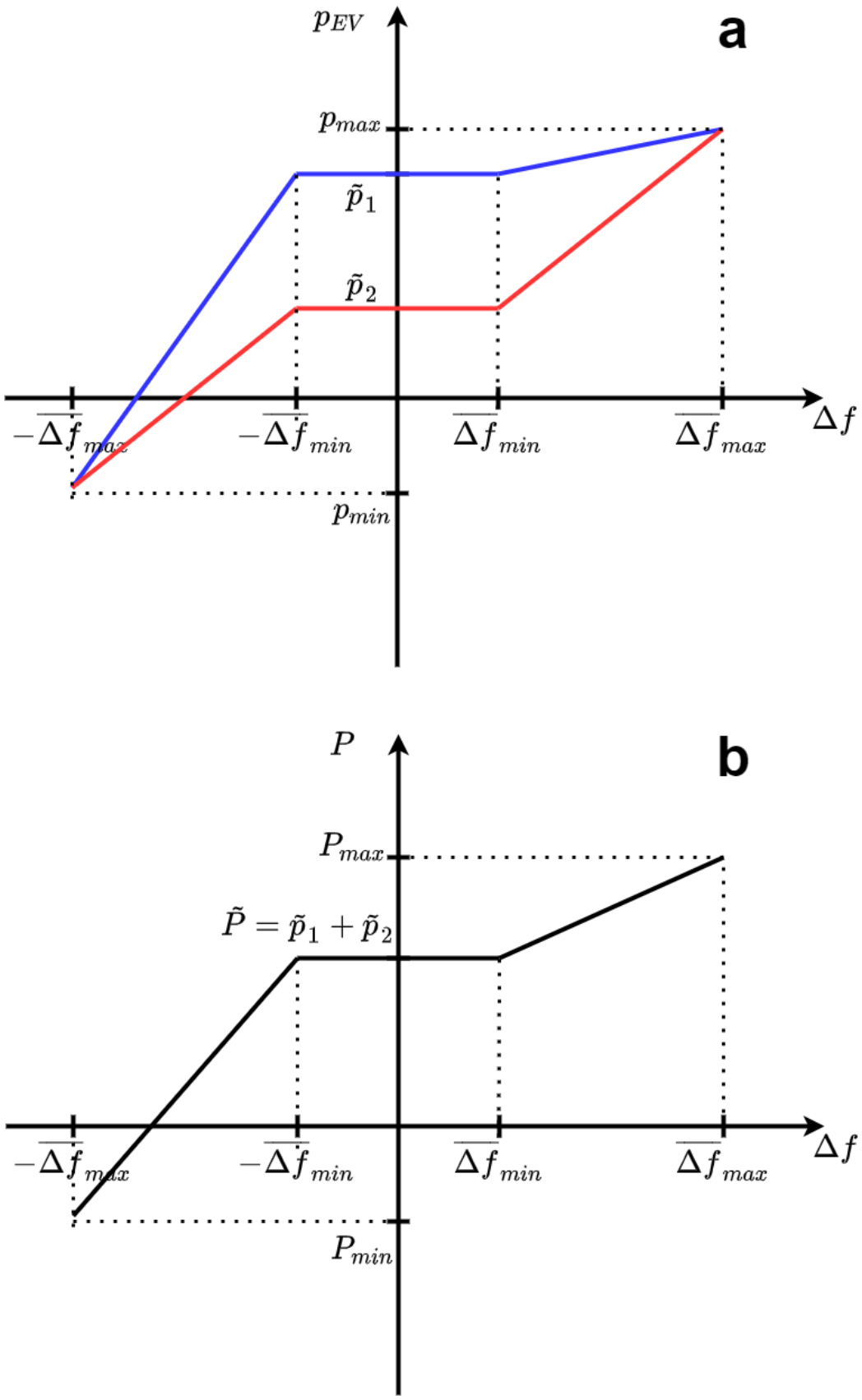

Figure 3.44: Case I - linear interpolation. a) p-f curve of two EVs, b) cumulative p-f curve

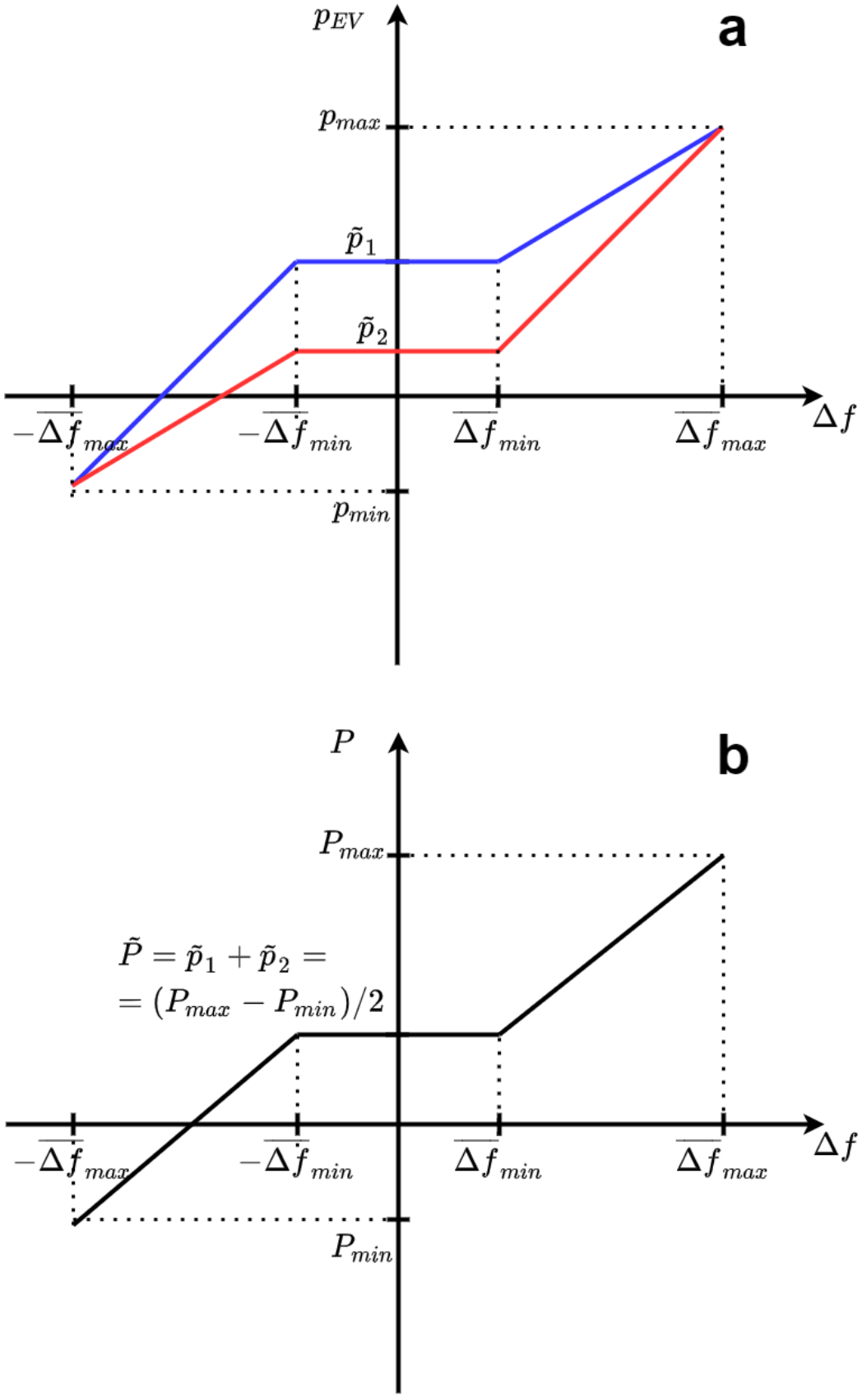

Figure 3.45: Case II - linear interpolation with load area control. a) p-f curve of two EVs, b) cumulative p-f curve

A more sophisticated strategy considers the implementation of a resource allocation algorithm, which assigns to each EVSE a specific p-f curve (even a nonlinear one), such that the aggregated load area curve satisfies all the requirements discussed before. The integration between the smart charging system and the resources allocation algorithm results in an integrated system that, managing the two services, allocates the resources considering drivers' requirements, balancing and distributing the service provisioning based on user profiling. The strategies presented before are less complex and easier to implement, while this last one requires the development of a resources allocation algorithm, that implies communications between EVSE and/or a deep integration with the smart charging system. In the next section, a formalization of the problem and a possible solution will be proposed.

3.2.2.5 Optimal Control of Plug-in Electric Vehicles Charging for Composition of Frequency Regulation Services

Figure 3.46 shows the reference scenario considered in this study. A set of PEVs are connected to charging stations that are remotely monitored and controlled by the CPO backend. The charging power setpoints actuated by the charging stations are periodically (e.g., every few minutes in [105]) computed by smart charging algorithms hosted in the "smart charging module". The goal of the smart charging module is to control the PEVs recharging in the load area, in such a way that the PEVs are recharged in compliance with the user preferences (e.g., time available for recharging and amount of energy to recharge), and in a way that is safe for the grid. In this section, I detail the control algorithm hosted in the "Local Droop Curves Computing module". This module periodically computes and sends to the charging stations the droop curves to be taken into account for frequency regulation. These are frequency/power curves that, given the current value of the network frequency, specify the power deviation with respect to the smart charging setpoint, i.e., how much the charging power setpoint computed by the smart charging module should be increased or decreased. One local droop curve is computed for each charging session, depending on the specific parameters of the ongoing charging session, as detailed next. This ensures that the two services, i.e., the smart charging service, and the frequency regulation one, can coexist.

In order to enable the charging stations to provide frequency regulation services, the system should be able to take a frequency measure and actuate the proper power setpoint to the PEV (increasing or reducing it based on the frequency deviation) within a very limited time (in the order of 300 ms, according to the *Fast Reserve* pilot project of TERNA [3]). In order to make the overall system economically feasible, it is not possible to install a frequency meter capable of the over-mentioned time requirements inside each charging station, but leveraging on new cellular communication technologies (e.g., 5G) it is possible to install just one (or few, for redundancy) frequency meter in each load area, and then spread the information to the other charging stations with negligible delay, thus matching the strict time requirements for the service.

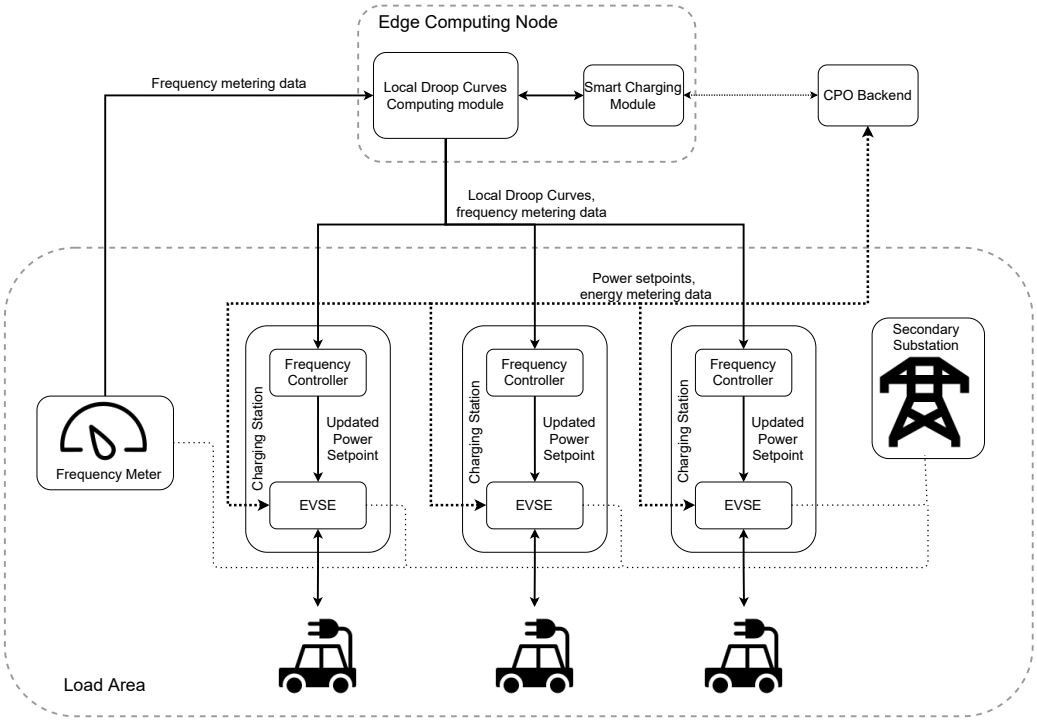

Figure 3.46: Reference System Architecture

Nomenclature and Problem Formulation In this section, I detail the proposed control algorithm hosted in the "local droop curves computing module", which periodically computes the local droop curves (i.e., one for each charging station), based on the current status of the ongoing charging sessions. First of all, the used nomenclature is introduced.

Let N be the number of PEVs connected at the generic time k in the load area. The generic n-th PEV at time k is characterized by:

- The current charging power level $P_{n,k}$;
- The maximum and the minimum possible charging power levels, respectively $P_n^{max} > 0$ and P_n^{min} (if $P_n^{min} < 0$, the PEV is enabled to discharging);
- The current SOC level $x_{n,k}$;
- The time left until the end of the charging session, $d_{n,k} > 0$;
- The error, $e_{n,k}$, between the desired SOC, x_n^{ref}, and the current one, $x_{n,k}$, i.e., $e_{n,k} := x_n^{ref} - x_{n,k}$;
- The power deviation, $\Delta P_{n,k}$, at time k, for the n-th PEV, due to the participation in the frequency regulation service. This value is computed from a droop curve.

The proposed algorithm is aimed at optimally coordinating the connected PEVs in the participation to the provisioning of ancillary services. More in details, the problem we tackle is that of optimally define p-f droop curves at single PEV level (which we call *local droop curves*), in such a way that, once combined, they match a given, desired droop curve (the *global droop curve*). The global droop curve defines how, *collectively*, the connected PEVs should react to frequency mismatches, as if they formed a unique entity participating in the provisioning of the ancillary service.

Figure 3.47 displays a general prototype of a global p-f curve. Focusing of the right-half plane, the parameter Δf_{min} defines the deadband: the power variation is zero if the deviation of the frequency with respect to the reference frequency value is in the interval $[0, \Delta f_{min}]$. Δf_{max} defines the frequency deviation limit after which the power variation saturates. m^{global} defines the droop, i.e., the ratio between the variation of the power and the frequency deviation.

The algorithm presented next recovers the global droop curve as the sum of N local droop curves. A notable aspect is that the design of each local droop curve takes into account the current status of the PEV's recharging process, as explained next.

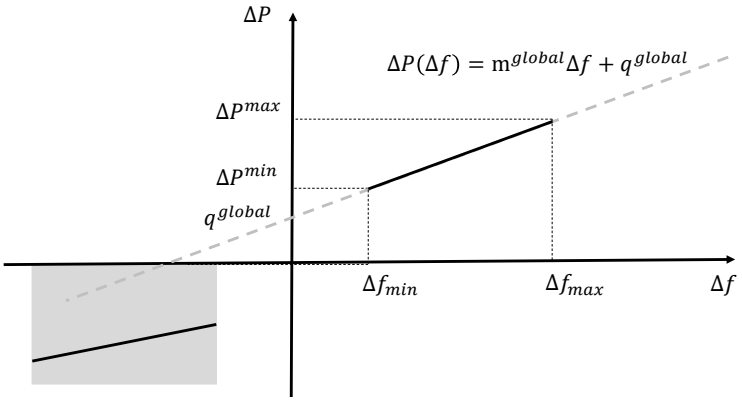

Figure 3.47: Global droop curve, with associated relevant parameters.

For the design of the local droop curves, we make the following assumption.

Assumption 3.3 (Shape of local droop curves)**.** *Local droop curves have a positive slope, and they are linear between* Δf_{min} *and* Δf_{max}*.*

Assumption 3.3 is included because it is in line with the common design principle of standard p-f droop curves (the algorithm discussed next works also without these assumptions). As implied by Assumption 3.3, the focus of this work is on linear droop curves, i.e., on curves described by the equation:

$$\Delta P_{n,k}(\Delta f) = m_{n,k}\Delta f + q_{n,k}. \tag{3.77}$$

I focus on linear local droop curves because standard droop curves are linear, and because working with such type of functions results in a linear optimization problem, which has low computational complexity.

The algorithm proposed in this work optimally designs each local droop curve by selecting the parameters $m_{n,k}$ and $q_{n,k}$, which are therefore the optimization variables of the problem. The algorithm is presented in the next section. To keep the description of the algorithm concise, and without loss of generality, we focus our attention on the design of the portion of the droop curves lying on the right half of the $\Delta f/\Delta P$ plane (see Figs. 3.47, 3.48). The part of the curve on the left half of the plane is designed in a similar way.

Proposed Local Droop Curves Design Algorithm The design of the generic local droop curve (3.77) must respect constraints related to the shape of the local curve, and others related to the shape of the global droop curve. It must also respect certain limitations imposed by the current status of the charging sessions, as explained next.

Local Droop Curve Design Constraints Figure 3.48 displays in gray the "design space" in which the generic n-th local droop curve can be drown. The

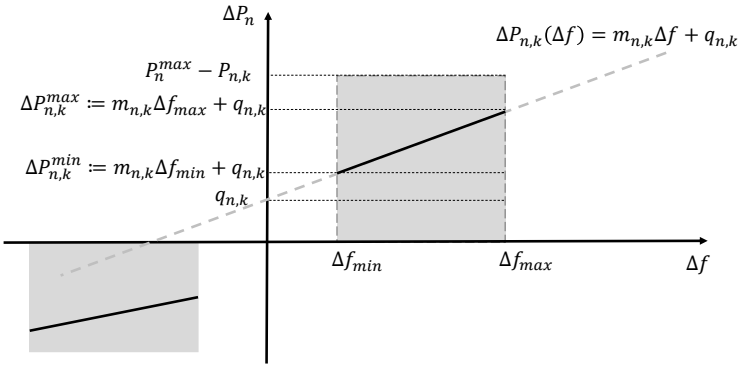

Figure 3.48: Local droop curve, with associated relevant parameters.

following constraints for each local curve are included.

$$0 \leq \Delta P_{n,k}^{min} := m_{n,k}\Delta f_{min} + q_{n,k} \leq P_n^{max} - P_{n,k} \tag{3.78}$$

$$0 \leq \Delta P_{n,k}^{max} := m_{n,k}\Delta f_{max} + q_{n,k} \leq P_n^{max} - P_{n,k} \tag{3.79}$$

The above two constraints state that, respectively, at Δf_{min} and Δf_{max}, the power increase for the single PEV must be between zero (i.e., corresponding to a null contribution to the frequency regulation services, and therefore having no impact on the current charging power level), and the maximum possible increase in charging power, i.e., $P_n^{max} - P_{n,k}$, which takes into account the current charging level, $P_{n,k}$, and the maximum possible one, P_n^{max}. Notice however that (3.79) alone is not sufficient, since the maximum power increase might be affected also by the current SOC. For example, the maximum power increase for a vehicle that is fully charged is zero. For this reason, the following constraint is added:

$$P_{n,k} + \Delta P_{n,k}^{max} \leq \frac{x_n^{max} - x_{n,k}}{T}. \tag{3.80}$$

Equation (3.80) states that the maximum power increment is limited by the maximum energy that can be charged into the battery in the unit of time. T is the sampling time of the algorithms, i.e., every T seconds the local droop curves are re-computed.

Given the focus on linear droop curves, (3.78), (3.79), and (3.80) ensure that the contribution of the single PEV is always feasible, also considering the current status of the charging session.

Next, in line with Assumption 3.3, local droop curves must have a positive slope, i.e.,:

$$m_{n,k} \geq 0. \tag{3.81}$$

This of course implies also that $\Delta P_{n,k}^{min} \leq \Delta P_{n,k}^{max}$.

Global Droop Curve Design Constraints The p-f droop curve arising from the superimposition of the local droop curves can be written as

$$\Delta P(\Delta f) = m_k \Delta f + q_k \tag{3.82}$$

where

$$m_k = \sum_{n=1}^{N} m_{n,k}, \quad q_k = \sum_{n=1}^{N} q_{n,k}. \tag{3.83}$$

The following additional constrains are included to ensure that the superimposition of the local droop curves matches the desired global droop curve:

$$m_k = m^{global} \tag{3.84}$$

$$q_k = q^{global}. \tag{3.85}$$

Target Function In the above paragraphs, I have presented the constraints that must be respected in the selection of the parameters $m_{n,k}$ and $q_{n,k}$, in order for the deriving local curves and global curve to be feasible d-f droop curves. In the following, I present the formulation of the proposed target function, to ensure that the parameters $m_{n,k}$ and $q_{n,k}$ are selected in an optimal way, according to the current status of the charging session of the PEVs participating in the provisioning of the ancillary service. The proposed target function to be *minimized* is:

$$\begin{aligned} J_k = \sum_{n=1}^{N} & -\alpha_1 e_k (\Delta P_{n,k}^{min} + \Delta P_{n,k}^{max}) + \alpha_2 d_k (\Delta P_{n,k}^{min} + \Delta P_{n,k}^{max}) \\ & + \alpha_3 m_k^{max} + \alpha_4 \Delta P_k^{max_r} + \alpha_5 \Delta P_k^{min_r} \end{aligned} \tag{3.86}$$

where $\alpha_1, ..., \alpha_5 \in [0, 1]$ are such that $\sum_{i=1}^{5} \alpha_i = 1$, and m_k^{max}, $\Delta P_k^{max_r}$, $\Delta P_k^{min_r}$, are auxiliary variables such that:

$$m_{n,k} \leq m_k^{max}, \quad m_k^{max} \geq 0. \tag{3.87}$$

$$\frac{\Delta P_{n,k}^{max}}{P_n^{max} - P_{n,k}} \leq \Delta P_k^{max_r} \quad \forall n \in N. \tag{3.88}$$

$$\frac{\Delta P_{n,k}^{min}}{P_n^{max} - P_{n,k}} \leq \Delta P_k^{min_r} \quad \forall n \in N. \tag{3.89}$$

Coefficients $\alpha_1, ..., \alpha_5$ can be used to weight the terms of the objective function. It is easy to see from (3.86) and (3.87) that, at the optimum, m_k^{max} is equal to the maximum value of $m_{n,k}$, for $i = 1, ..., N$. Hence, the inclusion of this term in (3.86) has the goal of minimizing the maximum value of $m_{n,k}$, i.e., of balancing the effort of the participation in the ancillary service provisioning among the PEVs, aiming to avoid that some vehicles are assigned steep droop curves (i.e., high values of $m_{n,k}$). The last two terms in (3.86), similarly to $m_{n,k}$, contribute to spread the effort between the vehicles, by minimizing the maximum share of the available power margin that each vehicle contributes to frequency regulation (see (3.88) and (3.89)).

The first and the second terms in (3.86) instead are included to take into account also the current status of the charging session of each PEV, and, specifically, to give priority to the PEVs with a larger SOC error (the first term - notice the minus sign), and the ones with a smaller remaining charging time (the second term). The local droop curves associated to these PEVs, will have a more pronounced slope and/or a higher power at Δf_{min}. As a result, they will contribute more to the provisioning of the ancillary service, which will help them in reaching earlier the desired SOC level. Notice that, when the SOC error e_k is negative (i.e., the current SOC is higher than the reference), then the PEV will contribute less to the provisioning of the service, which is a consistent behaviour. Finally, recall that, for the sake of brevity, we focused in the work in the design of the right-half part of the droop curves. The design of the left-half part of the curve, also in terms of the choice of the target function, can be carried out with similar considerations.

Numerical Tests Simulations have been performed in Julia [106], version 1.6.0, on an standard computer (3.3 GHz, I7 processor with 16 GB RAM). The simulation scenario is as follows. We consider a charging load area that participates to the frequency regulation service. We assume that the charging sessions active in the load area are enough to provide the required power-frequency curve, i.e., that the composition algorithm presented in Section 3.2.2.5 admits a solution.

In the following, two simulation scenarios are discussed, to validated the proposed approach:

1. Scenario 1: we run the algorithm in a balanced scenario, i.e., considering a set of charging sessions that are homogeneous in terms of power margin flexibility, SOC error, and charging time availability;

2. Scenario 2: we run the algorithm in a scenario in which the charging sessions have different power margins, different SOC errors, and time flexibility.

The two scenarios are meant to show that, from one side, the algorithm is able to come up with a fair and balanced assignment of local droop curves among the

participating PEVs while, on the other hand, taking always in consideration the real time SOC and time flexibility status of the participating PEVs, as determined by the respective charging session status, controlled by smart charging algorithms.

Scenario 1: Local Droop Curves Assignment in a Balanced Scenario The first set of simulations is aimed to show how the algorithm is able to design local droop curves that result in a balanced distribution of the regulation effort, among the participating PEVs. To this end, we consider 3 active charging sessions, characterized by the same dwelling time and SOC error. The distinguishing attribute between the sessions is the available margin of power, $\Delta P_{n,k}^{max}$, which reflects:

- The possible presence of different charging technologies in the load area, i.e., the fact that the charging sessions are characterized in general by different maximum power, depending on the charging technology;
- The presence of smart charging sessions, i.e., the fact that the charging sessions happen at different charging levels, which are in general different from the maximum possible charging level.

Indeed, the algorithm must be able to work in presence of smart charging sessions ongoing at different charging levels.

The first simulation in this scenario shows the case in which the charging sessions are characterized by the same power margin. Specifically, the charging sessions are characterized by a maximum charging power of 150 kW, and by a common charging setpoint of 100 kW, resulting in a power margin of 50 kW. The global droop curve, for over frequency events, is characterized by a maximum power deviation of 105 kW (70% of the available power margin of 150 kW), and by a frequency range $[\Delta f_{min}, \Delta f_{max}] = [500, 1500]$ mHz. In correspondence with the minimum of the bandwidth, the given global droop curve is characterized by a power deviation of 10 kW. Figure 3.49 shows the result of the algorithm.

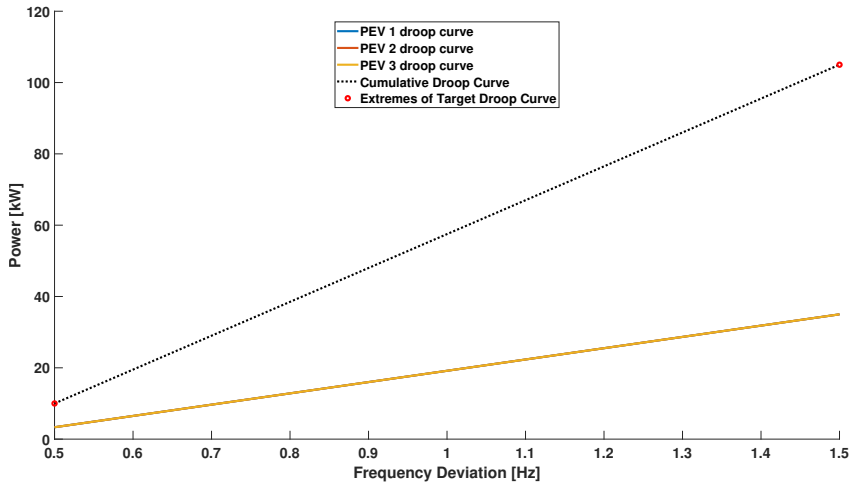

Figure 3.49: Scenario 1, balanced conditions: resulting local and global droop curves.

The algorithm determines the optimal distribution as an equal allocation of droop curves between the charging session. The target droop curve is identified in the plot with the red-dashed line, instead the resultant droop curve is represented by the black-dotted line. Figure 3.49 shows that the sum of the local curves matches exactly the target global one. The presence of the last term in the cost function determines an exact balancing of the frequency regulation service among the charging sessions, i.e., leading to identical local droop curves. Figure 3.50 shows the percentage of maximum usage of the power margin of each vehicle, i.e., the ratio between the value of the local droop curve corresponding to the frequency deviation Δf_{max} and the available margin of power. This plot confirms what already discussed: the algorithm distributes the effort in order to assign the same maximum relative usage to each vehicle's power margin, in this case 70%.

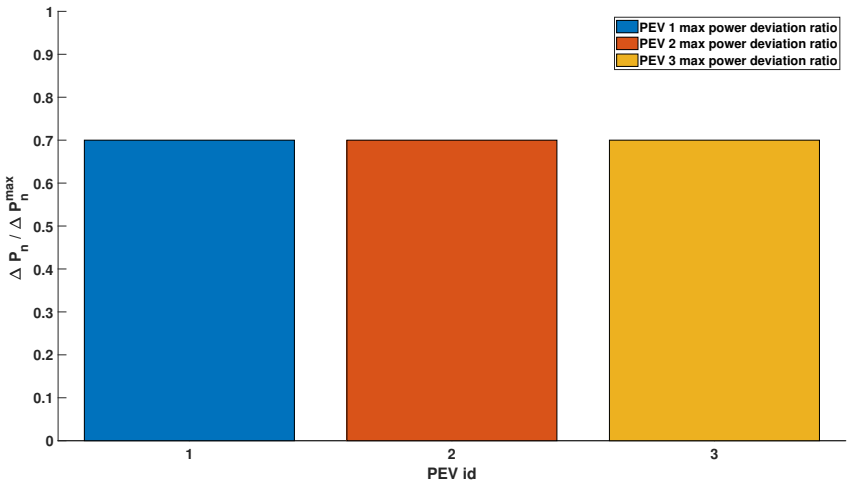

Figure 3.50: Scenario 1, balanced conditions: fraction of the maximum PEV power margin used for each PEV.

Typically, in smart charging, different charging power set-points are assigned to each charging session. As explained, this leads to different power margins, i.e., different levels of maximum contribution that could be provided by each PEV. This unbalance is considered by the proposed algorithm during the composition of the local droop curves. This is shown in the next simulation, which assumes three charging sessions characterized by different power margins, as summarized in Table 3.9.

Table 3.9: Charging sessions.

PEV ID	$P_{n,k}$ [kW]	P_n^{max} [kW]	e_k [%]	d_k [%]
1	75	150	10	10
2	50	100	10	10
3	25	50	10	10

The global droop curve that has to be composed is characterized by a a maximum droop value of 75 kW, i.e., 50% of the overall available margins. Note that all the charging sessions are performed at the 50% of maximum power, so they are characterized by different absolute power margins, $\Delta P_{n,k}$, but by the same percentage margin.

Figure 3.51 displays the droop curves assigned to each vehicle.

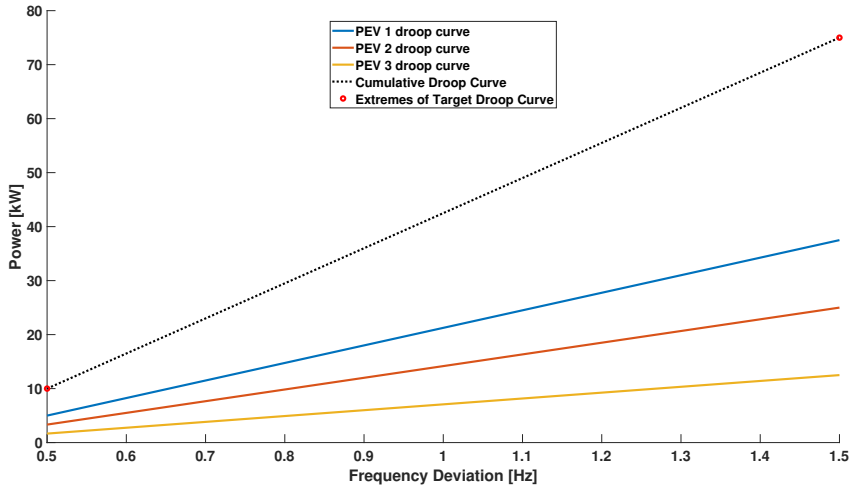

Figure 3.51: Scenario 1, different power margins: resulting local and global droop curves (request of 50% of the overall power margins).

The algorithm allocates the curves in order to distribute the relative effort equally between the sessions. Figure 3.52 highlights the equal distribution.

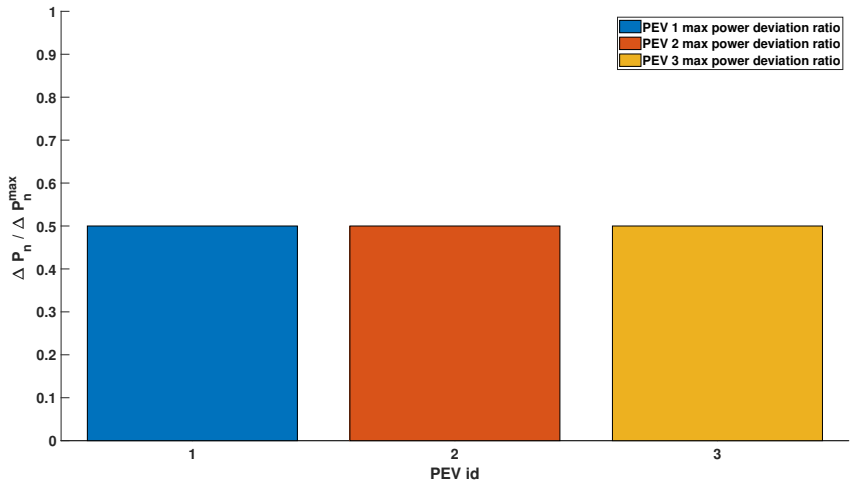

Figure 3.52: Scenario 1, different power margins: fraction of the maximum PEV power margin used for each PEV (request of 50% of the overall power margins).

It is interesting to see the result of the same simulation, when the overall max-

imum power deviation increases. The same simulation is now performed with a maximum global droop curve value of 105 kW, i.e. 70% of available margins. The increased request of power could be accomplished using the same strategy as before, so splitting the effort equally between the sessions. This strategy does not consider the fact that an equal distribution of power margins will impose a steeper droop curves to the sessions with larger margins, with a negative impact on the battery system. A steeper curve means a more aggressive response of the battery system to the frequency variations, with the consequently stress on power electronics and its effects on the battery temperature and cells health. The strategy presented in this work instead takes into account also the curve slope $m_{n,k}$ and the intercept $q_{n,k}$. As a result, the system distributes the additional effort needed to reach the new target droop curve less equally (Figure 3.54) but fair distributes the power electronics stress (Figure 3.53).

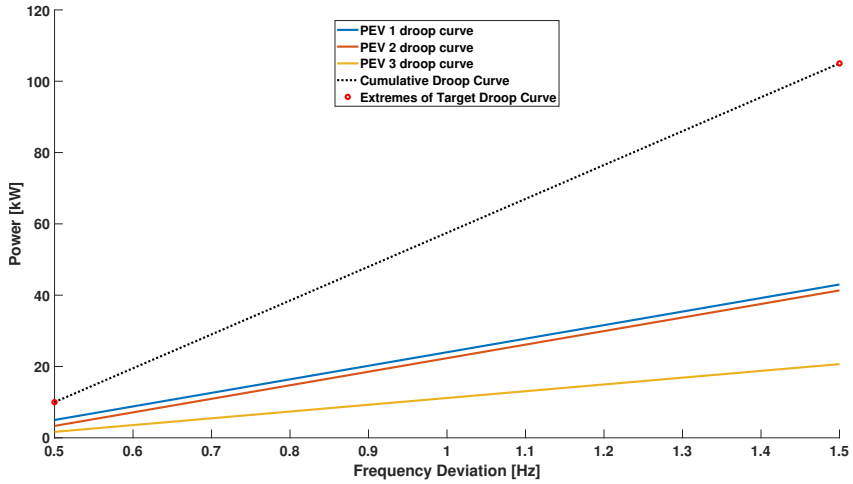

Figure 3.53: Scenario 1, different power margins: resulting local and global droop curves (request of 70% of the overall power margins).

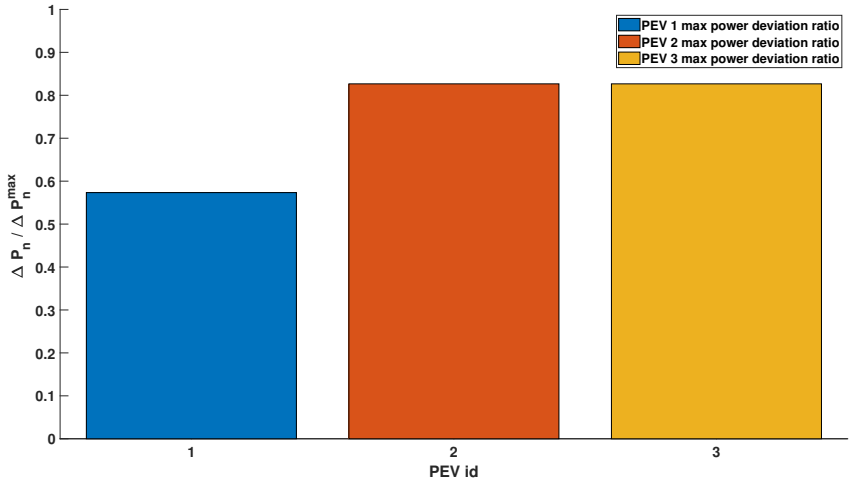

Figure 3.54: Scenario 1, different power margins: fraction of the maximum PEV power margin used for each PEV (request of 70% of the overall power margins).

Scenario 2: Local Droop Curves Assignment in an Unbalanced Scenario The interconnection between the smart charging and the frequency regulation service is done by considering the charging preferences expressed by the driver, i.e., the desired final state of charge and the charging time. Summarizing what already discussed about the target function (3.86), the algorithm gives a priority in the assignment of droop curves to the PEVs with grater state of charge error and/or a shorter dwelling time (i.e., to those PEVs that will benefit from an increase in the charging rate).

The simulations presented below will illustrate the capability of the designed algorithm to link the droop curve assignment with the charging status and the user preferences.

The balanced scenario is now re-proposed, but this time with different state of charge errors and dwelling times for the three PEVs. Table 3.10 summarizes the charging session status at the time when the proposed algorithm for allocating local droop curves is run.

PEV 1 is characterized by the grater SOC error, followed by PEV 2. The algorithm recognizes this condition and prioritizes the assignment of power to these two vehicles. The prioritization is in turn weighted by the respective SOC error.

Table 3.10: Charging sessions.

PEV ID	$P_{n,k}$ [kW]	P_n^{max} [kW]	e_k [%]	d_k [%]
1	150	100	80	10
2	150	100	40	10
3	150	100	30	10

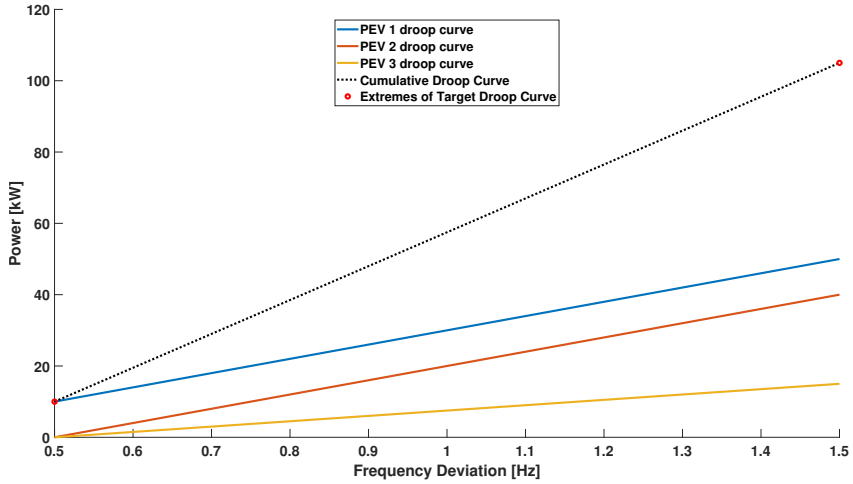

Figure 3.55: Scenario 2, balanced margins and unbalanced SOC errors: resulting local and global droop curves (request of 70% of the overall power margins).

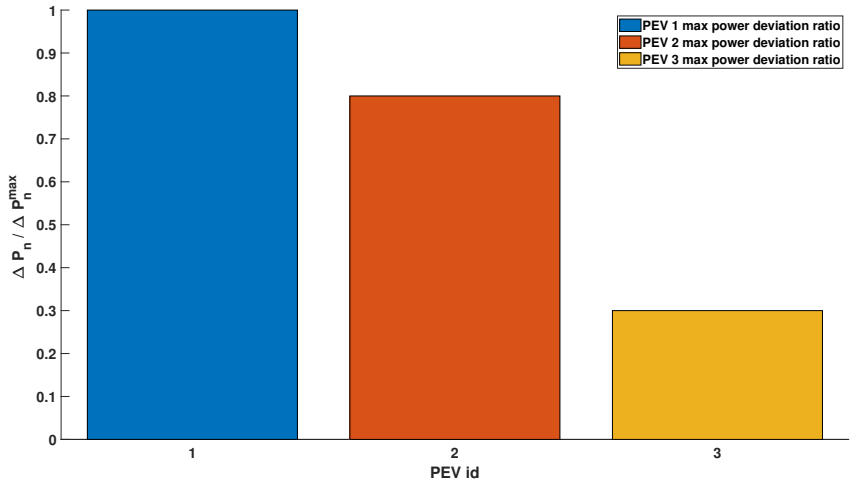

Figure 3.56: Scenario 2, balanced margins and unbalanced SOC errors: fraction of the maximum PEV power margin used for each PEV (request of 70% of the overall power margins).

The SOC error is one of the two charging preferences taken into account in the droop curve assignment. In the above simulation, the dwelling time was the same for the three PEVs. Figures 3.57 and 3.58 show the case in which the PEVs 1 charging session, characterized by a SOC error of 80%, is also characterized by a remaining dwelling time of 50%. In this case, the SOC error prioritization is compensated by the available dwelling time, so the algorithm identifies as optimal strategy to equal distribute the effort between the vehicles.

Notes on the Computational Complexity of the Algorithm The optimization problem associated to the proposed algorithm is linear. Quadratic cost functions could be also used for this kind of problem, as they are an efficient choice in terms of effort distribution (e.g., the third term in the objective function could be replaced by the term $\alpha_3 m_{n,k}^2$, and similarly the last two terms). However, quadratic problems are more complex, and require more computational resources than linear ones.

Considering that this algorithm is designed to work in conjunction with a smart charging system that updates the charging set points with a rate of minutes, and considering the amount of power needed for the participation to the frequency regulation services (e.g. in Italy, the Pilot Project *fast reserve* requires at least $5MW$ of aggregated power [3]), we have to face the issue of finding the solution of a large scale optimization problem in a short amount of time. For this reason, I decided to opt for a linear formulation. To test the scalability of the proposed algorithm, several simulation have been performed considering 100000 contemporary charging sessions. The solution time was always between 30 and 50 seconds, which is acceptable, in view of integrating the proposed algorithm with the smart charging algorithm.

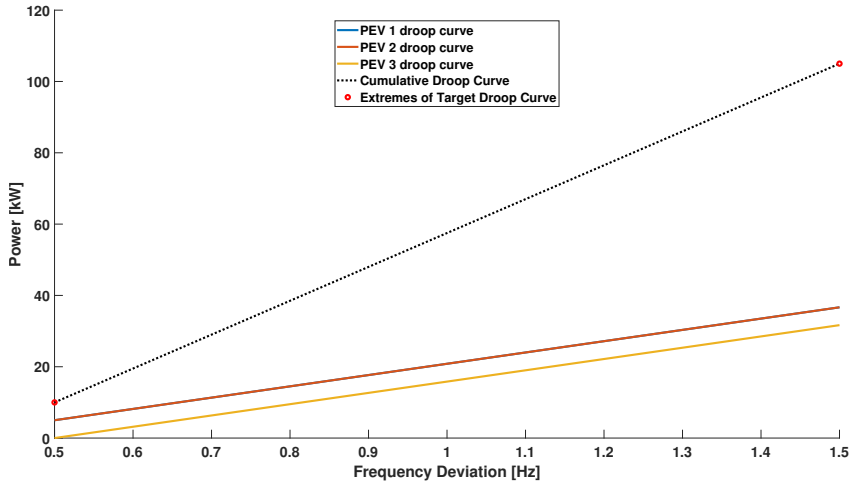

Figure 3.57: Scenario 2, balanced margins and unbalanced SOC errors and dwelling times: resulting local and global droop curves (request of 70% of the overall power margins).

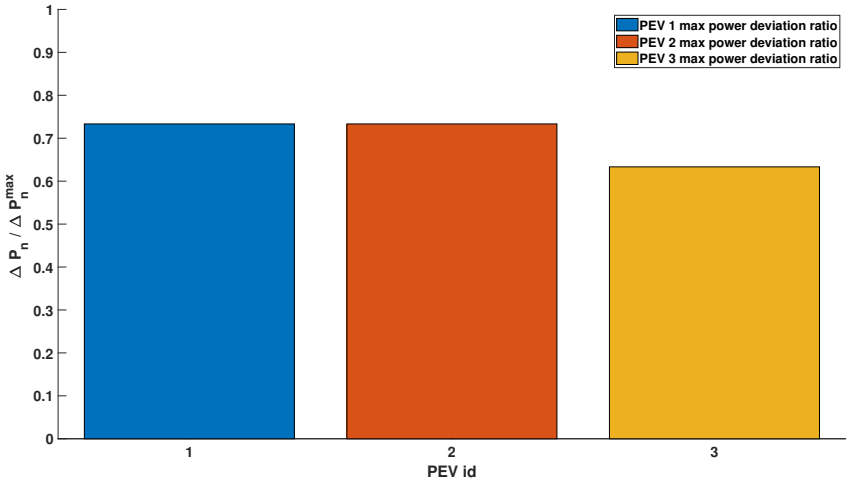

Figure 3.58: Scenario 2, balanced margins and unbalanced SOC errors and dwelling times: fraction of the maximum PEV power margin used for each PEV (request of 70% of the overall power margins).

3.2.2.6 The delay budget problem

In order to enable PEVs to the frequency regulation functions, some very strict constraints on the delay between the occurrence of the frequency disturbance and the actuation of the control signal by the EVSEs power unit on the PEVs have to be considered. In particular, the Pilot Project Fast Reserve requires an initial response from the PEVs within 300ms from the occurrence of the frequency disturbance event, and a full response of the system (the end of the transient and the establishment of a steady-state at the frequency-dependent power setpoint) within 1s.

As detailed in Fig. 3.59, and having in mind the proposed architecture in Fig. 3.41, the system in the first 300ms from the frequency disturbance event (happening at time t_0) have to:

- measure, through the frequency meter, the frequency disturbance;
- transmit it to the Master Control Agent hosted in the 5G MEC;
- the Master Control Agent has to propagate this frequency measure between all the Local Control Agents;
- the Local Control Agents have to compute the updated setpoints;
- the Local Control Agents have to communicate the new setpoints to the Control Units of the EVSEs.

Then, from $t_0 + 300$ms to $t_0 + 1$s, the PEVs must completely actuate the new power setpoints.

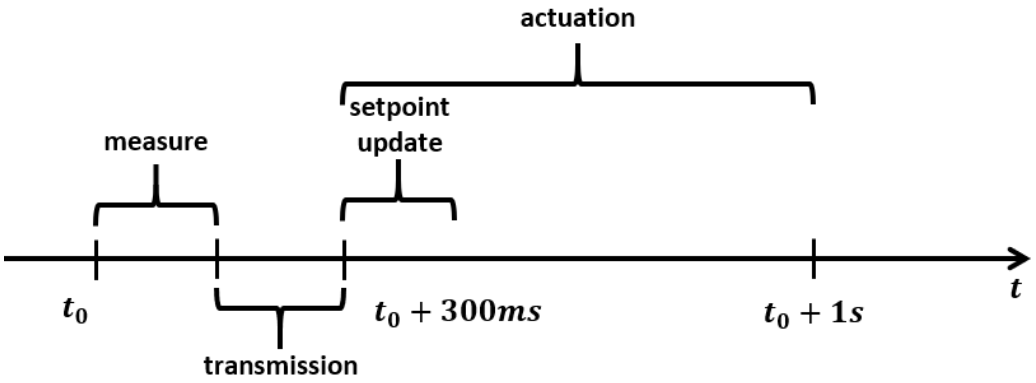

Figure 3.59: Delay Budget

Considering the frequency meters available on the market, it is possible to estimate a measurement delay in the order of few hundreds of milliseconds (usually 100ms-200ms), while the computation of the new setpoints, as explained in section 3.2.2.4, can be very simple, and so executed in less than a millisecond, or more advanced, and so executed in few dozen of milliseconds.

The transmission delay is a critical factor in the total delay budget, since the system components must receive the frequency measure well in advance of t_0+300ms, so to have time to process it and to update the power setpoints. Then, a maximum communication delay must be guaranteed by telco operators, as the TSO requesting the services may apply penalties to the CPO for not providing the service within the time constraints.

Using wired telecommunication technologies, this delay can be in the order of few milliseconds (for optic fiber), or in the order of dozen of milliseconds (for copper wires), that is in line frequency regulation service requirements. However, considering the dispersed nature of the EVSEs, this kind of solutions may be very expensive for the CPO, implying a cost that may be considerably high compared to the investment needed to install a frequency meter inside each EVSE.

Moreover, most of the EVSEs are nowadays connected through cellular networks to their back-end, so, in principle, it is possible to exploit the cellular connectivity already present on the EVSEs. However, the current cellular telecommunication technologies used by the EVSEs (3G, 4G) do not provide enough performances in terms of latency (or guaranteed latency) to perform such tasks. Indeed, 3G and 4G technologies have a end-to-end communication latency respectively in the order of hundreds of milliseconds and about 50-100 milliseconds. 3G communication delay occupies almost all (or even more than) the available time, while 4G latency may not guarantee that there is enough time for measurement and for computation. Moreover, both the technologies do not support slicing, so the overall performances and the end-to-end delay (at least on the radio access part of the network) cannot be guaranteed easily. On the contrary, 5G communication technologies further reduced the radio access delay (to few of milliseconds) as well as the end-to-end delay with a

novel fronthaul/backhaul/core network architecture made of Virtual Network Functions. Moreover, 5G introduces network slicing, so the telco operator may provide an exclusive slice of its communication resources to the CPO's frequency regulation system. Finally, 5G architecture introduced, as explained in section 3.2.2.3, the MEC at the edge of the radio access network. Indeed, deploying Master Control Agent module inside MEC, it is possible to communicate with the frequency meter and to the Local Control Agent with negligible delays (in the order of few milliseconds), making feasible the provisioning of frequency regulation services with PEVs.

Finally, since the EVSEs already have a modem installed, the only cost for the CPO is to replace it with a 5G-compatible one. This cost for the CPO is justified also by the obsolescence of older communication technologies, that may be discontinued in the next few years, forcing the CPO to change in any case the EVSEs modems.

3.2.2.7 Concluding remarks

This section has presented how plug-in electric vehicles can participate in the frequency regulation ancillary service provisioning. In this work, the reference scenario, the systems and actors involved are presented and discussed showing how the roles of CPOs and DSO will be expected to evolve in the next few years. The work provided a control architecture that exploits the novel 5G network architecture and its very low-latency. The section focused on the superposition between smart charging services and frequency regulation services, providing three different strategies and discussing their properties, pros and cons. The section also provided a deep discussion on the integration between the frequency regulation service, the ICT infrastructure and charging, measuring and communication components, providing quantitative considerations on the system feasibility also analysing the effects of different ICT technologies on the service quality.

This section has also presented a novel control algorithm for enabling the participation of smart charging plug-in electric vehicles (PEVs) to the provisioning of frequency regulation services. This has a positive value for the grid, providing an additional source of flexibility to ensure grid stability, and for the PEV drivers as well, providing to them an additional stream of revenues, which will lower the cost of ownership of the PEVs. The proposed algorithm computes local frequency-power droop curves, one for each active charging session. These curves specify how the charging power setpoint should be changed in real time, in response to frequency deviations from the nominal value. The local curves computation takes into account the real time status of the charging sessions (in terms of time left until the end of the charging session, current SOC, and energy left to charge), which is fundamental to ensure that the frequency regulation service is interdependent and harmonized with the smart charging service, and thus transparent to the PEV user. The superimposition of the local droop curves has to match a desired load area droop curve, which specify how the PEVs in the load area should collectively react to a frequency deviation. In this way, the aggregate of PEVs can provide frequency regulation ser-

vices to the market. Numerical simulations have shown that the proposed algorithm is effective in assigning local droop curves in a fair way, which takes into account the different status of the charging sessions. Also, the algorithm scales well, and is able to cope with aggregates of tens of thousands of PEVs. In future works, the proposed control strategy and its variants will be extended and tested using hybrid real/virtual test scenarios. The real components, such as 5G network nodes, charging infrastructures and measurement devices, will be used to validate the feasibility of the approach, while high-fidelity real time power network simulators will be used to analyse the impact of the service provisioning strategy.

3.2.3 Optimal Energy Storage System Placement for Robust Stabilization Against Dynamic Load Altering Attacks

Ancillary services are tools used by the Transmission System Operator to guarantee the secure operation of the transmission network. In section 3.2.2 I presented a strategy that exploits the e-mobility to support the network during frequency distortion events without specify the nature of the frequency distortion. In this section the investigation is focused on a particular situation in which the power imbalance is the effect of a malicious attack. This section presents a study on the "Dynamic Load Altering Attacks" (D-LAAs), their effects on the dynamics of a transmission network, and provides a robust control protection scheme, based on polytopic uncertainties, invariance theory, Lyapunov arguments and graph theory. The proposed algorithm provides as a result an optimal Energy Storage Systems (ESSs) placement, that minimizes the number of ESSs placed in the network, together with the associated control law that can robustly stabilize against D-LAAs. The work provides a contextualization of the problem and a power network subject to D-LAAs modelling approach suitable for the designed robust control protection scheme. The robust control protection scheme criteria is identified with the technological application. The work proposes a reference scenario for the study of the dynamics of the control actions and their effects in different cases, and different numerical simulations for the validation of the approach on large networks.

Nomenclature

Table 3.11: Nomenclature

Symbols	Meaning
δ	Voltage phase angle at generator buses
ω	Frequency deviation at generator buses
ϕ	Frequency deviation at load buses
M	Inertia matrix of the generators
n, m	number of generators and load buses
$\mathcal{M}_a, \mathcal{M}_p$	sets of vulnerable and secure buses
$\mathcal{M}_p^*$	optimal placement
$\mathcal{E}$	sets of transmission line
$\mathcal{M}_g$	Set of generation nodes
D, D^L	Damping coefficient matrices for the generators and loads
P^L	Power consumption at load buses
K^P, K^I	Generator controller gain matrices
K^{LG}	Attack gain matrix
α	Decrease rate of the Lyapunov function
u_{max}	Bound on the ESS power norm
Z	Impedance Matrix
$\mathbf{0}_n, \mathbf{1}_n$	Column vectors of zeros and ones of size n

3.2.3.1 Introduction

With the evolution of power systems towards more complex, intelligent, and dynamical systems, the power network has become a critical Cyber Physical System (CPS) in which the interaction of the physical domain with the ICT component of the system plays an evermore important role.

The digital innovations that are at the basis of the smart grid paradigm, such as demand-side management [107, 108] and vehicle-to-grid services [109], introduced in the power network several vulnerabilities that allow for the design of new and sophisticated attacks [110, 111, 112], which may deteriorate the power quality or even interrupt the service provision.

Among such kind of cyber-attacks, Dynamic-Load Altering Attacks (D-LAAs) [113, 99] were designed to destabilise the network by controlling some compromised loads (e.g., electric vehicles, appliances, smart factories) in a coordinated way.

In this section, a control scheme to defend against D-LAAs, by using the flexibility offered by Energy Storage Systems (ESSs) is proposed. The proposed control strategy is structured into two phases: (i) the off-line optimal placement of ESSs over the buses of the protected transmission network; (ii) the synthesis of a on-line control law that assures the stability of the network against the set of considered D-LAAs.

The remainder of the section is organised as follows: Section 3.2.3.2 provides an overview of the related works in this topic; Section 3.2.3.3 presents the needed preliminaries on the network model and on D-LAAs, together with the design of the on-line stabilizing control law; Section 3.2.3.4 discusses the optimal placement strategy of the ESSs over the network; Section 3.2.3.5 provides a validation scenario where a destabilizing D-LAA is demonstrated on a simple test network in both an uncontrolled and a controlled setting; Section 3.2.3.6 presents the result of the optimal ESS placement over two standard test networks, the IEEE-14 and the IEEE-39, while Section 3.2.3.7 draws the conclusions and highlights future works.

3.2.3.2 Related Works

CPSs are a contact point between computer science and control theory. Due to the deep linkage between the cyber and the physical domains that characterize CPSs, properties such as stability and robustness are typically studied together with concepts such as data integrity and intrusion detection.

The concept of security is of the utmost importance in the CPSs literature, as several critical systems such as utility networks, transport infrastructures and even healthcare systems have been modelled as CPSs. In general, a secure CPS provides guarantees on both the integrity of its data handling pipeline and on the safety of its physical process. In order to assure the safe operation of a CPS it is typically required to design a controller able to maintain certain critical quantities (e.g., temperature, voltage, pressure, ...) within some operative bounds, even when the CPS is subject to some form of adverse attack or event.

In this direction, CPSs have been widely modeled and studied as linear time-invariant descriptor systems [114, 111, 115] that describe, with differential equations and algebraic constraints, their dynamics. By properly designing the inputs and disturbances of such systems, researchers were able to model a wide range of attacks that may affect a CPS [111], such as state attacks (e.g., actuator or physical attacks), output attacks (e.g., data injection attacks) and even integrity attacks that compromise the control logic of a portion of a CPS.

The cyber-attacks I consider in this work are the so-called Dynamic-Load Altering Attacks (D-LAAs) [99], a complex dynamical attack that follows a control logic to employ a set of compromised electrical loads (e.g., loads that were part of a demand-side management program) with the aim of steering the transmission network towards instability. Several works studied such attacks, from both the defendant [116, 117] and attacker perspective [118], highlighting how the diffusion of demand-side management programs and large-scale controllable loads, such as smart factories and EV fleets, may introduce into the network a significant vulnerability.

This section proposes a control scheme to defend against D-LAAs, by using the flexibility offered by (ESSs). The proposed control strategy is structured into two phases: (i) the off-line optimal placement of ESSs over the buses of the protected transmission network; (ii) the synthesis of a on-line control law that assures the stability of the network against the set of considered D-LAAs;.

3.2.3.3 Preliminaries

This section reports some useful definitions and results that are required in the following analysis.

Definition 3.1. A Polytopic Linear Differential Inclusion (LDI) system is defined as [119]:

$$\dot{x} = A(\zeta)x + B(\zeta)u, \tag{3.90}$$

where

$$\zeta \in Z = \{[\zeta_1, \zeta_2, ..., \zeta_p]^T \mid \zeta_i \geq 0 \quad \forall i \ \in [1, p], \ \sum_{i=1}^{p} \zeta_i = 1\} \tag{3.91}$$

models the system uncertainties and the matrices $A(\zeta), B(\zeta)$ are elements of the convex hull of a finite set of known "vertex" matrices $A_i, B_i, i \in [1, p]$, i.e.:

$$A(\zeta) = \sum_{i=1}^{p} \zeta_i A_i, B(\zeta) = \sum_{i=1}^{p} \ \zeta_i B_i.$$

Definition 3.2. A Linear Time Invariant Switched Systems with arbitrary switching signal $\phi(t) : \mathbb{R}^+ \to S = \{1, 2, ..., s\}$ is defined as a system of the form [120, 121]:

$$\dot{x} = A_i x + B_i ui = \phi(t).$$

When modelling an uncertain system as a polytopic LDI system, one possible approach to study its asymptotic stability is related to the existence of a so-called "Common" Lyapunov Function [122]. In fact, to assure the asymptotic stability of a system of the form (3.92) under a state feedback $u = Kx$, it is sufficient to prove that, for any symmetric matrix $Q > 0$, there exist a single symmetric matrix $P > 0$ such that:

$$(A(\zeta) + B(\zeta)K)^T P + P(A(\zeta) + B(\zeta)K) = -Q, \forall \zeta \in Z, \tag{3.92}$$

which, due to the polytopic nature of the matrix uncertainties, is equalent to the existance of a symmetric matrix $P > 0$ that satisfies:

$$(A_i + B_i K)^T P + P(A_i + B_i K) < 0, \ \forall i \in [1, p]. \tag{3.93}$$

Furthermore, it is worth remarking that common quadratic Lyapunov functions (CQLFs) are also typically used to prove the quadratic, and hence asymptotic, stability of switched systems of the form (3.92) with analogous arguments and conditions of the ones reported above [120].
Quadratic stability and stabilizability of switched linear systems with polytopic uncertainties under state feedback has received a considerable amount of attention [123, 124, 125]. In general, the existence of a CQLF is only sufficient for the asymptotic stability and could hence be rather conservative, but the algebraic conditions

required to assure the existence of a CQLF for the switched system considered can not be trivially derived [121]. In the following, I will resort to numerical analysis to evaluate the existence of a CQLF for the system and the consequent feasibility of the related optimisat ion problem.

Definition 3.3. Given a symmetric matrix $P > 0$, the ellipsoid

$$\mathcal{E}(P) = \{x \in \mathbb{R}^n : x^T P^{-1} x \leq 1\} \tag{3.94}$$

centered at the origin of a linear system is said to be *invariant attractive* [126] for the closed loop system

$$\dot{x} = (A + BK)x \tag{3.95}$$

if for any $x_0 \in \mathcal{E}(P)$ the evolution of the system remains in $\mathcal{E}(P)$ and ultimately tends to the origin.

In this work the following theorem from [126] will be utilised:

Theorem 3.1. *Let P, Y be solution of following semidefinite programming problem:*

$$\max tr(P) s.t. \begin{bmatrix} AP + PA^T + BY + Y^T B^T & P \\ P & -I/\alpha \end{bmatrix} < 0, \begin{bmatrix} P & Y^T \\ Y & u_{max}^2 I \end{bmatrix} \geq 0$$

in the matrix variables $P = P^T$ and Y, with $\alpha > 0$. Then:

i) the control $u = Kx$, where $K = YP^{-1}$ asymptotically stabilizes the system (3.95),

ii) u is bounded on the ellipsoid $\mathcal{E}(P)$ so that $||u|| \leq u_{max}$,

iii) $V(x) = x^T P^{-1} x$ is a Lyapunov function for (3.95)

iv) the ellipsoid $\mathcal{E}(P)$ is the one that maximises the sum of its squared semiaxes among all the invariant ellipsoids of the system (3.95) over which $V(x)$ decreases not slower than $-\alpha \, ||x||^2$.

Preliminaries on Dynamic-Load Altering Attacks In this work, I will design a controller to defend against D-LAAs, which were originally introduced in [99]. This kind of attack is aimed at destabilising the transmission network by controlling some vulnerable loads in a closed loop fashion. This feedback can be obtained by the attacker by exploiting compromised network equipment. It was shown in [99] that a properly defined dynamic attack law is able to steer the network towards instability, in a limited amount of time.

In the work is proposed a state feedback controller to robustly stabilize transmission networks against D-LAAs, by employing Energy Storage Systems (ESSs) to provide a regulating action on the network. To this end, it was shown that a transmission network vulnerable to a set of D-LAAs of the form $P_v^{LV}(t) = -K_{vs}^{LG}(t)\omega_s(t)$ can be modelled as the parametric linear time variant system:

$$\begin{bmatrix}\dot{\delta}\\ \dot{\theta}\\ \dot{\omega}\end{bmatrix} = A\begin{bmatrix}\delta\\ \theta\\ \omega\end{bmatrix} + Bu =$$

$$= (A_1 + A_2)\begin{bmatrix}\delta\\ \theta\\ \omega\end{bmatrix} - \begin{bmatrix}0\\ (-D^L)^{-1}\\ 0\end{bmatrix}\bar{u}_T, \tag{3.96}$$

with

$$A_1 = \begin{bmatrix}0 & 0 & I\\ (-D^L)^{-1}L_{lg} & (-D^L)^{-1}L_{ll} & 0\\ M^{-1}(L_{gg}+K^I) & M^{-1}L_{gl} & M^{-1}(D+K^P)\end{bmatrix} \tag{3.97}$$

and

$$A_2 = \begin{bmatrix}0 & 0 & 0\\ 0 & 0 & (-D^L)^{-1}K^{LG}(t)\\ 0 & 0 & 0\end{bmatrix}, \tag{3.98}$$

The network model is the result of a DC linearization [127], a linearization technique based on the following assumptions:

- angular differences are small

$$|\delta_i(t) - \theta_j(t)| \ll 1 \ \forall L_{gl}(i,j) \neq 0$$
$$|\theta_i(t) - \theta_j(t)| \ll 1 \ \forall L_{ll}(i,j) \neq 0;$$

- the network is lossless;
- the network is equipotential;
- the swing equations are linearized.

L is the Laplacian matrix of the diagraph representation of the network

$$L = \left[\begin{array}{c|c} \overbrace{L_{gg}}^{(n\times n)} & \overbrace{L_{gl}}^{(n\times m)} \\ \hline \underbrace{L_{lg}}_{(m\times n)} & \underbrace{L_{ll}}_{(m\times m)} \end{array}\right]$$

is composed by the following blocks:

- L_{gg} is *diagonal*;
- L_{gl} contains nonzero-elements in correspondence to a direct generator bus - load bus connection;

- L_{lg} is the transpose of L_{gl};
- L_{ll} represents the load bus connections.

The model (3.96) takes into account the sensitivities of the load to the frequency variations using the diagonal damping matrix D^L, similarly the generators damping are modelled through diagonal matrix D. The inertia of the power system is represented by the diagonal matrix M in which each element is characterized by the inertia associated to the respective generator. In what follows, we assume that the speed control of each generator can be modeled as a PI control, thereafter, K^P and K_I entries represent, respectively, the integral and proportional controller coefficients of the generators at all generator buses [127]. Using a parametric uncertainties model approach, the transition matrix A can be split in two parts, the nominal dynamics of the network, indeed not subject to attacks, and the second part, which introduces the dynamics of the attacks and their impacts on the dynamics of the whole system. Respectively, the nominal and the attacked dynamics are represented by matrices A_1 and A_2.

It is worth noting that the matrix K^{LG} is a sparse matrix whose non-zero elements K_{vs}^{LG} represent the gains of the ongoing attacksD-LAAs. It is then possible to define an uncertainty range, as the various K_{vs}^{LG} that characterise every possible attack are bounded as in [99] by the amount of vulnerable load available on the node $v \in \mathcal{M}_a$, and by the availability of the measure of the frequency deviation at the generator node s. Due to the structure of (3.96), all possible uncertain dynamical matrices of system (3.98) lie in the compact set that is obtained by the product of the compact sets over which the various gains of the potential D-LAAs range. The convex hull of such set can be easily characterised by its vertices, as each vertex represent a distinct combination of the various possible D-LAAs each of which taken with its maximum gain K_{vs}^{LG}. Since all possible D-LAAs can be written as a convex combination of these vertices, it follows that the system (3.96) can be seen as a Polytopic Linear Differential Inclusion system of form (3.92). Note that if we also include in the analysis the ability of the attacker to modify in real time the gains that define the D-LAA, the network dynamics will switch between matrices that are included in the same polytope.

The term $\bar{u}_T$ represents the input of the system. Physically, the inputs are the power deviations (injections or withdraws) with respect to the operative point around which the system (3.96) is linearized on the various buses. For our purpose, the input of the system, $\bar{u}_T$, can be split into two terms: $\bar{u}_T = P^L + u$, the term P^L represents the power consumption at load buses, that can be used by the attacker to induce a frequency deviation that then may feed a D-LLAs, and the component u representing the ESS controlled power that implements the state feedback control $u = Kx$ to robustly stabilize the network.

Due to the structure of (3.96), the effects of D-LAAs can be seen as a form of parametric uncertainty affecting the nominal transition matrix of the network A.

The system (3.96) is studied as a switched system with polytopic uncertainty, and utilising the results from [126] it was proven that it was possible to design a controller

of the form $u(t) = Kx(t)$ able to defend against the set of considered D-LAAs, provided that the controller knows which buses are vulnerable and is provided with an estimation of the maximum power that can be compromised by the attackers. To determine the value of the control gain K, it was sufficient to solve the optimization problem

$$\begin{aligned} \max_{P,Y,\alpha,\bar{u}_{max}} \quad & \gamma_1\ tr(P) - \gamma_2\ \bar{u}_{max}\ +\ \gamma_3\ \alpha \\ & \text{s. t.} \quad \forall i = 1, ..., p \\ & \begin{bmatrix} A_iP + PA_i^T + BY + Y^TB^T & P \\ P & -I/\alpha \end{bmatrix} < 0 \\ & \begin{bmatrix} P & Y^T \\ Y & \bar{u}_{max}I \end{bmatrix} \geq 0 \\ & P = P^T \end{aligned} \tag{3.99}$$

and set $K = YP^{-1}$, where $\gamma_1, \gamma_2, \gamma_3$ represent the relative weights that their corresponding objectives have in the optimisation being the size the ellipsoid, the control saturation and its stabilising performances. In (3.99) it was set $\bar{u}_{max} = u_{max}^2$ to avoid increasing the complexity of the problem by maintaining the linear nature of its constraints and objective function.

In light of Theorem 3.1, the function $V(x) = xP^{-1}x$ is a CQLF for all the systems whose dynamics are represented by the vertices $(A_i + BYP^{-1})$ of (3.96). It follows that the feedback $u = YP^{-1}x$ will asymptotically stabilize the network under attack, independently of which attack is being performed. Additionally, u will be bounded in norm by u_{max} over the ellipsoid $\mathcal{E}(P)$, where $V(x)$ will decrease with a rate not slower than $-\alpha||x||^2$.

In what was presented so far, it was implicitly assumed u to be unbounded. This assumption is in general unreasonable, as the control effort provided by the available ESSs is limited by their operative power limits. Furthermore, the matrix $K = YP^{-1}$ is in principle dense, meaning that a portion of the control effort (i.e. stabilising power) could be distributed on every load bus. In realistic scenarios the number and location of ESSs to be placed in the network will be limited to a few units and specific, secured, buses previously identified with the set $\mathcal{M}_p$. The details on how both of these limitations are addressed are presented in the following.

Recalling that $\mathcal{M}_p$ was defined as the set of secure buses available for the installation of ESSs, and noting that the presence of a row of zeros in the matrix Y translates by construction to the matrix K, it is possible to restrict the number and locations of the ESSs by adding to (3.99) a set of constraints that forces the rows of the matrix Y corresponding to buses not contained in $\mathcal{M}_p$ to be formed by zeros. Doing this guarantees that the corresponding elements of the control vector u are identically zero, and hence no ESSs shall be placed on such buses.

Regarding the control saturation, recall that Theorem 3.1 states that over the invariant ellipsoid the inequality $||u|| \leq u_{max}$ holds. Having a bound on the norm of the control relates to having a limited amount of installed ESS power, and con-

sequently u_{max} can be used as an indicator for the sizing of the distributed storages. In fact, to avoid power outages the network state shall never leave its region of safe operation $\mathbb{X}^S$, as a frequency deviation higher than an operative bound would cause the security mechanisms to stop the service provision. Ideally, the network operator would desire to have the invariant ellipsoid over which the CQLF decreases with its desired rated to be enclosed by $\mathbb{X}^S$, so that the system evolutions are guaranteed to remain in its safe region. On the contrary, attacks that start from initial conditions in $\mathbb{X}^S$ but outside the ellipsoid would be successful in driving the system to instability, as the control effort would saturate.
Furthermore, having a larger invariant ellipsoid implies either worse transient performances or a higher maximum control effort (i.e. larger ESSs), while having a smaller ellipsoid may restrict too much the region of attraction in which the system is robustly stable. Recalling the multi-objective nature of the problem (3.99), the operator may iterativevly tune the weights $\gamma_1, \gamma_2, \gamma_3$ to attain a ESSs control configuration that satisfies its requirements. Additionally, the network operator may fix any of the three variables that appear in the objective function of (3.99) (e.g. in scenarios in which the installed ESSs power is predetermined) and run the optimisation to derive the robust control law, in compliance with its use case limitations.

Future research will cover automatic parameter tuning, by means of analytical analysis of the system stable and operative regions characteristics. In fact, a crucial aspect for usage on real scenarios is a proper, and direct, way of mapping the operative requirements of the operator onto the design parameters of the controller.

Remark 3.1. *The proposed control scheme protects the network also against D-LAAs in which the attacker changes the exploited load buses, or attack charateristics, over time. In fact, such attacks can be seen as switching the dynamics of the network in the sense of definition 3.2. Noting that the dynamical matrix* (3.96) *switches between matrices that are contained in the polytope characterised by the vertices over which $V(x) = xP^{-1}x$ is a CQLF, from standard switched system arguments it follows that the stability properties of the closed loop system are maintained.*

A challenge is related to the fact that the matrix K is in principle dense, which has some technical implications related to the physical meaning of the product $Kx(t)$. In particular, to protect the network with the proposed strategy, one would need:

1. access to the state measurements on all of the network nodes, as the matrix K does not have any column of zeroes (i.e., the vector $x(t)$ is required in its entirety to compute $u = Kx(t)$);

2. the presence of an ESS on every network node, as the matrix K does not have any row of zeroes (i.e., the vector $u = Kx(t)$ does not have any structurally zero element).

These two limitations significantly impact the likelihood of deploying the control strategy, as the technological requirements imposed to the operator may be too

demanding, for both economic and logistic constraints. In a realistic scenario, the number of installed ESSs will be limited to a few units, and their possible locations will include a limited subset of secured buses, $\mathcal{M}_p$, previously identified.

Due to the particular structure of the closed form $K = YP^{-1}$, it is always possible to avoid the placement of a storage on a specific node by setting a constraint in the optimisation problem (3.99), to force the elements of the corresponding row of the matrix Y to be zero. The limitation affecting this strategy is related to the placement of the ESSs, as their position in the network may have a significant impact on the defence performance. In fact, it was assumed that the network operator was free to deploy a storage on each of the buses in the set $\mathcal{M}_p$, but the identification of an optimal criteria for determining such set remained, at this moment, an open problem.

This work aims at overcoming this limitation, and, to do so, the following subsection discusses a solution for the optimal placement of ESSs.

3.2.3.4 Problem Fomulation

Optimal ESSs placement The determine the optimal locations to install the ESSs, the transmission network is modelled as a weighted unidirectional connected graph, in which the weights are given by the impedance values of the lines between the buses/nodes. Our goal is to find a prioritisation criteria to sort the secured buses in the set $\mathcal{M}_p$ that are candidates to host an ESS and, to this end, I designed an ad-hoc value function.

The nature of D-LAAs is to modify the power load on the nodes dynamically, based on measurements from a subset of state variables. This attack modifies the direction of the power flow through the network, in order to excite the generators (recall that, in our setting, for its structure the attack is based on the frequency deviation at the generator buses) to the point where their frequency diverges outside its operative bounds. To defend against such an attack, the optimal storage placement shall take into account two different concepts, as the ESSs have to:

1. reduce the power flow deviation;
2. relieve the affected generators to support the synchronization.

The optimal configuration sought by the algorithm is then characterised by a certain number of ESSs distributed over the network, so that their distance from vulnerable buses (i.e. potential attacks) and generators are both minimised and balanced.

In fact, on the one hand, having ESSs displaced too far from the vulnerable buses would imply that that the contribution of the ESSs would be filtered by the power network, requiring a considerable control effort when the attack is located far from the defence/ESS location. On the other hand, having ESSs located near the generators allows to unload the on-board regulating systems of the generators, partially uncoupling the disturbances generated on the network from the self-regulating control actions.

Having set this criterion, is now need to define in our setting the concept of distance between two nodes. A natural quantity that serves the purpose of "electrical distance" when dealing with power networks is the minimum impedance observed on the paths that connect two nodes. To compute this quantity it is sufficient to employ off-line an implementation of the Dijkstra algorithm, whose complexity in the considered setting is treatable, as it is linear in the number of busses and linearithmic in the number of lines [128].

Having these concepts in mind, the value function has to capture the cumulative electrical distance (impedance) a given location has with respect to the set of vulnerable nodes and the generators. This can be obtained by setting, for every node $i \in |\mathcal{M}_p|$, a value index d_i:

$$\begin{aligned} d_i =& \rho_a \sum_{j|x_j \in M_a} \phi(Z,i,j) + \rho_g \sum_{j|x_j \in M_g} \phi(Z,i,j) \ \forall i \in |\mathcal{M}_p| \\ & \rho_g = 1 - \rho_a, \quad \rho_a \in [0,1] \end{aligned} \tag{3.100}$$

where $\mathcal{M}_a$ and $\mathcal{M}_g$ are the set of vulnerable and generator nodes respectively, $\phi(Z,i,j)$ is the minimum impedance between the nodes i,j, Z is the line impedance matrix and ρ_a and ρ_g are complementary coefficients that weight the operator's choice for the prioritization of the distance from vulnerable nodes and generators.

Having defined a value index d_i for every secured node in the network, it is now possible to sort and prioritise their locations for the optimal placement strategy. In the following, we will assume the nodes in $\mathcal{M}_p$ to be sorted in descending order according to their values of d_i.

Optimisation algorithm In the presentation above we neglected the aspects related to determining the minimum number of ESSs to be installed. The minimisation of ESSs is a crucial requirement for the operator, as their cost is not negligible. In order to find such minimum number, I propose an iterative procedure: starting from the empty set and adding to it, one by one, the remaining buses ordered according to their priority index d_i, find the minimum number of nodes for which (3.99) admits a solution.

In other words, iteratively increase $\mathcal{I}$ from 1 to $|\mathcal{M}_p|$, until

Algorithm 1:

Result: Storage placement and controller
Sort the nodes $i \in \mathcal{M}_p$ according to the value function (3.100)
Initialize: $\mathcal{I} = 1$; $x_i = 0 \ \forall$ nodes $i \in |\mathcal{M}_p|$
while $\mathcal{I} \leq |\mathcal{M}_p|$ **do**
  $x_i = 1 \ \forall i \leq \mathcal{I}$
  if (3.99) *has a solution* **then**
    $K = YP^{-1}$
    Output: Set of nodes for ESSs placement, given by $\mathcal{I}$;
    Defence control law, defined by its gain K
  else
    $\mathcal{I} \leftarrow \mathcal{I} + 1$
  end
end
Output: No placement protects from the given attacks

$$
\begin{aligned}
\max_{P,Y,\alpha,\bar{u}_{max}} \quad & \gamma_1 \ tr(P) - \gamma_2 \ \bar{u}_{max} \ + \ \gamma_3 \ \alpha \\
& \text{s. t.} \quad \forall i = 1, ..., p \\
& \begin{bmatrix} A_i P + P A_i^T + BXY + XY^T B^T & P \\ P & -I/\alpha \end{bmatrix} < 0 \\
& \begin{bmatrix} P & Y^T X^T \\ XY & \bar{u}_{max} I \end{bmatrix} \geq 0 \\
& P = P^T \\
& X \text{ is diagonal} \\
& X(i,i) = x_i \ \forall i \in \mathcal{M}_p \text{ and } X(i,i) = 0 \text{ otherwise} \\
& x_i \text{ binary} \\
& \sum_{i \in \mathcal{M}_p} x_i = \mathcal{I} \\
& x_i \geq x_j \text{ for } i > j
\end{aligned}
\tag{3.101}
$$

becomes feasible. The last two constraints model the prioritisation of nodes given by the values d_i (recall that we assumed the set $\mathcal{M}_p$ to be ordered), while the diagonal matrix X defines the structure of the controller: if the element (i,i) of the matrix X is zero, then the corresponding i^{th} row of the control as $U = Kx = XYP^{-1}x$ is zero, implying that no storage will be placed on node i.

The resulting algorithm is reported in Table 1.

Once the placement is completed and the matrix K is determined, the control law can be deployed to defend against D-LAAs in real time.

3.2.3.5 Real-Time Controller and D-LAA Validation Scenario

In this section we consider the *IEEE 9 bus test system* reported in Figure 3.60 to validate the proposed real-time defence control law and the capabilities of the D-LAAs. In particular, Section 3.2.3.5, at the beginning describes the scenario considered and details the attack sequence implemented, also demonstrating how the attack is able to de-stabilize the network in the uncontrolled case, while ends with a report on the effects of the proposed real-time control law for the protection of the network.

Reference Scenario From an attack point of view, we consider a scenario in which two different attacks are deployed: one on the node 5, driven by the frequency deviation of generator 1, and one on the bus 9, driven by the the frequency deviation of the generator 2. For our initial testing, I modified the standard network by adding the presence of one ESS on the node 7. The attack gains $-K_{vs}^{LG}$ are bounded respectively by the values of 20 and 10. In all the simulations we will consider attacks based on a measurements from all generator buses. The modeled sequence of attacks consists of the following:

1. an initial static load altering attack on nodes 5 and 9 of 0.1 $p.u.$, from time $t = 1s$ to $t = 2s$, to induce a non-negligible frequency deviation in the network;
2. a D-LAA on node 5 from time $t = 3s$ to $t = 12s$, with maximum attack gain;s
3. a D-LAA on node 9 from time $t = 7s$ to $t = 22s$, with maximum attack gain;
4. a static load altering attack on nodes 5 and 9 of 0.01 $p.u.$, from time $t = 21s$ to $t = 22s$, to further perturb the network;
5. two contemporary D-LAAs on nodes 5 and 9, respectively, from times $t = 21s$ and $t = 23s$, up to times $t = 36s$ and $t = 40s$, with their corresponding maximum attack gains.

Figure 3.61 reports the attack sequence: the first plot shows the time evolution of the static load altering attacks on nodes 5 and 9, while the second one represents the percentage of the attack gain for the D-LAA on node 5 and the last graph represents the same quantity for node 9.

Figure 3.62 shows how, for the uncontrolled case (i.e., when the ESS is deactivated), the D-LAAs, exploiting the frequency deviation generated by the initial Static Load Altering Attack (S-LAA) to steer the injection of power on the nodes in order to excite the controllers of the generators to induce an unstable behaviour in the network.

Figure 3.63 reports the magnitude of the attacks expressed in p.u., highlighting how power is injected in the network when the generator is in sub synchronous and vice versa. This counter-phase power injection, guided by a state feedback attack, is due to the unstable eigenvalues induced in the system by the D-LAAs [99] and

is able to destabilise the system in a few seconds. This can be esily seen from the comparison of the Figures 3.62 and 3.63, where it is possible to see that all the generators go out of the operational range ($|\omega_i| < 2$) [99] around $t = 9s$. I mention that the linearized model becomes inaccurate when the generators' frequencies are steered away from their nominal equilibrium values.

In what follows, we will consider a scenario in which an Anomaly detection system (IADS) [129, 130, 131] is utilised to detect ongoing attacks from the analysis of data coming from the Supervisory Control and Data Acquisition (SCADA) system to provide better situational awareness to the defence controllers. In this perspective, the ESSs are not utilised to regulate the network if an attack is not detected, as it is a reasonable assumption that ESSs are employed to only defend against ongoing attacks ands compensate significant frequency deviations. For this reason, the ESS are not to be considered as a virtual inertia to cover the normal network imbalance, but should be fed and maintained at some specific value of charge [131, 132], in order to be ready to interview in case of need.

Under the assumptions of the presence of IADS and the independence of the control action w.r.t. the SOC of the ESS, we are then able to demonstrate the effectiveness of the proposed state feedback controller.

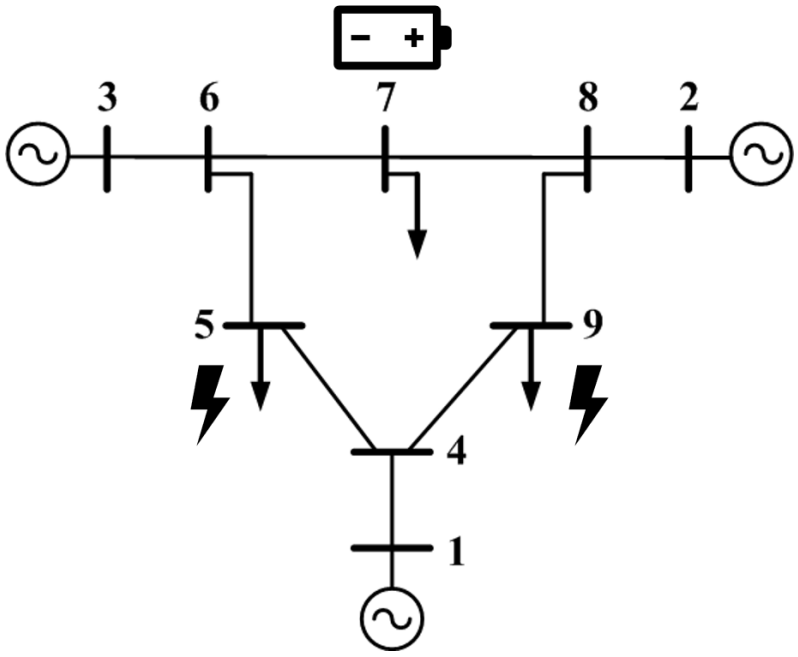

Figure 3.60: Modified IEEE 9 bus test system

Controlled scenario Activating the control action for the ESS on node 7, I demonstrate in this section that the network is successfully stabilised and the attack is compensated.

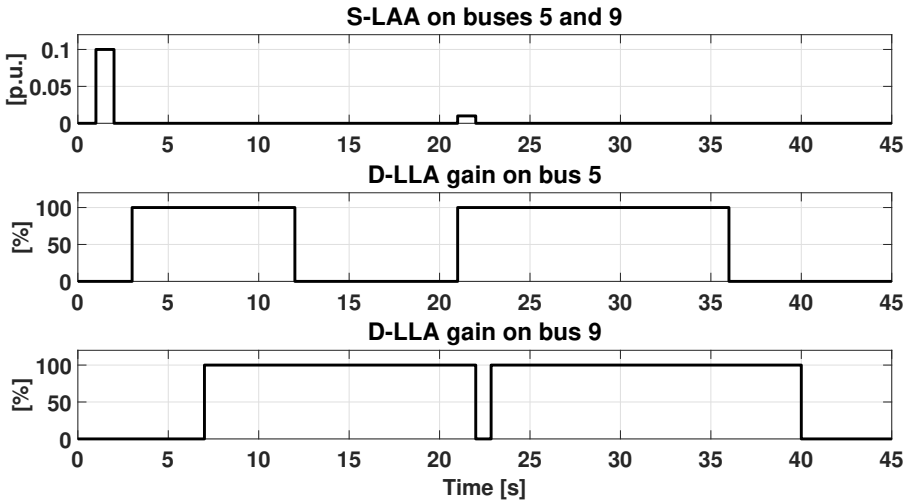

Figure 3.61: Attacks sequence on IEEE 9 bus test system

Figure 3.64 shows the frequency deviations on the generators, while Figure 3.65 shows the shape and the magnitude of the attacks. The presence of the pre-emptive S-LAA from $t = 1$ to $t = 2$ is designed in order to induce a initial unbalance in the network, so that the following D-LAAs will meet favourable conditions to be effective [99].

For the sake of presentation, we assume that the first S-LAA is not recognized as an attack by the IADS, implying that the ESS control is not activated. Exploiting the unbalance generated by the S-LAA an D-LAA starts on the node 5, driven by the frequency deviation arisen on generator 1 at time $t = 3s$. This attack (reported in the first plot of Figure 3.65) start to excite the unstable modes of the system (see the zoom in Figure 3.64), as at this stage the defense strategy is not yet activated. At $t = 7$, a second D-LAA arises on node 9, driven by the the frequency deviation measured on generator 2. In this scenario, we assume that the IADS recognises the ongoing attacks a time 7.5, activating hence the control. The effect of the control are related to the minimization of the frequency deviations that drive the attacks, meaning that, due to the state feedback nature of the D-LAAs, by regulating the network frequencies the ESSs are able also to annihilate the attacking power. I recall that the identified controller, obtained solving the optimization problem (3.99), asymptotically stabilizes the network robustly with respect to all the possible combinations of the considered D-LAAs. The rejection effect that the controller attains against the D-LAAs is shown in Figure 3.65.

Figure 3.66 reports the power injection on the controlled node 7: when at the time 7.5 the IADS recognizes the abnormal behavior, the controller is triggered. The measured frequency deviation generates a spike in the control effort, but after this peak has some regulating effects on the on-going attack, the control magnitude reduces significantly.

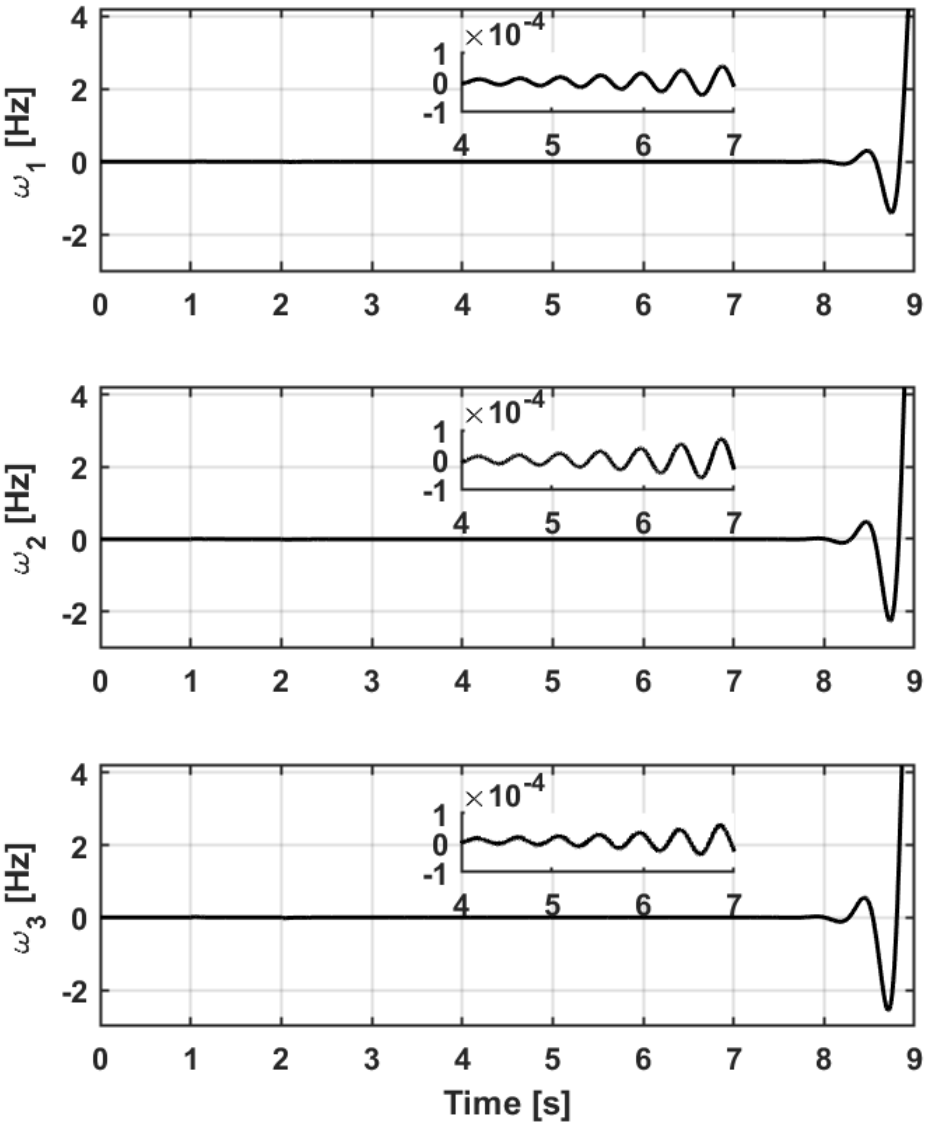

Figure 3.62: Frequency deviation of the uncontrolled IEEE 9 bus test system case

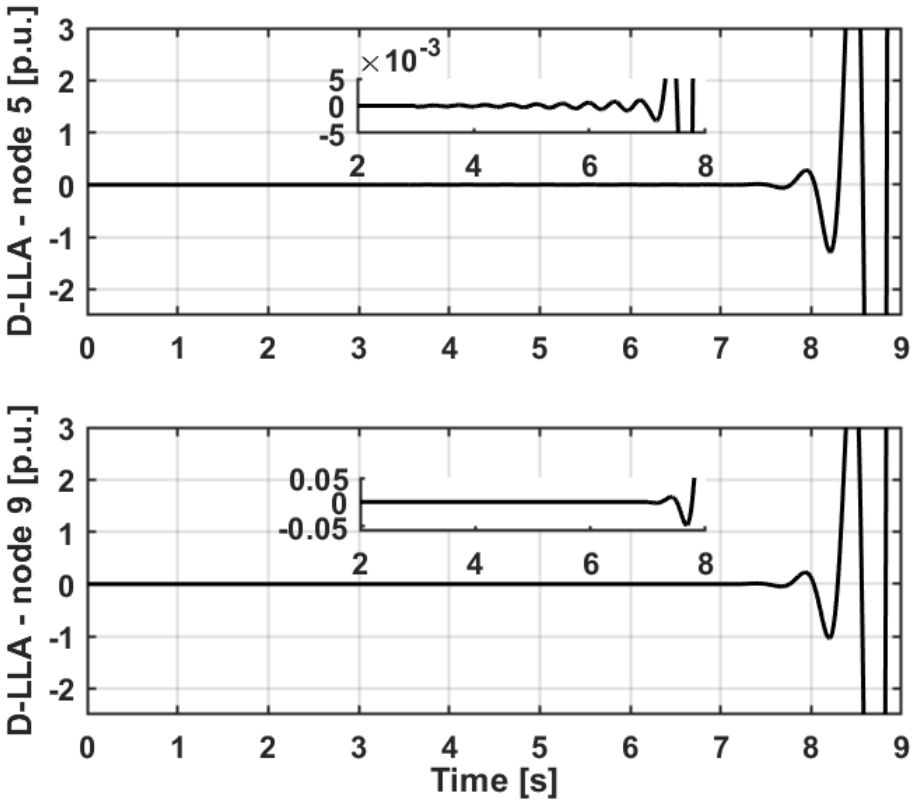

Figure 3.63: D-LAA magnitude of the uncontrolled IEEE 9 bus test system case. First plot shows the attack node 5, related to the frequency deviation ω_1 of generator 1, second plot shows the attack on node 9 driven by the frequency deviation ω_2 on generator 2

For the sake of comparison, Figure 3.67 reports the control action if the IADS is able to recognize the anomaly in a more efficient way, activating the control at time $t = 6s$.

An important difference between D-LAA and S-LAA resides in the fact that S-LAA are not able to move the eigenvalue of the network to the instability region [99], but they are still necessary to introduce a frequency deviation needed to activate the D-LAA. In the considered scenario, a second S-LAA is then applied from time $t = 21s$ to $t = 22s$ on nodes 5 and 9, with the purpose to create an addition frequency deviation to amplify the D-LAAs. Note that the defence strategy obtained from the optimization problem (3.99) is not designed to face S-LAAs, but the asymptotic stability property of the controlled system brings the induced frequency deviation to zero (see zoom in Figure 3.64 between time 20 and 25). The drawback of employing ESSs to respond to such attacks consists in the request of a non-negligible control effort from the ESS, as depicted by the spikes of Figure 3.66.

Simulations were performed using OPAL-RT 4510, a real-time digital simulator, which enables accurate validation of smart grid control algorithms. It is one of the reference simulation tools used in the electric power industries [133].

3.2.3.6 Simulations with optimal ESS placement

In this section I will demonstrate on two different network test systems (the IEEE-14 and the IEEE-39) the optimal ESS placement procedure to defend against the considered D-LAAs. With reference to Figures 3.68 and 3.69, we now consider three different classes of attacks:

1. YELLOW attacks: attacks that are spread all over the network
2. RED attacks: attacks that are concentrated in a single mesh of the network
3. PURPLE attacks: attacks that are concentrated on generation nodes.

The two Figures detail the attack locations on their corresponding test networks.

Unsecured IEEE-14 bus test system In our first testing the 14 bus test system IEEE will be used to test the placement algorithm. I bound the gains of all the attacks reported in 3.68 with a maximum value of 10^6. In particular, the attacks considered are color-coded as follows:

- YELLOW attacks, that are spread over the network, on nodes $2, 7, 11, 13$
- RED attacks, that are located in a single mesh, on nodes $10, 11, 13, 14$
- PURPLE attacks, that are on the generator buses, on nodes $1, 3, 6, 8$.

Tables 3.12 and 3.13 report the results of the optimal placement problem. In particular, in Table 3.12 YELLOW and PURPLE attacks are considered for various values of ρ_a and ρ_g. Overall, all proposed placements are similar, with minor changes

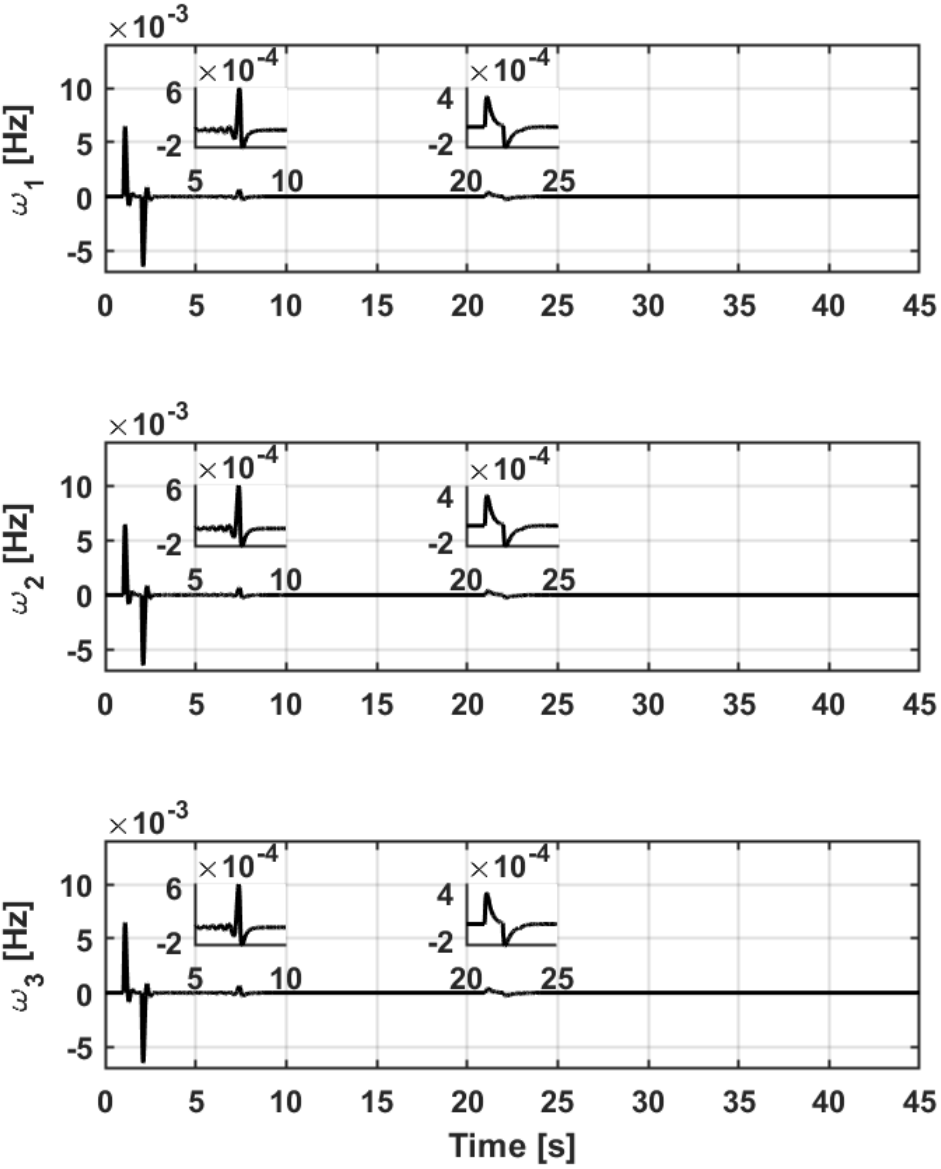

Figure 3.64: Frequency deviation of the controlled IEEE 9 bus test system case

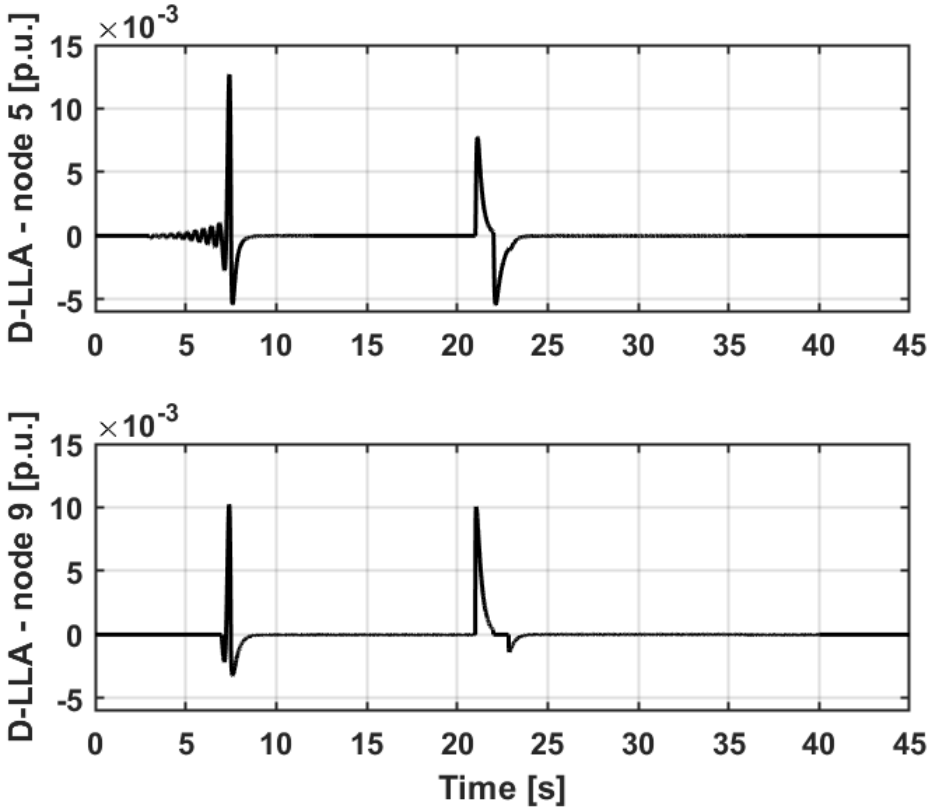

Figure 3.65: D-LAA magnitude of the controlled IEEE 9 bus test system case. First plot shows the attack node 5, related to the frequency deviation ω_1 of generator 1, second plot shows the attack on node 9 driven by the frequency deviation ω_3 on generator 3

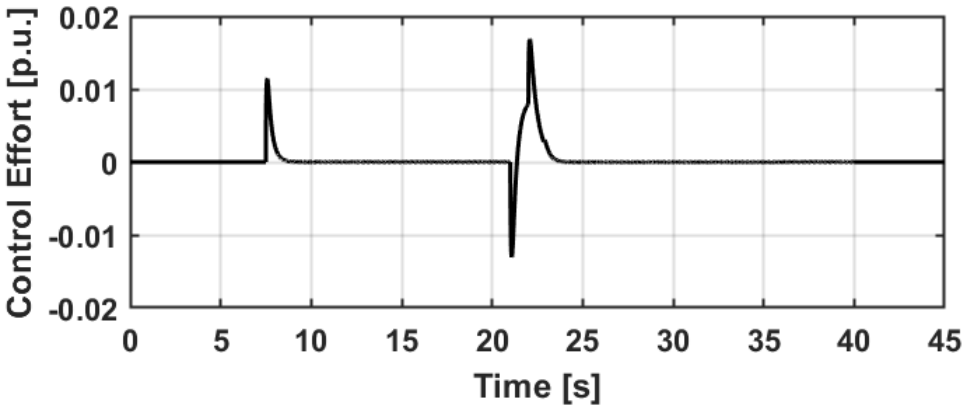

Figure 3.66: Control action on node 7

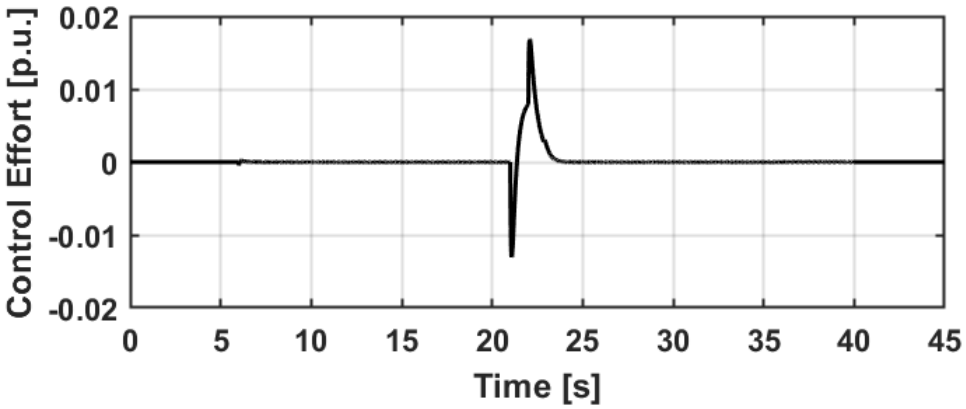

Figure 3.67: Control action on node 7 - efficient IADS

Weights		Yellow Attacks	Purple Attacks
ρ_a	ρ_g	$\mathcal{M}_p^*$	$\mathcal{M}_p^*$
1.0	0.0	{9,14}	{2,5,4}
0.7	0.3	{5,9}	{2,5,4}
0.5	0.5	{5,4}	{2,5,4}
0.3	0.7	{5,4}	{2,5,4}

Table 3.12: ESSs placement-14 bus-Yellow and PURPLE Attacks

Weights		Red Attacks
ρ_a	ρ_g	$\mathcal{M}_p^*$
1.0	0.0	{6,12,9}
0.7	0.3	{6,12,9}
0.5	0.5	{6,9}
0.3	0.7	{2,5,4}

Table 3.13: ESSs placement-14 bus-Red Attack

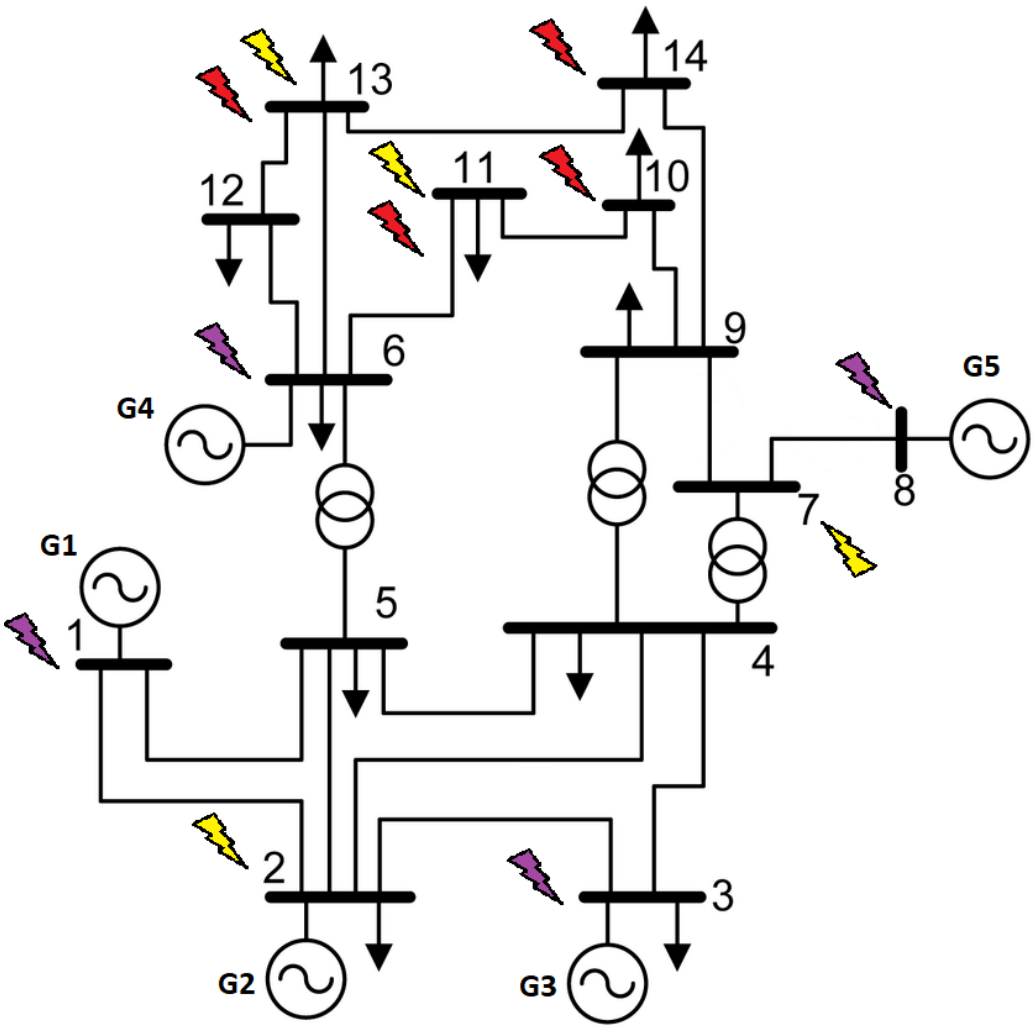

Figure 3.68: Unsecured IEEE-14 bus test system- In red, YELLOW and PURPLE the considered attacks.

in the prioritization of the busses due to the different definitions of d_i. The contribution of the weights ρ_a and ρ_g becomes more significant in the case of protection against RED attacks, as reported in Table 3.13. From the table, we can note how when the position of the generators is not considered (i.e., $\rho_g = 0$) the number of the ESSs required for the robust stabilization is 3, as the aggregation of the attacks drives the placement in a limited area with the intent of absorb/redirect the flows of power caused by the attack as soon as they start affecting the network. Balancing the weights (e.g., the case $\rho_a = \rho_g = 0.5$) the algorithm is able to find a solution that involves the presence of only 2 ESSs, placed on buses that divide the zone under attack (top) from the secure (bottom) one. Setting the weights as $\rho_a = 0.3$ $\rho_g = 0.7$ moves the *center-of-mass*, with respect to the electrical distance defined in (3.100), of the network in the lower portion of the network. As a consequence, the network is divided by the nodes 5 and 4 instead of 6 and 9, with the need of an additional protection on node 2 to better defend the generators.

Unsecured IEEE-39 bus test system To test the scalability of the algorithm, we now consider a larger scale power network. The target network is the IEEE-39 bus test system composed by 29 load buses and 10 generators, as shown in Figure 3.69. Two sets of attacks are considered, with the same color-coding as before: the RED attacks, concentrated on a single mesh, on nodes {1,3,4,9} with a maximum gain of 10^2; and the YELLOW attacks, spread all over the network, on nodes {9,13,22,27} with a maximum gain of 10^3. Similar to the previous case, several tests have been performed varying the weights ρ_a and ρ_g, Tables 3.14 and 3.15 summarize the results.

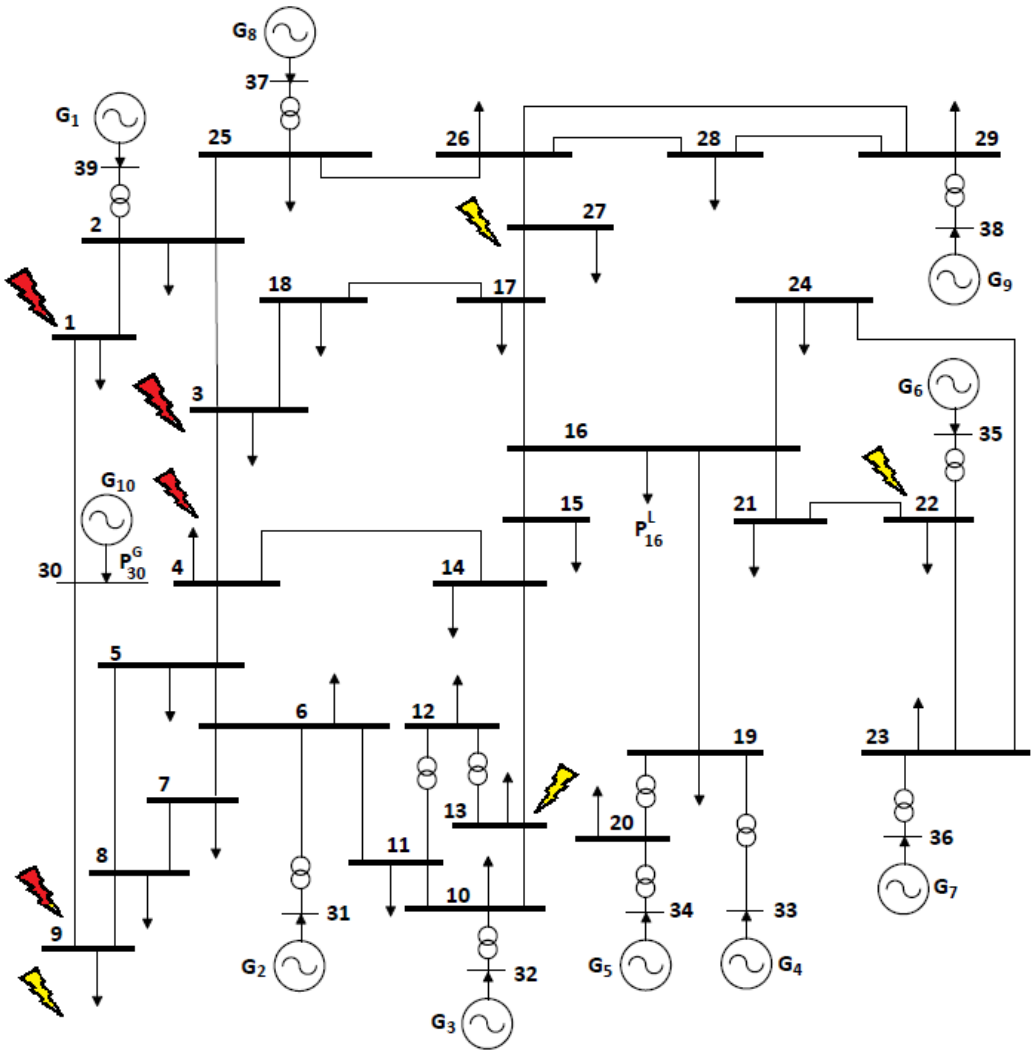

Figure 3.69: Unsecured IEEE-39 bus test system - In RED and YELLOW the considered attacks

Weights		Red Attacks
ρ_a	ρ_g	$\mathcal{M}_p^*$
1.0	0.0	{2,30, 8}
0.7	0.3	{2,30,14,5}
0.5	0.5	{2,14,25,15,30,26,18,5}
0.3	0.7	{14,2,15,2,26,27,29}

Table 3.14: ESSs placement-39 bus-RED Attacks

In the tables 3.14 and 3.15 we can see how the heavily distributed attacks (yellow)

Weights		Yellow Attacks
ρ_a	ρ_g	$\mathcal{M}_p^*$
1.0	0.0	{4,14,2}
0.7	0.3	{14,4,3}
0.5	0.5	{14,4,15,25}
0.3	0.7	{14,4,15,25}

Table 3.15: ESSs placement-39 bus-Yellow Attacks

can be compensated by a limited number of central nodes, whereas attacks that are focused on a specific mesh require more ESSs to separate the portion of the network under attack from the secure part.

3.2.3.7 Concluding remarks

This section presented an optimization algorithm to determine the optimal placement for Energy Storage Systems (ESSs), integrated with a control law based on Polytopic Linear Differential Inclusion system theory and Lyapunov-Invariance, to protect a transmission network vulnerable to Dynamic Load Altering Attacks. The designed algorithm exploits the geometrical structure of the attack to synthesize a defence control law for ESSs able to robustly stabilize the network against any combination of the considered attacks.

The optimal placement obtained was demonstrated to be able to protect the network against various types of attacks on both the IEEE-19 and the IEEE-39 networks. Future research will focus on a procedure for the optimal sizing of the invariance ellipsoid used to assure network stable operation, and the ensurance of component-wise constraints on the control effort replacing the bound on its norm assured in the present work. Automatic tuning of the design parameters of the controller will also be explored, to better support the network operator in satisfying its requirements. Future research directions involve the explicit inclusion of the ESS capacity and its state-of-charge-dynamics in the placement problem.

Chapter 4

Conclusion

This manuscript has presented the reasons and the story of my three years work of PhD. The thesis has provided a contextualization of the Electricity Energy Market and its next evolution. The manuscripts provides a panoramic on the new roles that the energy players will take on in the next periods and the associated potentialities.

Starting from these discussions, the opportunities introduced by the Electricity Energy Market are transformed in incremental case studies that gradually highlighted potentialities and obstacles. Each case study is faced and possible solution, from control algorithm and architectural points of view control are provided, accomplish with a critical analysis on the gaps, limitations and possible improvements associated to the proposed solution.

The flexibility is built from the bottom, so the works started with studies dedicated to the control of single load of the distribution network. The first work presented in this thesis dealt with the derivation and application of optimal control strategy for controlling the recharging of plug-in electric vehicles in a service area equipped with an energy storage system. The main result of this work is to provide a proof of concept on the effectiveness on the control applied on flexible loads for network benefits.

The concept of network interaction was delve into, the recharging of plug-in electric vehicles was modelled in a more actuated way and computational and privacy aspects, inherent in this situation, were take into account. The optimal control strategy was replaced with a real time decentralised control strategy for electric vehicles charging. The main result of this work is to show the potential of the proposed approach, which can be implemented in practice in scenarios where the sampling time of the control action is in the typical range of power systems metering and scheduling applications.

Until this point the network interaction is limited on a behaviour that the charging area try to maintain, in order to reduce as much as possible his impact on the network. The paradigm was changed and improved with a more intense interaction between the network and the load area. Using the same control strategy as before, the recharging of plug-in electric vehicles has modeled as a consensus with regularization optimization problem, increasing the efficiency in terms of user satisfaction and network interaction. Also the associated computational strategy was revised in order to guarantee the convergence of the associated optimization problem. The main result of this work is to jointly meet control requirements at load area level (reference charging power tracking) and at PEVs level (charging preferences and

privacy), showing a realistic example of network service provisioning at DSO level.

The results obtained were analysed not only by means of control theory perspective, the implementability of the proposed approaches was investigated. The computational effort related to the decentralized optimization algorithm has been preliminary assessed in terms of number of needed iterations to reach optimality and computation time, assuming zero communication latency among optimization agents.

Following, a control architecture suitable for the presented control strategy was designed and discussed. The discussion concerned on the limitations associated to the proposed distributed strategy and evaluation, supported by tests are reported. The evaluations concerned on the communication latency, that affects the computational time needed for the solving of the optimal control problem, and on the additional requirements, not modelled in the previous parts, related to the real application and international standard (ISO 15118).

The discussions I have gone through are related to the local ancillary service provisioning. The algorithms and the control architectures were extended to the global ancillary service provisioning. The discussion was focused on the Italian Market and regulations and was shown the consistency of the proposed strategy with. The analysis was supported also by representative simulations.

Starting from these results obtained on the Demand Side Management (DSM) service, the attention was move on the frequency regulation ancillary service provisioning. The reference scenario, the systems and actors involved are presented and discussed showing how the roles of CPOs and DSO will be expected to evolve in the next few years. I made a focus on the superposition between smart charging services and frequency regulation services, providing different strategies and discussing their properties, pros and cons, also in terms of ICT infrastructure and charging, measuring and communication components.

The section also provided a deep discussion on the integration between the frequency regulation service, the , providing quantitative considerations on the system feasibility also analysing the effects of different ICT technologies on the service quality. The work provided a control architecture that exploits the novel 5G network architecture and its very low-latency.

In this perspective I also presented a novel control algorithm for enabling the participation of smart charging plug-in electric vehicles (PEVs) to the provisioning of frequency regulation services taking into account the real time status of the charging sessions (in terms of time left until the end of the charging session, current SOC, and energy left to charge) and harmonized with the smart charging service, and thus transparent to the PEV users.

Finally, I investigated the possibility of integrating the current frequency regulation service not only to support the transmission network during normal operation but also in presence of malicious attacks. I presented an optimization algorithm to determine the optimal placement for Energy Storage Systems (ESSs) to protect a transmission network vulnerable to Dynamic Load Altering Attacks.

Glossary

Ancillary Service are the services necessary to guarantee the safety of the entire electricity system. They can, in principle, be classified into global ancillary services (or global services), if necessary for the safe operation of the national electricity system and into local ancillary services (or local services), if necessary for the safe operation of distribution networks only (or portions of them). They consist in a variation of the power injection/withdraw .

Balance Responsible Party Balance Responsible Party' (BRP) in the electricity market is a market participant or its chosen representative responsible for its imbalances (Commission Regulation (EU) 2017/2195 of 23 November 2017 establishing a guideline on electricity balancing, Article 2(7)). It is underlined in Article 17(1) and (2) of the said Regulation 2017/2195 that each BRP must strive to be balanced in real time, and that BRP is financially responsible for the imbalances to be settled with the connecting TSO..

Balancing Service Provider Balancing Service Provider (BSP) in the European Union Internal Electricty Market is a market participant providing balancing services to its Connecting TSO, or in case of the TSO-BSP Model, to its Contracting TSO. According to Article 2(6) of the Electricity Balancing Network Code (Commission Regulation (EU) 2017/2195 of 23 November 2017 establishing a guideline on electricity balancing - EBGL), Balancing Service Provider is a market participant with reserve-providing units or reserve-providing groups able to provide balancing services to Transmission System Operators (TSOs). Article 14(1) of the said Commission Regulation stipulates that each TSO is responsible for procuring balancing services from BSPs in order to ensure operational security..

Charging Point Operator is a company operating a pool of charging points. A Charging Point Operator provides value by connecting smart charging devices to E-mobility Service Provider.

Charging Station A system dedicated to the recharging of PEVs, hosting all the necessary equipment (breakers, protections, meters, controllers, transformers, etc.). The CS does not include the cable assembly necessary to connect the PEV to the CS..

Dispatching Service is the service aimed at maintaining the balance between the input and withdrawal of electrical energy, with necessary reserve margins. The service consists in activities aimed at issuing instructions for the coordinated use and operation of production plants, the transmission grid and ancillary services..

Disptatching Activity are the procurement and consequent provision of services necessary to ensure the safety of the national electricity system, as well as the regulation of economic items resulting from the execution of contracts and actual imbalances.

Distribution System Operator is the operating managers (and sometimes owners) of energy distribution networks, operating at low, medium and, in some member states, high voltage levels (LV, MV).

Electricity Energy Market is a system enabling purchases, through bids to buy; sales, through offers to sell; and short-term trading, of the electricity energy generally in the form of financial or obligation swaps. Bids and offers use supply and demand principles to set the price. Long-term trades are contracts similar to power purchase agreements and generally considered private bilateral transactions between counter-parties. .

Flexible Load is an asset or a group of assets that can modify electricity production or consumption in response to variability, expected or otherwise.

Frequency Regulation Services Automatic regulation to adapt the output of a generation unit following a frequency variation..

Transmission System Operator is the responsible for the reliable transmission of power from generation plants to regional or local electricity distribution operators (DSOs) by way of a high voltage electrical grid. Since TSOs are usually a natural monopoly, they are subject to state regulation. TSOs provide grid access to the electricity market players (i.e. generating companies, traders, suppliers, distributors and directly connected customers) according to non-discriminatory and transparent rules..

Bibliography

[1] "GME web page," https://www.mercatoelettrico.org/it/default.aspx, year = 2021. (Cited on pages vi, 6 and 8).

[2] "Next kraftwerke gmbh web page," https://www.next-kraftwerke.com/, year = 2021. (Cited on pages vi and 9).

[3] TERNA. Pilot project fast reserve. [Online]. Available: https://www.terna.it/en/electric-system/pilot-projects-pursuant-arera-resolution-300-2017-reel/fast-reserve-pilot-project (Cited on pages vii, 90, 92, 93, 98 and 110).

[4] European Parliament, Council of the European Union, "Communication from the commission to the european parliament, the council, the european economic and social committee and the committee of the regions - stepping up europe's 2030 climate ambition - investing in a climate-neutral future for the benefit of our people," 2020, https://eur-lex.europa.eu/legal-content/EN/ALL/?uri=CELEX:52020DC0562. (Cited on page 2).

[5] ——, "Regulation (EC) No 714/2009 of the European Parliament and of the Council of 13 July 2009 on conditions for access to the network for cross-border exchanges in electricity and repealing Regulation (EC) No 1228/2003," *Official Journal of the European Union*, vol. L 211, p. 15–35, 14.8.2009. [Online]. Available: https://eur-lex.europa.eu/legal-content/EN/ALL/?uri=CELEX:32009R0714 (Cited on page 2).

[6] European Commission, Directorate-General for Energy, "Commission Regulation (EU) 2017/2195 of 23 November 2017 establishing a guideline on electricity balancing (Text with EEA relevance.)C/2017/7774," *Official Journal of the European Union*, vol. L 312, p. 6–53, 28.11.2017. [Online]. Available: https://eur-lex.europa.eu/legal-content/en/ALL/?uri=CELEX:32017R2195 (Cited on page 2).

[7] European Parliament, Council of the European Union, "Directive 96/92/EC of the European Parliament and of the Council of 19 December 1996 concerning common rules for the internal market in electricity," *Official Journal of the European Union*, vol. L 27, p. 20–29, 30.1.1997. [Online]. Available: https://eur-lex.europa.eu/legal-content/EN/TXT/?uri=CELEX:31996L0092 (Cited on page 5).

[8] ——, "Directive (EU) 2019/944 of the European Parliament and of the Council of 5 June 2019 on common rules for the internal market for electricity and amending Directive 2012/27/EU," *Official Journal of the European Union*, vol. 158, p. 125–199, 14.6.2019. [Online].

Available: https://eur-lex.europa.eu/legal-content/EN/TXT/?uri=CELEX:31996L0092 (Cited on page 7).

[9] AREA, "Documento per la consultazione dell'Autorità ,322/2019/R/eel, Testo Integrato del Dispacciamento elettrico (TIDE) - Orientamenti complessivi," 23.7.2019. [Online]. Available: https://www.arera.it/allegati/docs/19/322-19.pdf (Cited on pages 7, 8, 73, 74, 89 and 90).

[10] ——, "Prima apertura del mercato per il servizio di dispacciamento (MSD) alla domanda elettrica edalle unità di produzione anche da fonti rinnovabili non già abilitate nonché ai sistemi di accumulo. Istituzione di progetti pilota in vista della costituzione del testo integrato dispacciamento elettrico (tide) coerente con il balancing code europeo," 5.5.2017. [Online]. Available: https://www.arera.it/it/docs/17/300-17.htm (Cited on pages 8, 73, 74, 77 and 80).

[11] "Terna web page," https://www.terna.it/en, year = 2021. (Cited on pages 8, 73 and 77).

[12] S. Koohi-Fayegh and M. Rosen, "A review of energy storage types, applications and recent developments," *Journal of Energy Storage*, vol. 27, p. 101047, 2020. [Online]. Available: https://www.sciencedirect.com/science/article/pii/S2352152X19306012 (Cited on page 12).

[13] M. Schücking, P. Jochem, W. Fichtner, O. Wollersheim, and K. Stella, "Charging strategies for economic operations of electric vehicles in commercial applications," *Transportation Research Part D: Transport and Environment*, vol. 51, pp. 173–189, 2017. (Cited on page 12).

[14] J. Neubauer and E. Wood, "The impact of range anxiety and home, workplace, and public charging infrastructure on simulated battery electric vehicle lifetime utility," *Journal of Power Sources*, vol. 257, pp. 12–20, 2014. (Cited on page 12).

[15] M. Neaimeh, S. D. Salisbury, G. A. Hill, P. T. Blythe, D. R. Scoffield, and J. E. Francfort, "Analysing the usage and evidencing the importance of fast chargers for the adoption of battery electric vehicles," *Energy Policy*, vol. 108, pp. 474–486, 2017. (Cited on page 12).

[16] T. Gnann, S. Funke, N. Jakobsson, P. Plötz, F. Sprei, and A. Bennehag, "Fast charging infrastructure for electric vehicles: Today's situation and future needs," *Transportation Research Part D: Transport and Environment*, vol. 62, pp. 314–329, 2018. (Cited on page 12).

[17] C. Bruni, F. Delli Priscoli, G. Koch, and I. Marchetti, "Resource management in network dynamics: An optimal approach to the admission control problem," *Computers & Mathematics with Applications*, vol. 59, no. 1, pp.

305–318, 2010. [Online]. Available: https://www.sciencedirect.com/science/article/pii/S0898122109004842 (Cited on page 13).

[18] A. Fiaschetti, V. Suraci, and F. D. Priscoli, "The shield framework: How to control security, privacy and dependability in complex systems," in *2012 Complexity in Engineering (COMPENG). Proceedings*, 2012, pp. 1–4. (Cited on page 13).

[19] M. S. Misaghian, M. Saffari, M. Kia, A. Heidari, P. Dehghanian, and B. Wang, "Electric vehicles contributions to voltage improvement and loss reduction in microgrids," in *2018 North American Power Symposium (NAPS)*, 2018, pp. 1–6. (Cited on page 13).

[20] A. Kavousi-Fard and A. Khodaei, "Efficient integration of plug-in electric vehicles via reconfigurable microgrids," *Energy*, vol. 111, pp. 653–663, 2016. (Cited on page 13).

[21] X. Wu, X. Hu, X. Yin, and S. J. Moura, "Stochastic optimal energy management of smart home with pev energy storage," *IEEE Transactions on Smart Grid*, vol. 9, no. 3, pp. 2065–2075, 2018. (Cited on page 13).

[22] P. Kou, Y. Feng, D. Liang, and L. Gao, "A model predictive control approach for matching uncertain wind generation with pev charging demand in a microgrid," *International Journal of Electrical Power & Energy Systems*, vol. 105, pp. 488–499, 2019. (Cited on page 13).

[23] P. Kou, D. Liang, L. Gao, and F. Gao, "Stochastic coordination of plug-in electric vehicles and wind turbines in microgrid: A model predictive control approach," *IEEE Transactions on Smart Grid*, vol. 7, no. 3, pp. 1537–1551, May 2016. (Cited on pages 13 and 41).

[24] E. Hossain, R. Perez, S. Padmanaban, and P. Siano, "Investigation on the development of a sliding mode controller for constant power loads in microgrids," *Energies*, vol. 10, no. 8, 2017. (Cited on pages 14 and 88).

[25] M. Lei and M. Mohammadi, "Hybrid machine learning based energy policy and management in the renewable-based microgrids considering hybrid electric vehicle charging demand," *International Journal of Electrical Power & Energy Systems*, vol. 128, p. 106702, 2021. (Cited on page 14).

[26] N. Kim, S. Cha, and H. Peng, "Optimal Control of Hybrid Electric Vehicles Based on Pontryagin's Minimum Principle," *IEEE Tran. on Control Systems Technology*, vol. 19, no. 5, pp. 1279–1287, Sep. 2011. (Cited on page 14).

[27] B. Heymann, J. F. Bonnans, P. Martinon, F. J. Silva, F. Lanas, and G. Jiménez-Estévez, "Continuous optimal control approaches to microgrid energy management," *Energy Systems*, vol. 9, no. 1, pp. 59–77, Feb 2018. (Cited on page 14).

[28] S. Xie, X. Hu, Z. Xin, and J. Brighton, "Pontryagin's minimum principle based model predictive control of energy management for a plug-in hybrid electric bus," *Applied Energy*, vol. 236, pp. 893–905, 2019. (Cited on page 14).

[29] H. Dagdougui, A. Ouammi, and R. Sacile, "Optimal control of a network of power microgrids using the pontryagin's minimum principle," *IEEE Transactions on Control Systems Technology*, vol. 22, no. 5, pp. 1942–1948, Sep. 2014. (Cited on page 14).

[30] C. Zheng, W. Li, and Q. Liang, "An energy management strategy of hybrid energy storage systems for electric vehicle applications," *IEEE Tran. on Sustainable Energy*, vol. 9, no. 4, pp. 1880–1888, Oct 2018. (Cited on page 14).

[31] A. Nguyen, J. Lauber, and M. Dambrine, "Optimal control based algorithms for energy management of automotive power systems with battery/supercapacitor storage devices," *Energy Conversion and Management*, vol. 87, pp. 410–420, 2014. (Cited on page 15).

[32] L. Redouane, A. Redouane, O. Mohamed, A. E. Hasnaoui, and I. E. Harraki, "Optimal control in micro grid system under state constraint," in *AIP Conference Proceedings*, vol. 2056, no. 1. AIP Publishing, 2018, p. 020017. (Cited on page 15).

[33] J. Yong and X. Y. Zhou, *Stochastic controls: Hamiltonian systems and HJB equations*. Springer Science & Business Media, 1999, vol. 43. (Cited on page 23).

[34] European Parliament, Council of the European Union , "Directive (EU) 2018/844 of the European Parliament and of the Council of 30 May 2018 amending Directive 2010/31/EU on the energy performance of buildings and Directive 2012/27/EU on energy efficiency (Text with EEA relevance)," *Official Journal of the European Union*, vol. L 156, p. 75–91, 19.6.2018. [Online]. Available: http://data.europa.eu/eli/dir/2018/844/oj (Cited on page 25).

[35] European Parliament, Council of the European Union, "Directive 2009/33/EC of the European Parliament and of the Council of 23 April 2009 on the promotion of clean and energy-efficient road transport vehicles (Text with EEA relevance)," *Official Journal of the European Union*, vol. L 120, p. 5–12, 15.5.2009. [Online]. Available: https://eur-lex.europa.eu/legal-content/EN/ALL/?uri=CELEX:32009L0033 (Cited on page 25).

[36] J. Kang, S. J. Duncan, and D. N. Mavris, "Real-time scheduling techniques for electric vehicle charging in support of frequency regulation," *Procedia Computer Science*, vol. 16, pp. 767–775, 2013, 2013 Conference on Systems Engineering Research. [Online]. Available: http://www.sciencedirect.com/science/article/pii/S1877050913000811 (Cited on page 25).

[37] A. Di Giorgio, F. Liberati, R. Germanà, M. Presciuttini, L. R. Celsi, and F. Delli Priscoli, "On the control of energy storage systems for electric vehicles fast charging in service areas," in *2016 24th Mediterranean Conference on Control and Automation (MED)*. IEEE, June 2016. [Online]. Available: https://doi.org/10.1109/med.2016.7535947 (Cited on pages 25 and 41).

[38] S. Deilami, A. S. Masoum, P. S. Moses, and M. A. S. Masoum, "Real-time coordination of plug-in electric vehicle charging in smart grids to minimize power losses and improve voltage profile," *IEEE Transactions on Smart Grid*, vol. 2, no. 3, pp. 456–467, Sep. 2011. (Cited on page 25).

[39] P. Richardson, D. Flynn, and A. Keane, "Local versus centralized charging strategies for electric vehicles in low voltage distribution systems," *IEEE Transactions on Smart Grid*, vol. 3, no. 2, pp. 1020–1028, June 2012. (Cited on page 25).

[40] D. T. Nguyen and L. B. Le, "Joint optimization of electric vehicle and home energy scheduling considering user comfort preference," *IEEE Transactions on Smart Grid*, vol. 5, no. 1, pp. 188–199, Jan 2014. (Cited on page 26).

[41] E. Sortomme and M. A. El-Sharkawi, "Optimal charging strategies for unidirectional vehicle-to-grid," *IEEE Transactions on Smart Grid*, vol. 2, no. 1, pp. 131–138, March 2011. (Cited on page 26).

[42] A. Di Giorgio, F. Liberati, and S. Canale, "Electric vehicles charging control in a smart grid: A model predictive control approach," *Control Engineering Practice*, vol. 22, pp. 147–162, 2014. (Cited on pages 26, 42, 43, 55 and 95).

[43] M. C. Kisacikoglu, F. Erden, and N. Erdogan, "Distributed control of pev charging based on energy demand forecast," *IEEE Transactions on Industrial Informatics*, vol. 14, no. 1, pp. 332–341, Jan 2018. (Cited on page 26).

[44] F. Liberati, A. Mercurio, L. Zuccaro, A. Tortorelli, and A. Di Giorgio, "Electric vehicles charging load reprofiling," in *22nd Mediterranean Conference on Control and Automation*, June 2014, pp. 728–733. (Cited on pages 26 and 42).

[45] C. L. Floch, E. C. Kara, and S. Moura, "Pde modeling and control of electric vehicle fleets for ancillary services: A discrete charging case," *IEEE Transactions on Smart Grid*, vol. 9, no. 2, pp. 573–581, March 2018. (Cited on page 26).

[46] F. Soares, P. R. Almeida, and J. P. Lopes, "Quasi-real-time management of electric vehicles charging," *Electric Power Systems Research*, vol. 108, pp. 293–303, 2014. [Online]. Available: http://www.sciencedirect.com/science/article/pii/S0378779613003210 (Cited on page 26).

[47] F. Mwasilu, J. J. Justo, E.-K. Kim, T. D. Do, and J.-W. Jung, "Electric vehicles and smart grid interaction: A review on vehicle

to grid and renewable energy sources integration," *Renewable and Sustainable Energy Reviews*, vol. 34, pp. 501–516, 2014. [Online]. Available: http://www.sciencedirect.com/science/article/pii/S1364032114001920 (Cited on page 26).

[48] A. Di Giorgio, A. Giuseppi, F. Liberati, and A. Pietrabissa, "Controlled electricity distribution network black start with energy storage system support," in *2017 25th Mediterranean Conference on Control and Automation (MED)*, July 2017, pp. 781–786. (Cited on page 26).

[49] A. Di Giorgio, A. Giuseppi, F. Liberali, A. Ornatelli, A. Rabezzano, and L. R. Celsi, "On the optimization of energy storage system placement for protecting power transmission grids against dynamic load altering attacks," in *2017 25th Mediterranean Conference on Control and Automation (MED)*, 2017, pp. 986–992. (Cited on page 26).

[50] J. Rivera, C. Goebel, and H.-A. Jacobsen, "A distributed anytime algorithm for real-time ev charging congestion control," in *Proceedings of the 2015 ACM Sixth International Conference on Future Energy Systems*, ser. e-Energy '15. New York, NY, USA: ACM, 2015, pp. 67–76. (Cited on page 26).

[51] S. Studli, E. Crisostomi, R. Middleton, J. Braslavsky, and R. Shorten, *Distributed Load Management Using Additive Increase Multiplicative Decrease Based Techniques*. Singapore: Springer Singapore, 2015, pp. 173–202. [Online]. Available: https://doi.org/10.1007/978-981-287-302-6_7 (Cited on page 26).

[52] B. Jiang and Y. Fei, "Decentralized scheduling of pev on-street parking and charging for smart grid reactive power compensation," in *2013 IEEE PES Innovative Smart Grid Technologies Conference (ISGT)*, Feb 2013, pp. 1–6. (Cited on page 26).

[53] O. Ardakanian, C. Rosenberg, and S. Keshav, "Distributed control of electric vehicle charging," in *Proceedings of the Fourth International Conference on Future Energy Systems*, ser. e-Energy '13. New York, NY, USA: ACM, 2013, pp. 101–112. [Online]. Available: http://doi.acm.org/10.1145/2487166.2487178 (Cited on page 26).

[54] W. Qi, Z. Xu, Z. M. Shen, Z. Hu, and Y. Song, "Hierarchical coordinated control of plug-in electric vehicles charging in multifamily dwellings," *IEEE Transactions on Smart Grid*, vol. 5, no. 3, pp. 1465–1474, May 2014. (Cited on page 26).

[55] X. Luo, S. Xia, and K. W. Chan, "A decentralized charging control strategy for plug-in electric vehicles to mitigate wind farm intermittency and enhance frequency regulation," *Journal of Power Sources*, vol. 248, pp. 604–614, 2014. (Cited on page 26).

[56] A. Malhotra, G. Binetti, A. Davoudi, and I. D. Schizas, "Distributed power profile tracking for heterogeneous charging of electric vehicles," *IEEE Transactions on Smart Grid*, vol. 8, no. 5, pp. 2090–2099, Sep. 2017. (Cited on page 26).

[57] P. Kong and G. K. Karagiannidis, "Charging schemes for plug-in hybrid electric vehicles in smart grid: A survey," *IEEE Access*, vol. 4, pp. 6846–6875, 2016. (Cited on page 26).

[58] M. Amjad, A. Ahmad, M. H. Rehmani, and T. Umer, "A review of evs charging: From the perspective of energy optimization, optimization approaches, and charging techniques," *Transportation Research Part D: Transport and Environment*, vol. 62, pp. 386–417, 2018. [Online]. Available: http://www.sciencedirect.com/science/article/pii/S1361920917306120 (Cited on page 26).

[59] Y. Shi, H. D. Tuan, A. V. Savkin, T. Q. Duong, and H. V. Poor, "Model predictive control for smart grids with multiple electric-vehicle charging stations," *IEEE Transactions on Smart Grid*, vol. 10, no. 2, pp. 2127–2136, March 2019. (Cited on page 26).

[60] G. Wenzel, M. Negrete-Pincetic, D. E. Olivares, J. MacDonald, and D. S. Callaway, "Real-time charging strategies for an electric vehicle aggregator to provide ancillary services," *IEEE Transactions on Smart Grid*, vol. 9, no. 5, pp. 5141–5151, Sep. 2018. (Cited on page 26).

[61] A. S. Gazafroudi, J. M. Corchado, A. Keane, and A. Soroudi, "Decentralised flexibility management for evs," *IET Renewable Power Generation*, vol. 13, pp. 952–960(8), April 2019. [Online]. Available: https://digital-library.theiet.org/content/journals/10.1049/iet-rpg.2018.6023 (Cited on page 26).

[62] E. Xydas, C. Marmaras, and L. M. Cipcigan, "A multi-agent based scheduling algorithm for adaptive electric vehicles charging," *Applied Energy*, vol. 177, pp. 354–365, 2016. [Online]. Available: http://www.sciencedirect.com/science/article/pii/S0306261916306286 (Cited on page 26).

[63] M. A. Tajeddini and H. Kebriaei, "A mean-field game method for decentralized charging coordination of a large population of plug-in electric vehicles," *IEEE Systems Journal*, vol. 13, no. 1, pp. 854–863, March 2019. (Cited on page 26).

[64] D. Mayne, J. Rawlings, C. Rao, and P. Scokaert, "Constrained model predictive control: Stability and optimality," *Automatica*, vol. 36, no. 6, pp. 789–814, 2000. [Online]. Available: http://www.sciencedirect.com/science/article/pii/S0005109899002149 (Cited on pages 27 and 43).

[65] C. Bruni, F. Delli Priscoli, G. Koch, A. Palo, and A. Pietrabissa, "Quality of experience provision in the future internet," *IEEE Systems Journal*, vol. 10, no. 1, pp. 302–312, March 2016. (Cited on page 28).

[66] A. Pietrabissa, F. Delli Priscoli, A. D. Giorgio, A. Giuseppi, M. Panfili, and V. Suraci, "An approximate dynamic programming approach to resource management in multi-cloud scenarios," *International Journal of Control*, vol. 90, no. 3, pp. 492–503, 2017. [Online]. Available: https://doi.org/10.1080/00207179.2016.1185802 (Cited on page 28).

[67] J. Borwein and A. S. Lewis, *Convex analysis and nonlinear optimization: theory and examples*. Springer Science & Business Media, 2010. (Cited on pages 30 and 40).

[68] European Parliament, Council of the European Union, "Directive 2012/27/EU of the European Parliament and of the Council of 25 October 2012 on energy efficiency, amending Directives 2009/125/EC and 2010/30/EU and repealing Directives 2004/8/EC and 2006/32/EC Text with EEA relevance," *OJ*, vol. L 315, p. 1–56, 25/10/2012. [Online]. Available: https://eur-lex.europa.eu/legal-content/EN/TXT/?uri=OJ:L:2012:315:TOC (Cited on page 41).

[69] European Parliament, Council of the European Union , "Directive (EU) 2018/2001 of the European Parliament and of the Council of 11 December 2018 on the promotion of the use of energy from renewable sources (Text with EEA relevance.)," *OJ*, vol. L 328, p. 82–209, 11/12/2018. [Online]. Available: https://eur-lex.europa.eu/legal-content/EN/TXT/?uri=OJ:L:2018:328:TOC (Cited on pages 41 and 89).

[70] S. Chowdhuri and A. Mukherjee, "Decision making on load management for plug-in hybrid electric vehicle in smart grid," in *2017 IEEE Calcutta Conference (CALCON)*, Dec 2017, pp. 288–291. (Cited on page 41).

[71] N. Thie, E. Junge, S. Hillenbrand, and M. Konermann, "Evaluation of grid compatible load management concepts for e-mobility in distribution grids," in *2019 54th International Universities Power Engineering Conference (UPEC)*, Sep. 2019, pp. 1–5. (Cited on page 41).

[72] M. A. Azzouz, M. F. Shaaban, and E. F. El-Saadany, "Real-time optimal voltage regulation for distribution networks incorporating high penetration of pevs," *IEEE Transactions on Power Systems*, vol. 30, no. 6, pp. 3234–3245, Nov 2015. (Cited on page 41).

[73] C. Wu, H. Mohsenian-Rad, J. Huang, and J. Jatskevich, "Pev-based combined frequency and voltage regulation for smart grid," in *2012 IEEE PES Innovative Smart Grid Technologies (ISGT)*, Jan 2012, pp. 1–6. (Cited on page 41).

[74] M. Zeraati, M. E. Hamedani Golshan, and J. M. Guerrero, "A consensus-based cooperative control of pev battery and pv active power curtailment for voltage regulation in distribution networks," *IEEE Transactions on Smart Grid*, vol. 10, no. 1, pp. 670–680, Jan 2019. (Cited on page 41).

[75] S. Han, H. Aki, and S. Han, "Optimal charging strategy of a pev battery considering frequency regulation and distributed generation," in *2012 IEEE Vehicle Power and Propulsion Conference*, Oct 2012, pp. 1014–1019. (Cited on page 41).

[76] K. R. Reddy and S. Meikandasivam, "Load flattening and voltage regulation using plug-in electric vehicle's storage capacity with vehicle prioritization using anfis," *IEEE Transactions on Sustainable Energy*, vol. 11, no. 1, pp. 260–270, Jan 2020. (Cited on page 41).

[77] S. Khatiri-Doost and M. Amirahmadi, "Peak shaving and power losses minimization by coordination of plug-in electric vehicles charging and discharging in smart grids," in *2017 IEEE International Conference on Environment and Electrical Engineering and 2017 IEEE Industrial and Commercial Power Systems Europe (EEEIC / I CPS Europe)*, June 2017, pp. 1–5. (Cited on page 41).

[78] S. Pazouki, A. Mohsenzadeh, S. Ardalan, and M. Haghifam, "Simultaneous planning of pev charging stations and dgs considering financial, technical,and environmental effects," *Canadian Journal of Electrical and Computer Engineering*, vol. 38, no. 3, pp. 238–245, Summer 2015. (Cited on page 41).

[79] R. Yu and Z. Ma, "A distributed charging coordination of plug-in electric vehicles based on potential game considering feeder overload constraint," in *2015 18th International Conference on Electrical Machines and Systems (ICEMS)*, Oct 2015, pp. 1114–1118. (Cited on page 41).

[80] S. Deb, P. Harsh, J. P. Sahoo, and A. K. Goswami, "Charging coordination of plug-in electric vehicle for congestion management in distribution system integrated with renewable energy sources," in *2018 IEEE International Conference on Power Electronics, Drives and Energy Systems (PEDES)*, Dec 2018, pp. 1–6. (Cited on page 41).

[81] M. Moghbel, M. A. S. Masoum, and F. Shahnia, "Coordinated charging of pevs in unbalanced residential network based on worst node voltage profile," in *2013 IEEE Power Energy Society General Meeting*, July 2013, pp. 1–5. (Cited on page 41).

[82] A. Hamidi, D. Nazarpour, and S. Golshannavaz, "Optimal scheduling of unbalanced distribution networks to improve the contribution of renewables and network balancing performance," in *2017 Iranian Conference on Electrical Engineering (ICEE)*, May 2017, pp. 1236–1241. (Cited on page 41).

[83] M. González Vayá and G. Andersson, "Self scheduling of plug-in electric vehicle aggregator to provide balancing services for wind power," *IEEE Transactions on Sustainable Energy*, vol. 7, no. 2, pp. 886–899, April 2016. (Cited on page 41).

[84] A. G. Fiorese, Y. R. Rodrigues, A. C. Z. de Souza, and M. C. Passaro, "On effects of pevs in islanded microgrids resilience," in *2019 IEEE PES Innovative Smart Grid Technologies Conference - Latin America (ISGT Latin America)*, Sep. 2019, pp. 1–6. (Cited on page 41).

[85] D. Wu, X. Ke, N. Radhakrishnan, and A. Reiman, "Optimization methods for evaluating pev charging considering customer behavior," in *2018 IEEE Power Energy Society General Meeting (PESGM)*, Aug 2018, pp. 1–5. (Cited on page 41).

[86] A. Kulvanitchaiyanunt, V. C. P. Chen, J. Rosenberger, P. Sarikprueck, and W. Lee, "A linear program for system-level control of regional phev charging stations," *IEEE Transactions on Industry Applications*, vol. 52, no. 3, pp. 2046–2052, May 2016. (Cited on page 41).

[87] A. Chiş, J. Lundén, and V. Koivunen, "Reinforcement learning-based plug-in electric vehicle charging with forecasted price," *IEEE Transactions on Vehicular Technology*, vol. 66, no. 5, pp. 3674–3684, May 2017. (Cited on page 41).

[88] K. K. Monfared, H. Iman-Eini, and R. Razi, "Control of single-phase bidirectional pev/ev charger based on fcs-mpc method for v2g reactive power operation," in *2019 10th International Power Electronics, Drive Systems and Technologies Conference (PEDSTC)*, Feb 2019, pp. 641–646. (Cited on page 41).

[89] M. Rahmani-Andebili and M. Fotuhi-Firuzabad, "An adaptive approach for pevs charging management and reconfiguration of electrical distribution system penetrated by renewables," *IEEE Transactions on Industrial Informatics*, vol. 14, no. 5, pp. 2001–2010, May 2018. (Cited on page 41).

[90] European Commission. (2012, 2015) FP7 - ICT. [Online]. Available: https://cordis.europa.eu/project/id/314328/es (Cited on page 41).

[91] Applied Research to Technologies (Ares2t). (2013). [Online]. Available: https://www.ares2t.com/wordpress/ (Cited on page 41).

[92] S. Boyd, N. Parikh, E. Chu, B. Peleato, and J. Eckstein, "Distributed optimization and statistical learning via the alternating direction method of multipliers," *Foundations and Trends in Machine Learning*, vol. 3, no. 1, pp. 1–122, 2011. [Online]. Available: http://dx.doi.org/10.1561/2200000016 (Cited on pages 42 and 45).

[93] A. Fiaschetti, V. Suraci, and F. Delli Priscoli, "The SHIELD framework: How to control security, privacy and dependability in complex systems," in *2012 Complexity in Engineering (COMPENG). Proceedings.* IEEE, June 2012. [Online]. Available: https://doi.org/10.1109/compeng.2012.6242962 (Cited on page 42).

[94] A. Di Giorgio, L. Zuccaro, G. Coppola, and F. Caleno, "Plug-in electric vehicles smart charging in italy: Control system architecture and field test results," in *2018 IEEE International Conference on Environment and Electrical Engineering and 2018 IEEE Industrial and Commercial Power Systems Europe (EEEIC / I CPS Europe)*, June 2018, pp. 1–5. (Cited on page 42).

[95] A. Di Giorgio, A. Giuseppi, R. Germanà, and F. Liberati, "Decentralised model predictive control of electric vehicles charging," in *2019 IEEE International Conference on Systems, Man, and Cybernetics, SMC 2019*, October 2019, pp. 1–7. (Cited on page 42).

[96] 5G-SOLUTIONS Consortium. (2019) H2020. [Online]. Available: https://www.5gsolutionsproject.eu/ (Cited on pages 42 and 88).

[97] I. S. 31, "Road vehicles — Vehicle to grid communication interface," International Organization for Standardization, Geneva, CH, Standard, 2019. (Cited on page 66).

[98] ENTSO-E, "High penetration of power electronic interfaced power sources (hpopeips)," no. March, p. 37, 2017. (Cited on page 72).

[99] S. Amini, F. Pasqualetti, and H. Mohsenian-Rad, "Dynamic load altering attacks against power system stability: Attack models and protection schemes," *IEEE Transactions on Smart Grid*, vol. 9, no. 4, pp. 2862–2872, 2016. (Cited on pages 82, 116, 117, 119, 121, 127, 128, 129 and 132).

[100] P. Kundur, N. J. Balu, and M. G. Lauby, *Power system stability and control*. McGraw-hill New York, 1994, vol. 7. (Cited on page 88).

[101] F. Liberati, A. D. Giorgio, A. Giuseppi, A. Pietrabissa, E. Habib, and L. Martirano, "Joint model predictive control of electric and heating resources in a smart building," *IEEE Transactions on Industry Applications*, vol. 55, no. 6, pp. 7015–7027, Nov. 2019. [Online]. Available: https://doi.org/10.1109/tia.2019.2932954 (Cited on page 88).

[102] U. Tamrakar, D. Shrestha, M. Maharjan, B. P. Bhattarai, T. M. Hansen, and R. Tonkoski, "Virtual inertia: Current trends and future directions," *Applied Sciences*, vol. 7, no. 7, 2017. [Online]. Available: https://www.mdpi.com/2076-3417/7/7/654 (Cited on page 88).

[103] C. Peng, J. Zou, and L. Lian, "Dispatching strategies of electric vehicles participating in frequency regulation on power grid: A review," *Renewable and Sustainable Energy Reviews*, vol. 68, pp. 147–152, 2017. [Online]. Available: https://www.sciencedirect.com/science/article/pii/S1364032116306426 (Cited on page 88).

[104] B. De Wachter (Elia /Project Team convenor), Gerard Doorman (Statnett), S. De Carlo (Terna), C. Neumann (TenneT), F. Paul Sapp (Amprion), K. Smolira (PSE), M. Ángel Martínez (REE), C. Payement (RTE), S. Heather (NG ESO), and M. Foresti (ENTSO-E), "Options for the design of European Electricity Markets in 2030 About ENTSO-E," no. March, 2021. [Online]. Available: https://eepublicdownloads.entsoe.eu/clean-documents/Publications/Market/Committee/publications/210331_Market_design2030.pdf (Cited on page 90).

[105] R. Germanà, F. Liberati, and A. Di Giorgio, "Decentralized model predictive control of plug-in electric vehicles charging based on the alternating direction method of multipliers," in *2020 28th Mediterranean Conference on Control and Automation (MED)*, 2020, pp. 739–745. (Cited on pages 95 and 98).

[106] J. Bezanson, A. Edelman, S. Karpinski, and V. B. Shah, "Julia: A fresh approach to numerical computing," *SIAM review*, vol. 59, no. 1, pp. 65–98, 2017. (Cited on page 103).

[107] D. Groppi, A. Pfeifer, D. A. Garcia, G. Krajačić, and N. Duić, "A review on energy storage and demand side management solutions in smart energy islands," *Renewable and Sustainable Energy Reviews*, vol. 135, p. 110183, Jan. 2021. (Cited on page 116).

[108] R. Jing, M. N. Xie, F. X. Wang, and L. X. Chen, "Fair p2p energy trading between residential and commercial multi-energy systems enabling integrated demand-side management," *Applied Energy*, vol. 262, p. 114551, Mar. 2020. (Cited on page 116).

[109] E. L. Karfopoulos and N. D. Hatziargyriou, "Distributed coordination of electric vehicles providing v2g services," *IEEE Transactions on Power Systems*, vol. 31, no. 1, pp. 329–338, Jan. 2016. (Cited on page 116).

[110] C. Kwon and I. Hwang, "Cyber attack mitigation for cyber–physical systems: hybrid system approach to controller design," *IET Control Theory & Applications*, vol. 10, no. 7, pp. 731–741, Apr. 2016. (Cited on page 116).

[111] F. Pasqualetti, F. Dorfler, and F. Bullo, "Cyber-physical attacks in power networks: Models, fundamental limitations and monitor design," in *IEEE Conference on Decision and Control and European Control Conference*. IEEE, Dec. 2011. (Cited on pages 116 and 117).

[112] K. Chatterjee, V. Padmini, and S. A. Khaparde, "Review of cyber attacks on power system operations," in *2017 IEEE Region 10 Symposium (TENSYMP)*. IEEE, July 2017. (Cited on page 116).

[113] S. Amini, H. Mohsenian-Rad, and F. Pasqualetti, "Dynamic load altering attacks in smart grid," in *2015 IEEE Power Energy Society Innovative Smart Grid Technologies Conference (ISGT)*, 2015, pp. 1–5. (Cited on page 116).

[114] "Control-theoretic methods for cyberphysical security: Geometric principles for optimal cross-layer resilient control systems," *IEEE Control Systems*, vol. 35, no. 1, pp. 110–127, Feb. 2015. [Online]. Available: https://doi.org/10.1109/mcs.2014.2364725 (Cited on page 117).

[115] F. Pasqualetti, F. Dorfler, and F. Bullo, "Attack detection and identification in cyber-physical systems," *IEEE Transactions on Automatic Control*, vol. 58, no. 11, pp. 2715–2729, Nov. 2013. [Online]. Available: https://doi.org/10.1109/tac.2013.2266831 (Cited on page 117).

[116] E. Baron-Prada, E. Osorio, and E. Mojica-Nava, "Resilient transactive control in microgrids under dynamic load altering attacks," in *2017 IEEE 3rd Colombian Conference on Automatic Control (CCAC)*. IEEE, Oct. 2017. [Online]. Available: https://doi.org/10.1109/ccac.2017.8276400 (Cited on page 117).

[117] A. Gusrialdi and Z. Qu, "Smart grid security: Attacks and defenses," in *Smart Grid Control*. Springer International Publishing, Sept. 2018, pp. 199–223. (Cited on page 117).

[118] V. Katewa and F. Pasqualetti, "Optimal dynamic load-altering attacks against power systems," in *2021 American Control Conference (ACC)*. IEEE, May 2021. (Cited on page 117).

[119] J. C. Geromel and P. Colaneri, "Robust stability of time varying polytopic systems," *Systems & Control Letters*, vol. 55, no. 1, pp. 81–85, 2006. (Cited on page 118).

[120] M. S. Mahmoud, "Switched time-delay systems." Springer, 2010. (Cited on page 118).

[121] H. Lin and P. J. Antsaklis, "Stability and stabilizability of switched linear systems: a survey of recent results," *IEEE Transactions on Automatic control*, vol. 54, no. 2, pp. 308–322, 2009. (Cited on pages 118 and 119).

[122] H. Horisberger and P. Belanger, "Regulators for linear, time invariant plants with uncertain parameters," *IEEE Transactions on automatic control*, vol. 21, no. 5, pp. 705–708, 1976. (Cited on page 118).

[123] G. Zhai, H. Lin, and P. J. Antsaklis, "Quadratic stabilizability of switched linear systems with polytopic uncertainties," *International Journal of Control*, vol. 76, no. 7, pp. 747–753, 2003. [Online]. Available: https://doi.org/10.1080/0020717031000114968 (Cited on page 118).

[124] D. Liberzon, "Switching in systems and control. boston: Birkhäuser," 2003. (Cited on page 118).

[125] D. Liberzon, J. P. Hespanha, and A. S. Morse, "Stability of switched systems: a lie-algebraic condition," *Systems & Control Letters*, vol. 37, no. 3, pp. 117–122, 1999. (Cited on page 118).

[126] B. Polyak and P. Shcherbakov, "Ellipsoidal approximations to attraction domains of linear systems with bounded control," in *2009 American Control Conference*. IEEE, 2009, pp. 5363–5367. (Cited on pages 119 and 121).

[127] F. Pasqualetti, A. Bicchi, and F. Bullo, "A graph-theoretical characterization of power network vulnerabilities," in *Proceedings of the 2011 American Control Conference*, June 2011, pp. 3918–3923. (Cited on pages 120 and 121).

[128] M. Barbehenn, "A note on the complexity of dijkstra's algorithm for graphs with weighted vertices," *IEEE Transactions on Computers*, vol. 47, no. 2, p. 263, 1998. [Online]. Available: https://doi.org/10.1109/12.663776 (Cited on page 125).

[129] V. Graveto, L. Rosa, T. Cruz, and P. Simões, "A stealth monitoring mechanism for cyber-physical systems," *International Journal of Critical Infrastructure Protection*, vol. 24, pp. 126–143, 2019. [Online]. Available: http://www.sciencedirect.com/science/article/pii/S1874548218300672 (Cited on page 128).

[130] F. Adamsky, M. Aubigny, F. Battisti, M. Carli, F. Cimorelli, T. Cruz, A. D. Giorgio, C. Foglietta, A. Galli, A. Giuseppi, F. Liberati, A. Neri, S. Panzieri, F. Pascucci, J. Proenca, P. Pucci, L. Rosa, and R. Soua, "Integrated protection of industrial control systems from cyber-attacks: the atena approach," *International Journal of Critical Infrastructure Protection*, vol. 21, pp. 72–82, 2018. (Cited on page 128).

[131] A. Giuseppi, R. Germana, and A. Di Giorgio, "Risk adverse virtual power plant control in unsecure power systems," 2018, pp. 210–216. (Cited on page 128).

[132] A. Di Giorgio, F. Liberati, A. Lanna, A. Pietrabissa, and F. Delli Priscoli, "Model predictive control of energy storage systems for power tracking and shaving in distribution grids," *IEEE Transactions on Sustainable Energy*, vol. 8, no. 2, pp. 496–504, 2017. (Cited on page 128).

[133] OPAL-RT. Opal-rt website. [Online]. Available: https://www.opal-rt.com/ (Cited on page 132).